BEHAVIOUR OF BURIED RECTANGULAR STRUCTURES DURING EARTHQUAKE

DİKDÖRTGEN KESİTLİ GÖMÜLÜ YAPILARIN DEPREM SIRASINDAKİ DAVRANIŞI

SABAHAT TUĞBA İLERİ

PROF. DR. BERNA UNUTMAZ

Supervisor

Submitted to

Graduate School of Science and Engineering of Hacettepe University

as a Partial Fulfilment to the Requirements

for be Award of the Degree of Master of Science

in Civil Engineering

2022

To My Family

ABSTRACT

BEHAVIOUR OF BURIED RECTANGULAR STRUCTURES DURING EARTHQUAKE

Sabahat Tuğba İLERİ

Master of Science, Department of Civil Engineering

Supervisor: Prof. Dr. Berna UNUTMAZ

December 2022, 95 pages

In recent years, due to the increasing population, underground construction has started as well as superstructures. In addition to underground tunnels used for transportation, the design of rectangular structures such as subway stations, ventilation structures etc. is very common. Today, the calculation of loads on such embedded structures during earthquakes is calculated in a similar to retaining walls and this leads to uneconomical solutions. Within the scope of this paper, the displacement of embedded rectangular cross-section structures during earthquakes has been defined and the behavior of these types of structures under cyclic loading has been tried to be determined. In this study, one-dimensional soil response and two-dimensional finite element analyzes were performed using various structure- earthquake- soil combinations and in embedded structures, the horizontal displacements that occurred after an earthquake have been evaluated. At this stage, the important parameters are considered to be the soil–structure stiffness ratio, the stiffness of the soil, and the properties of the structure. Two-dimensional finite element based numerical analyzes were performed. For different states of structural stiffness, soil stiffness, and earthquake magnitudes, the relative displacements between the top and bottom of the structure were determined. Finally, the analysis used finite element method was performed using the easily obtainable soil-structure-earthquake parameters (depth,

length, width of the structure etc.; soil stiffness; internal friction angle etc.) and results obtained from analysis were compared.

Keywords: Soil – Structure Interaction, Finite Element Method, Simplified Frame Method, Site Response Analysis, Unit Stiffness, Racking Coefficient

ÖZET

DİKDÖRTGEN KESİTLİ GÖMÜLÜ YAPILARIN DEPREM SIRASINDAKİ DAVRANIŞI

Sabahat Tuğba İLERİ

Yüksek Lisans, İnşaat Mühendisliği Bölümü

Tez Danışmanı: Prof. Dr. Berna UNUTMAZ

Aralık 2022, 95 sayfa

Son yıllarda artan nüfus artışı ile yer üstünde olduğu gibi yer altında da yapılaşma başlamıştır. Özellikle ulaşım için kullanılan yer altı tünellerine ek olarak, metro istasyonları, havalandırma yapıları vb. dikdörtgen kesitli yapıların tasarımına sıklıkla rastlanılır olmuştur. Günümüzde deprem sırasında bu tip gömülü yapıların tasarımı, yer üstündeki istinat duvarlarına benzer şekilde yapılmakta ve böylece aşırı derecede güvenli tarafta kalınarak, hiç de ekonomik olmayan çözümlerin üretilmektedir. Bu çalışma kapsamında gömülü dikdörtgen kesitli yapıların deprem sırasında yapacakları yer değiştirmeler belirlenerek, bu tip yapıların bu tekrarlı yükler altındaki davranışı belirlenmeye çalışılmıştır. Bu kapsamda çeşitli yapı – deprem – zemin kombinasyonları kullanılarak, bir boyutlu zemin tepki ve iki boyutlu sonlu elemanlar analizleri yapılmış ve gömülü yapıda deprem sonrasında oluşacak yatay deplasmanlar hesaplanmaya çalışılmıştır. Bu aşamada önemli parametreler, zemin – yapı rijitlik oranı, zeminin

rijitliği, ve yapının özellikleri olduğu düşünülmüş ve bu kapsamda iki boyutlu sayısal analizler gerçekleştirilmiştir. Farklı senaryo koşulları altında (farklı yapı rijitlikleri, farklı zemin rijitlikleri ve farklı deprem büyüklükleri) bu tip yapılarda oluşacak göreceli yer değiştirmeler belirlenmiştir. Sonrasında kolay elde edilebilir yapı – zemin – deprem parametreleri kullanılarak (yapının derinliği, boyu, genişliği vb.; zeminin rijitliği, içsel sürtünme açısı vb., maksimum yer ivmesi vb.) sonlu elemanlar yöntemi ile hesaplanmış ve elde edilen sonuçlar karşılaştırılmıştır.

Anahtar kelimeler: Zemin – Yapı Etkileşimi, Sonlu Elemanlar Yöntemi, Basitleştirilmiş Çerçeve Yöntemi, Zemin Tepki Analizi, Birim Rijitlik, Yamulma Katsayısı

ACKNOWLEDGMENT

First of all, I would like to express my deepest gratitude to my thesis supervisor Prof. Dr. Berna UNUTMAZ for her endless understanding, patience, guidance, support and encouragement throughout this thesis journey. This thesis would not have been possible without her continuous motivation, understanding, unlimited assistance, academic and professional support. I am very lucky to have a supervisor who always helped me for my engineering and academic life. I am forever grateful to her for magical touches in my life.

I would like to express my gratefulness to Assoc. Prof. Dr. Mustafa Kerem KOÇKAR and Assoc. Prof. Dr. Mustafa Abdullah SANDIKKAYA for their technical support, great motivation and valuable help during my academic life. It was a pleasure to have an opportunity to work with them.

I would also like to thank to Prof. Dr. Zeynep GÜLERCE and Assoc. Prof. Dr. Alper ALDEMİR for their constructive comments and insightful recommendations in my thesis committee.

Sincere thanks to my director, my manager and my colleagues who have encouraged me in ASSYSTEM – Site Services / Geo-Engineering Team for their support and motivation.

My special thanks go to my girls, Tuğba YILDIZLI, Zeynep MANDACIOĞLU, Merve BAYRAKTAR and Sercan ÇALIŞ for precious friendship and continuous support. I am very thankful for always being by my side and sharing my joy or sadness. Having such friends in life is my luck. We always find a way to bring hearts together no matter how many miles there are between them.

I am very thankful to my friend, Zeynep YADAŞ for her motivations and supports.

The last but not the least, I would also like to express my deepest love and appreciation to my family. I am grateful to my beloved mother Sevil and father Fatih for their invaluable love, endless patience and unconditional support. They always believe in me each decision that I take. I am more than happy and lucky to be their little girl throughout my life. Also, my beloved sister Tuğçe, her presence always gave me strength and happiness. Thank you for all the beauties you brought to my life.

TABLE OF CONTENTS

LIST OF FIGURES

LIST OF TABLES

SYMBOLS AND ABBREVIATIONS

Symbols

a	Width of the structure (Huo et al., 2006; Tsinidis and Pitilakis, 2018; this study)
a_i	Geometrical parameters in any control perimeter of soil
a_{max}	Maximum soil accelerations
b	Height of the structure (Huo et al., 2006; Tsinidis and Pitilakis, 2018; this study)
b_i	Geometrical parameters in any control perimeter of soil
c	Cohesion
c_i	Geometrical parameters in any control perimeter of soil
C	Embedment depth of the tunnel (Patil et al., 2018)
d_1, d_2	Diagonals lengths of the deformed tunnel section
D_O	Overburden depth
D	Diameter of the tunnel (Patil et al., 2018)
D_B	Founded level above the bedrock
D_{co}	Critical burial depth
d_i	Geometrical parameters in any control perimeter of soil
E	Elasticity modulus
E_1	Young's modulus of the lining material
E_s	Stiffness of the structure element
EA	Normal stiffness
EI	Flexural rigidity
F	Flexibility ratio
F^w	Wang's flexibility ratio

G	Shear modulus of surrounding soil
G_{max}	Small-strain shear modulus
Gs	Strain – compatible shear modulus of the soil
h	Burial depth of structure
H	Height of the structure
H_i	Geometrical parameters in any control perimeter of soil
I	Moment of inertia of the lining (per unit width)
I_b	Wall bending inertia
I_s	Structure moment of inertia
I_w	Slab bending inertia
K_0	The coefficient of earth pressure at rest condition
$K_{AVG,H}$	The average horizontal shear stiffness of the soil and structure ensemble
$K_{AVG,V}$	The average vertical shear stiffness of the soil and structure ensemble
K_{BOT}	The shear stiffness for bottom layer
K_{CENT}	The shear stiffness for central layer
$K_{CENT,V}$	The vertical shear stiffness for central layer
K_H	The shear stiffness of separated block for horizontal force
K_{INT}	The shear stiffness for intermediate layer
$K_{INT,H}$	The horizontal shear stiffness for intermediate layer
k_l	Lateral stiffness coefficient proposed by Penzien (2000)
K_{LEFT}	The shear stiffness for left layer
K_{RIGHT}	The shear stiffness for right layer

K_s	The force required to cause unit racking deflection of the structure (or is the required concentrated force to induce a unit racking deflection of the top of the structure)
K_{SOIL}	Soil shear stiffness
K_{STRU}	Structure shear stiffness
$K_{STRU,H}$	The shear stiffness of structure for horizontal force
$K_{STRU,V}$	The shear stiffness of structure for vertical force
k_{s0}	Soil stiffness coefficient
k_{si}	Second soil parameter
K_{TOP}	The shear stiffness for top layer
K_v	The shear stiffness of separated block for vertical force
M	Coefficient depend on the shape of the structure (proposed by Huo et al., 2006)
M_w	Magnitude of earthquake
N	Coefficient depend on the shape of the structure (proposed by Huo et al., 2006)
L_s	Coefficient depend on the stiffness of the structure and soil (proposed by Huo et al., 2006)
L	Width of the rectangular structure (Debiasi et al., 2013)
L_i	Geometrical parameters in any control perimeter of soil
P	Pseudo-concentrated force
$\widetilde{R}$	Approximate and conditional racking coefficient based on the block behavior assumption
R	Racking coefficient
R_{Deep}	The racking coefficient for a deeply buried case
R_{jb}	The Joyner-Boore distance
R_n	Racking ratios by numerically calculated

R_R	Racking ratio produced by rocking rotation (Debiasi et al., 2013)
R_{rup}	The closest distance to rupturing fault plane
R_{TOT}	Racking ratio (Debiasi et al., 2013)
R_Z	The ratio of the racking coefficient at a certain depth Z
t	Lining thickness
u_1	Rigid body movement of the tunnel section
u_2	Displacement because of the rotation of the tunnel section
u_3	Displacement because of the racking distortion of the tunnel section
u_A	Lateral displacement of soil at point A (in this study)
u_B	Lateral displacement of soil at point B (in this study)
u_x	Total horizontal displacement of soil or plate
W	Width of the structure
V_s	Shear wave velocity
V_{s30}	The average shear-wave velocity (V_S) to a depth of 30 meters
Z	Burial depth of the structure (Gordo-Mons´o et al., 2021)
α	Numerical parameters proposed by Gordo-Mons´o et al. (2021)
α_S	The principal lining - soil racking ratio
B	Numerical parameters proposed by Gordo-Mons´o et al. (2021)
γ	The total sheared angle
γ_{AVG}	Shear distortion of the outer perimeter
$\gamma_{AVG,H}$	The average horizontal shear strain
$\gamma_{AVG,V}$	The average vertical shear strain
$\gamma_{CENT,V}$	Central layer vertical shear strain
γ_{FF}	Free field shear distortion
γ_{ff}	Free-field shear strain
γ_R	Rocking distortion of the shallow structure

γ_S	Shear distortion of the shallow structure
γ_s	The average racking angle of the tunnel section
γ_{STRU}	The underground structure shear deformation
γ_{INN}	Shear distortion of the inner structure
$\gamma_{INT,H}$	Intermediate layer horizontal shear strain
γ_{unsat}	Dry unit weight
Δ	Displacement difference between the bottom and top elevations of the rectangular box structures by using proposed equation in this study
Δ_A	The differential sideways movement of top elevations of rectangular structures
Δ_B	The differential sideways movement of bottom elevations of rectangular structures
Δ_{diff}	The differential sideways movements between the top and bottom elevations of rectangular structures
$\Delta_{free-field}$, Δ_{ff}	Lateral racking deformation of the free-field soil
$\Delta_{p_2^i}$	The deformation of the structure due to a linear normal stress distribution
Δ_R	The differential horizontal displacement produced by rocking rotation
$\Delta_{structure}$, Δ_{str}, Δ_s	Lateral racking deformation of the structure embedded in the soil
Δ_{t^i}	Deformation of the structure due to a shear stress
Δ_{TOT}	The differential horizontal displacement produced by racking displacement and rocking rotation
δ_θ	Half of the horizontal displacement caused by the rocking rotation of the tunnel section
δ_{ff}	Tunnel axis soil racking distortion at free-field
δ_{str}	Seismic racking deformations of the tunnel section

$\delta_{str,a}$	The actual seismic racking distortions
θ	Rocking rotation of the tunnel section
λ	Aspect ratio of the structure (Huo et al., 2006 and Tsinidis, 2018)
μ	Interface of between the soil and the tunnel
ν	Poisson's ratio
ν_S	Poisson's ratio of the soil
ρ	Unit mass of the soil
σ'	Vertical effective stress
τ	Pure shear stress state
τ_{ff}	Free field shear stress
τ_l	Intensity of shear stress proposed by Penzien (2000)
ϕ	Internal friction angle of soil
Ω	Stiffness ratio

Abbreviations

1-D	One Dimensional
2D	Two Dimensional
EC8	Eurocode 8
EQ	Earthquake
FE	Finite Element
FEM	Finite Element Method
FHWA	Federal Highway Administration
JSCE	Japan Society of Civil Engineers
NCHRP	National Cooperative Highway Research Program
PEER	Pacific Earthquake Engineering Research
PGA	Peak Ground Acceleration
PGV	Peak Ground Velocity

PI	Plasticity Index
PIV	Particle Image Velocimetry
SRA	Site Response Analysis
TBEC	Turkish Building Earthquake Code

1. INTRODUCTION

1.1. Research Statement

Underground structures play crucial role in the infrastructure of contemporary life because they take part in many important applications ranging from transportation to storage systems.

Behavior of underground structures subjected to the seismic excitations differ from the ones above the ground surface. Also, the seismic response of underground structures depend upon the seismic behavior of the surrounding soil and aboveground structures are not subject to free vibrations (Hashash, 2015). Buried structures are subjected to displacement similar to that of the soil because they are constrained by the surrounding soil (Hashash et al., 2010; Bobet et al., 2008; Huo et al., 2005).

The literature shows that buried structures, such as rectangular tunnels or box culverts can be affected by shaking motion. These structures generally have a rectangular cross-section and they are usually in soils. The soil-structure interaction effects are especially significant under some conditions. Tunnel is a box-type structure that is built in urban areas (or sometimes adjacent to an existing structure above the surface) and they have a strategic importance role in railway and highway transportation networks.

In seismic design, racking distortion is regarded to be the most critical situation (Merrit et al., 1985). Racking displacements of rectangular underground structures can be assessed using several methods such as fully non-linear, simplified linear, pseudo-static model, dynamic soil–structure interaction. Pseudo-static free-field displacement calculations (Merrit et al., 1985; Hendron and Fernandez, 1983) generate the early initiatives to study the linked behavior between underground structure and soil subjected to the seismic condition. Numerical dynamic soil-structure interaction analysis constitutes very complex and detailed methods to investigate the response of an underground structure during an earthquake. To avoid the complex non-linear soil–structure interaction analysis, a great extent of simplified methodology has been recommended in last years by designers. The aim of this thesis is to investigate the new approaches such as simplified frame analyses with results emerging from soil-structure interaction analysis.

1.2. Research Objectives

This thesis focuses on the seismic response and behavior of buried rectangular structures commonly used for culvert, tunnels, water or sewage transportation ducts and metro structures. The research objectives of this thesis are described as follow;

1. To analyze the buried rectangular structures behaviors accounting for the effect of the geometry of the cross section (in terms of burial depth, single or double barrel and lining thickness), the embedment depth, the subjected to different earthquake excitation.
2. To propose a new equation for assessing the racking displacement of the rectangular structures based on pseudo static soil-structure analysis.

1.3. Outline of the Thesis

This thesis is divided into five chapters. The contents of these chapters are as follow;

Chapter 1 presents an introduction to the thesis and refers the research statement and objectives.

Chapter 2 provides literature review on the various aspects of behavior of buried rectangular structures subjected to seismic action under different conditions. Several design considerations are also presented in this chapter.

Chapter 3 explains the simplified frame methodology and presents the sequence of parametric study followed through the research. The one-dimensional site response analysis, two-dimensional finite element analysis, racking ratio and flexibility coefficient procedures are also introduced in this chapter.

Chapter 4 consists of the explanation of sample case and results of parametric study from two-dimensional finite element analysis. Moreover, the proposed equation based on simplified parameters are also presented in this part.

Chapter 5 concludes summary of parametric study results and presents proposed equation for future studies.

2. LITERATURE SURVEY

This chapter presents design methods for seismic response assessment of buried rectangular structures that are performed in the literature.

Effects of earthquake on underground structures can be categorized into two categories:

- ground shaking
- ground failures such as liquefaction, fault displacement and slope stability (Hashash et. al., 2001)

It was thought that the behavior of a tunnel would approximate that of an elastic beam subjected to deformations exerted by the surrounding soil. Response of the underground structures to ground vibrations induced by the seismic motion is classified as axial extension and compression (Figure 1 a and Figure 1 b), longitudinal bending (Figure 1 c and Figure 1 d) and racking/ovaling (Figure 1 e and Figure 1 f) (Owen and Scholl, 1981). Racking deformation of tunnel section occurs when shear waves propagate normal direction or nearly normal direction to the tunnel axis. Procedures of design for racking response are in the transverse direction (Hashash et. al., 2001).

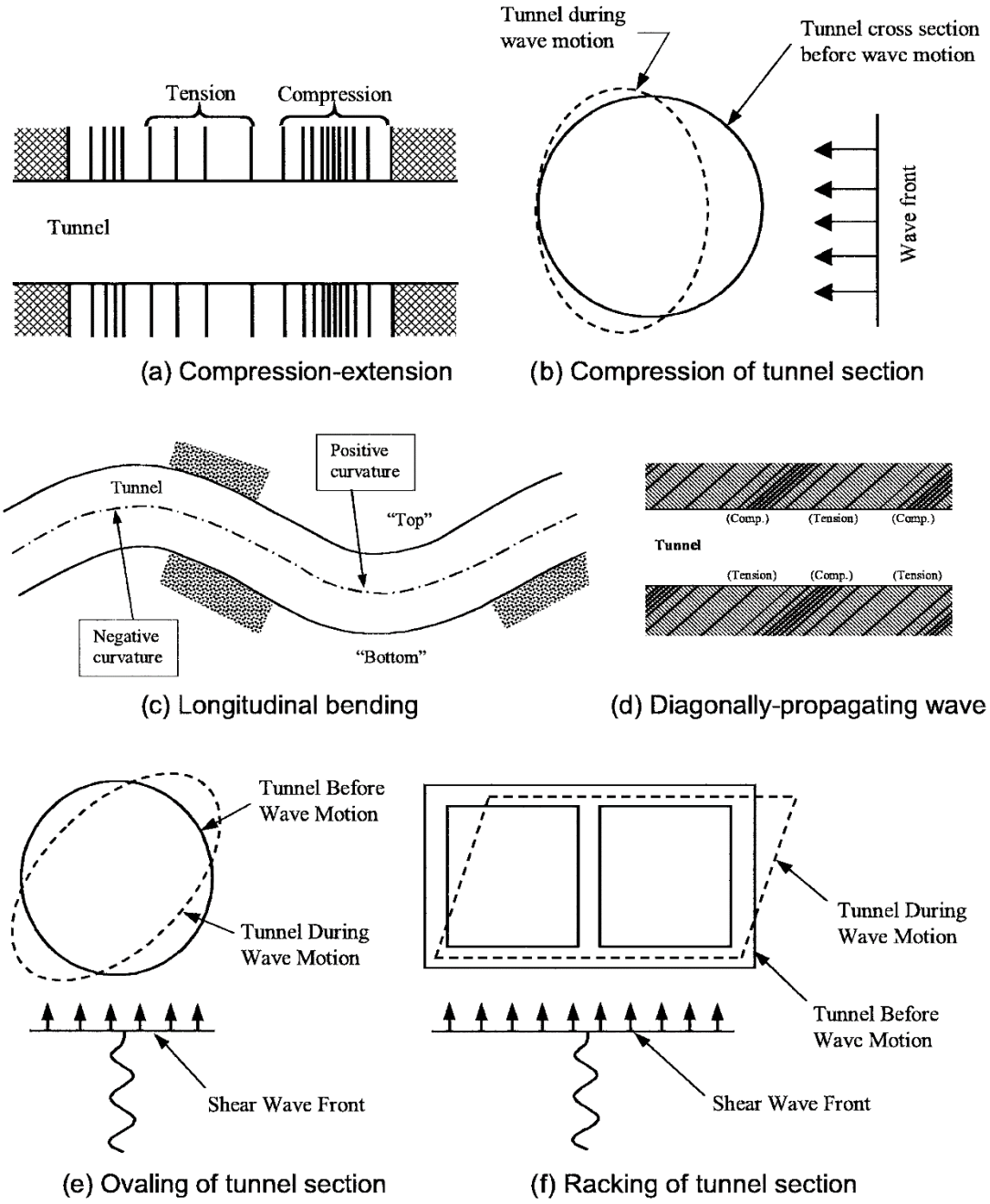

Figure 1 Tunnels deformation modes because of seismic waves (after Owen and Scholl, 1981)

Seismic design and construction of underground structures have large uncertainties that can be accounted for by conducting different design methods. However, seismic resistant culvert/pipeline structure design and construction should never be overlooked because many buried structures have suffered moderate to major damage from earthquakes (FHWA, 2011). As a consequence, a safe design to perform a reliable evaluation of the

interaction between the surrounding soil and the buried structure is necessary. To understand the seismic design of the buried structures and explain the critical parameters of their seismic response, numerical and analytical solutions, simplified methods have been developed on a large scale. In addition to these tests, physical tests (dynamic centrifuge test, shaking table test etc.) has also been conducted.

Mononobe-Okabe methodology as proposed by Seed and Whitman (1970) and the Japanese Society of Civil Engineers (JSCE, 1975), used for calculating the increase in lateral earth pressure, undertake earthquake loads to be induced by the inertial force of surrounding soil (Hashash et. al.,2001). This method is associated with a decided seismic coefficient and the parameters of soil (Hashash et. al.,2001).

According to Hashash et. al. (2001), this method gives unrealistic results for buried rectangular structures under plane strain conditions. The estimated seismic lateral earth pressures are less reliable for the deeper buried tunnel. Therefore, as seismic ground motions vary with depth, it becomes important to take this effect into account.

Another study on dynamic earth pressure was proposed by Wood (1973). By supposing infinitely rigid wall and foundation, Wood (1973) proposed a total dynamic thrust that is almost 1.5 to 2.0 times the thrust calculated by the Mononobe-Okabe methodology (Wang, 1993).

Commonly, rectangular tunnels are designed using the assumption that racking deformation imposes the same shear distortions on the structure as the surrounding soil has free-field shear distortion (Wang,1993). Differential distortion and free-field soil deformation to be used in the analysis of the buried rectangular structures are shown in Figure 2.

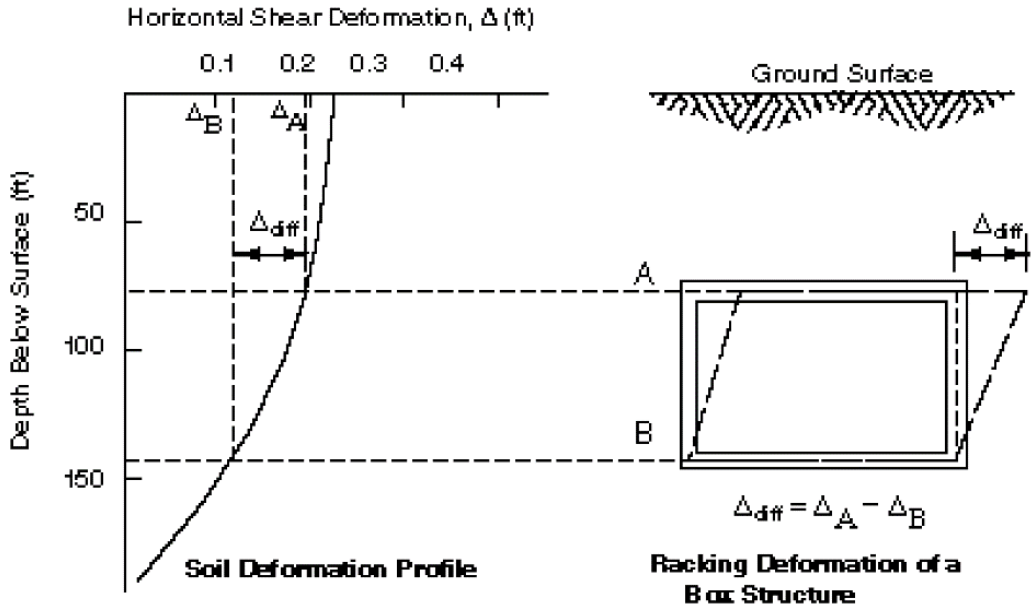

Figure 2 Buried rectangular structure exposed to free-field racking deformation (Wang, 1993; source: St. John and Zahrah, 1987)

Wang (1993) emphasized relative flexibility ratio as an important parameter to find out the seismically-induced deformation of buried structures.

Embedment depth, structure geometry, and earthquake motion are critical parameters in the behavior of the soil-structure interaction system, also a fundamental factor is the relative shear stiffness between the structure it displaces and the surrounding soil (Wang 1993). So, Wang (1993) proposed a simplified analytical method (referred to as simplified frame analysis model) to explain soil-structure interaction in estimating the racking deformation of rectangular structures and also performed finite element analysis using structure geometry having different types.

Wang (1993) carried out extensive studies and evaluated seismic design approaches for an underground structure. Some assumptions of these analyses are no-slip case between the soil-structure interface and linear-elastic deformations of structure and ground. Researchers concluded that the flexibility ratio and racking coefficient are correlated. According to Wang, the flexibility ratio (F) is identified to represent the relative stiffness between soils and rectangular structures and the racking coefficient (R) is the ratio of the

displacement of the tunnel and free-field surrounding soil. The method of Wang (1993) was presented in Figure 3.

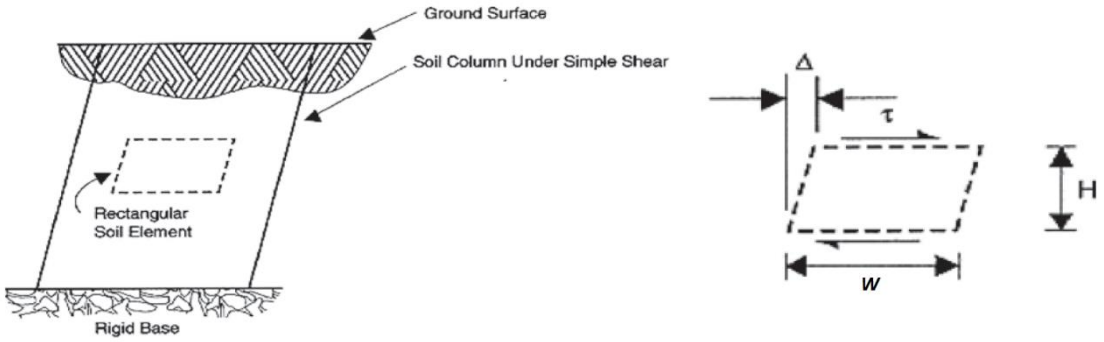

Figure 3 Wang (1993) simplified frame analysis method

Flexibility ratio is:

$$F = \frac{G\,W}{K_s\,H}$$

where

W: rectangular structure width

H: rectangular structure height

G: shear modulus of soil

K_S: force required to cause unit racking deflection of the structure

The racking coefficient is:

$$R = \frac{\Delta_{structure}}{\Delta_{free-field}}$$

Where,

$\Delta_{free-field}$: lateral shear deformation of the free-field condition

$\Delta_{structure}$: lateral racking deformation of the structure

The F-R relationship curves of Wang are presented in Figure 4.

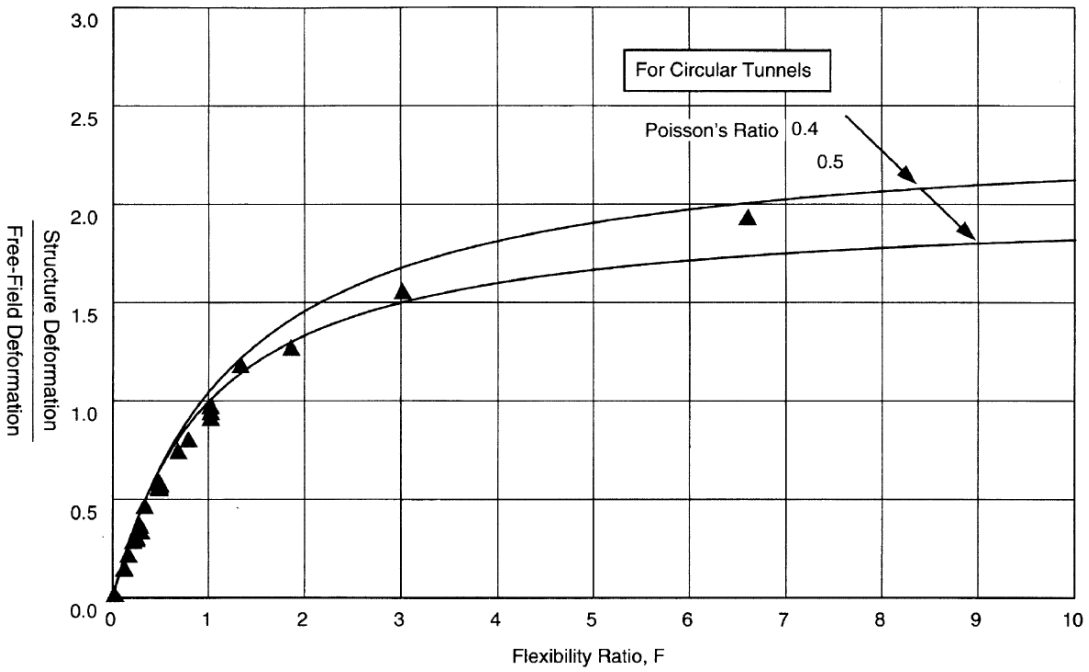

Figure 4 Flexibility ratio - Racking coefficient curve suggested by Wang (1993)

Wang (1993) reported that the structure is less stiff than the surrounding soil for $F > 1$ whereas it is stiffer than the surrounding soil for $F < 1$.

Penzien (2000) proposed an analytical methodology to calculate the racking deformation for rectangular structures during an earthquake loading. Penzien stated that if a rectangular cavity having W and H cross-section dimension exist in an unstrained medium, it will have the same free-field racking (γ_{ff}) provided the free-field shear stress (τ_{ff}) equal to $G_S\gamma_{ff}$ is applied as external loading to the cavity surface (Figure 5).

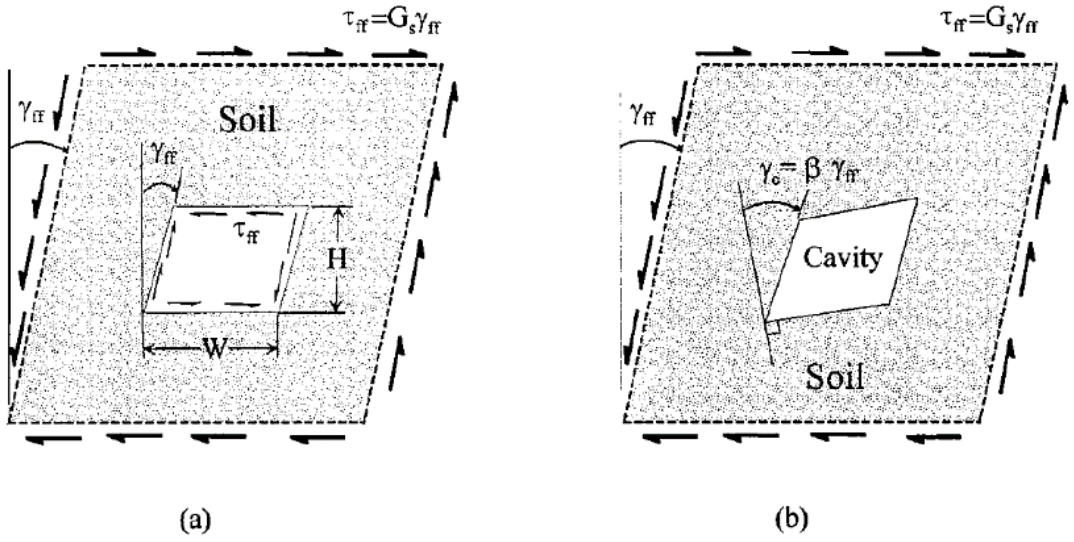

Figure 5 Deformation of the rectangular cavity under a uniform shear strain environment

Some assumptions made by Penzien in these analyses:

- No inertial effects (soil-structure interaction is relatively small)
- Soil has a uniform strain field

The methodology process can be summarized:

- So as to obtain the racking coefficient, lateral stiffness k_l must be found. Stiffness coefficient k_l is defined that the intensity of shear stress τ_l (Figure 6).

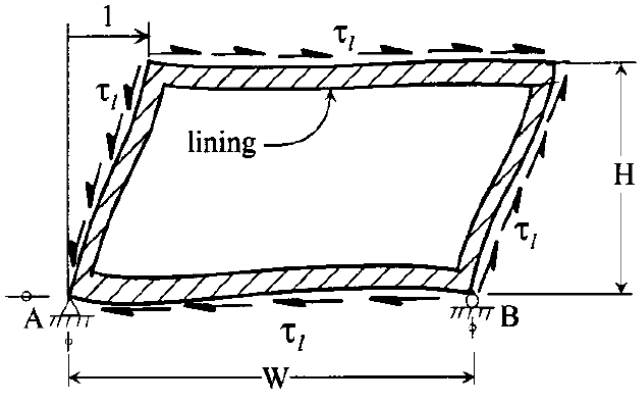

Figure 6 Stiffness coefficient k_l

- Soil stiffness coefficient k_{s0} and second soil parameter k_{si} is estimated as given in equations:

$$k_{s0} = \frac{G_S}{(3 - 4\nu_S)\, H}$$

$$k_{si} = \frac{G_S}{H}$$

- $\alpha_S = (3 - 4\nu_S)\, \frac{k_l}{k_{si}}$

Where ν_S is Poisson's ratio of the soil.

- Racking coefficient of the structure is:

$$R = \frac{4\,(1 - 4\nu_S)}{1 + \alpha_S}$$

A graph of F (stiffness ratio or flexibility ratio, $\frac{k_{si}}{k_l}$) versus racking coefficient (R) is presented in Figure 7 for discrete values of Poisson's ratio of the soil (ν_S) equal to 0.5 and 0.4.

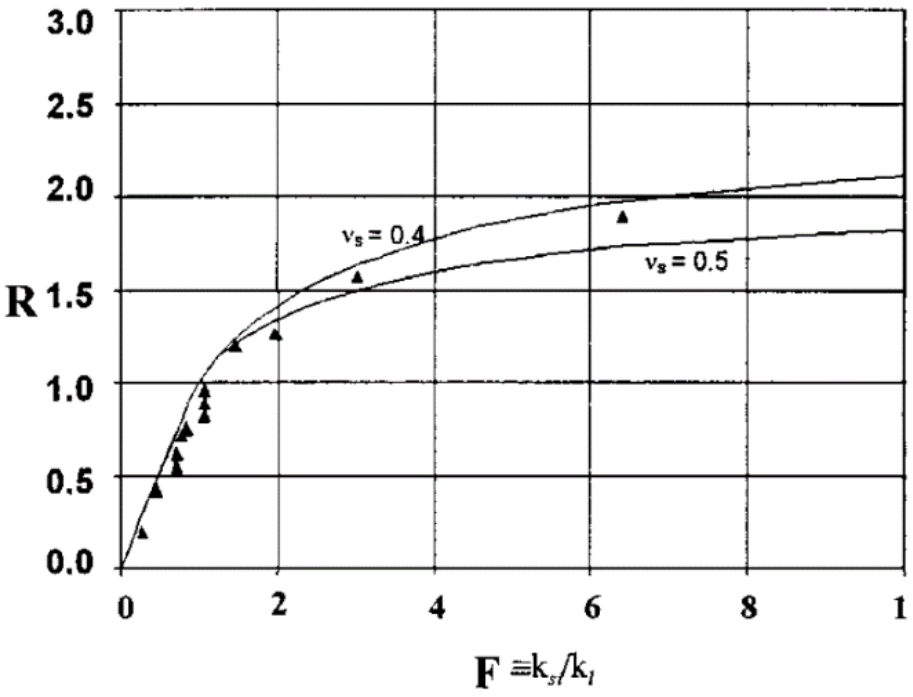

Figure 7 Racking coefficient R vs. stiffness ratio Penzien (2000)

Penzien (2000) reported that the racking coefficient R increases for lower Poisson's ratios.

Huo et al. (2006) suggested a new analytical procedure to predict seismic induced distortions in embedded deep rectangular structures, considering the soil and the structure interaction condition.

This new analytical solution has some assumptions (Figure 8):

- isotropic and homogeneous soil
- elastic response of the surrounding soil and structure
- deep rectangular structure in an infinite medium
- pseudo-static analysis
- plane strain conditions.

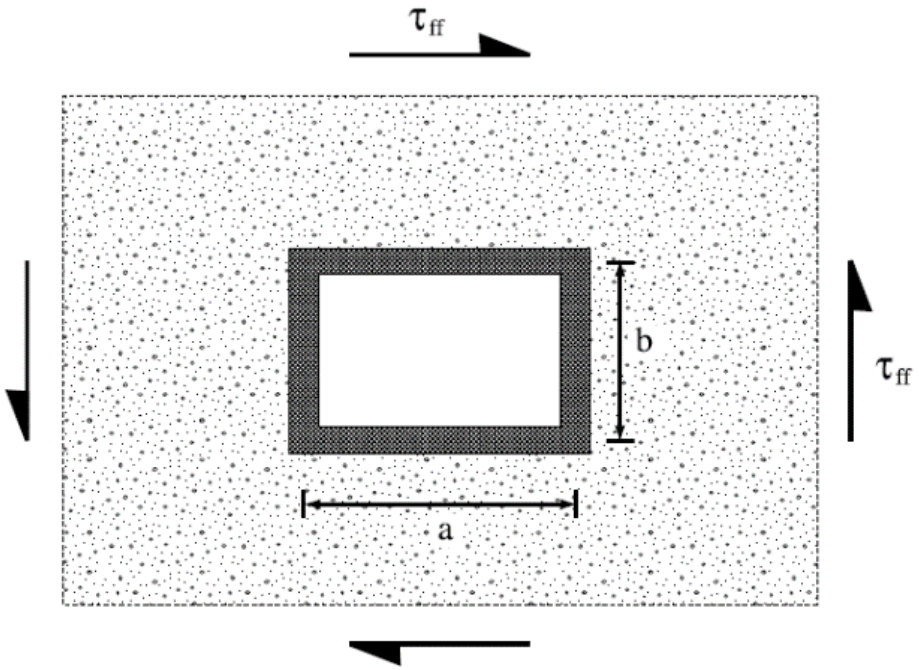

Figure 8 Structure having rectangular cross section in an infinite medium

The methodology of Huo et al. (2006) can be described:

- The aspect ratio λ is calculated by dividing the width of the structure (a) by the height of the structure (b).

$$\lambda = \frac{a}{b}$$

- Stiffness ratio Ω can be calculated by:

$$\Omega = \frac{E_s I_s}{G\, b^3}$$

where

E_s: stiffness of structure elements

I_s: structure moment of inertia

G: stiffness of the soil

- Δ_{t^i} and $\Delta_{p_2^i}$ are calculated by following equation for racking coefficient

$$\Delta_{t^i} = \frac{(1+\lambda)}{24\ (E_s I_s)}\ \lambda\, b^4$$

$$\Delta_{p_2^i} = \frac{(1+\lambda)}{60\ (E_s I_s)}\ b^4$$

where

Δ_{t^i} is the structure deformation because of a shear stress

$\Delta_{p_2^i}$ is the structure deformation because of a linear normal stress distribution

- M and N coefficients based upon the cross section of the rectangular structure, coefficient L_s depends upon the stiffness of the structure and soil. These coefficients are calculated by Figure 9 and Figure 10.

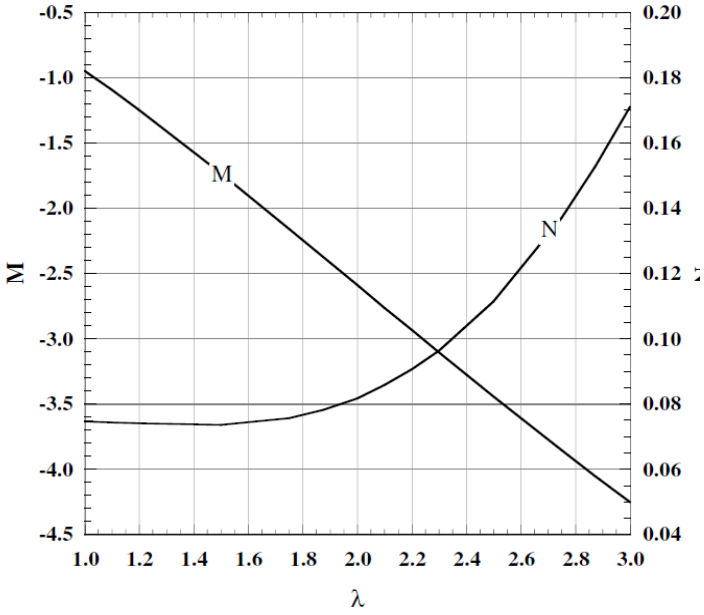

Figure 9 M and N coefficients

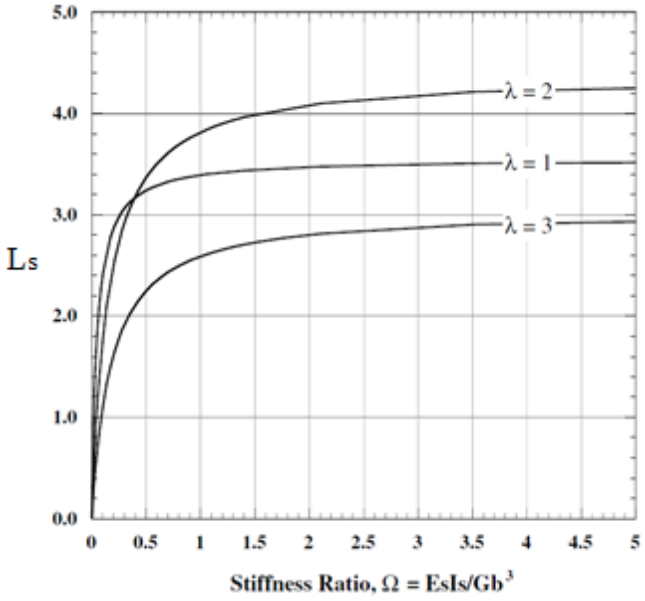

Figure 10 L_s coefficient

- Huo et al. (2006) proposed the formula for normalizing the deformation of the structure as follows:

$$\frac{\Delta_{str}}{\Delta_{ff}} = R = (1 - \nu_s^2)\,[\,N\,\Delta_{p_2^i} + (M\,\Delta_{p_2^i} + \Delta_{t^i})L_s]\frac{G}{b}$$

Comparison between existing literature and Huo et al. (2006) correlations are shown in Figure 11. This study shows that the racking coefficient increases than results from Penzien (2000) and Wang (1993) for flexibility ratios greater than 1. Also, results are similar to other studies for flexibility ratio is less than 1. In addition to this, aspect ratio (λ) affects the racking deformation for the same Poisson ratios.

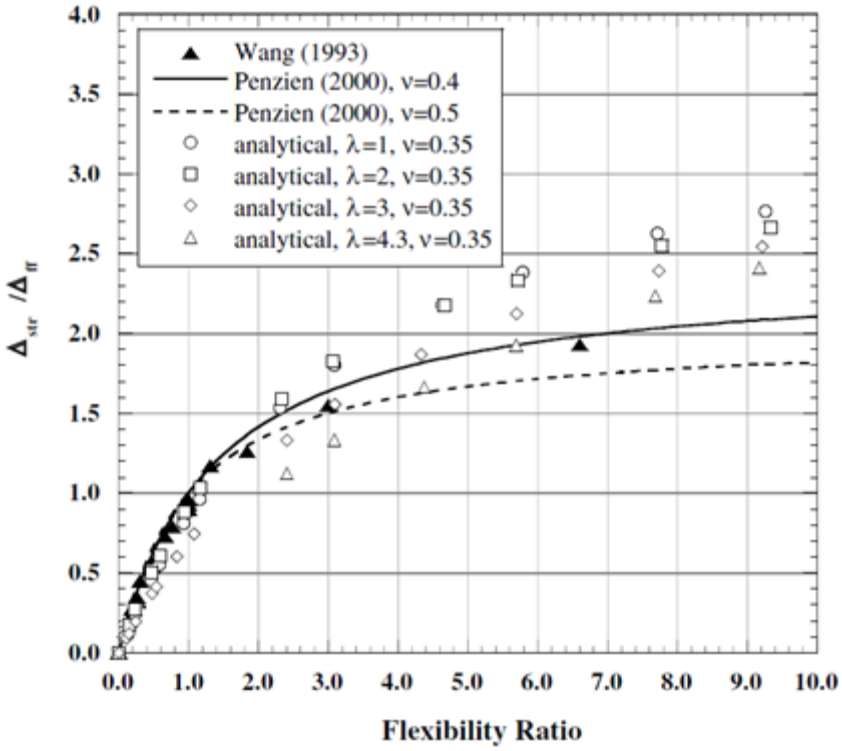

Figure 11 Comparison of results between existing literature and Huo et al. (2006) correlations

Hashash (2010) reviewed simplified solutions in literature and conducted numerical pseudo-static and dynamic soil-structure interaction analysis. Several analyses were performed on single- and double-barrel rectangular structures (Figure 12). Both nonlinear and equivalent linear site response analysis were conducted in the study.

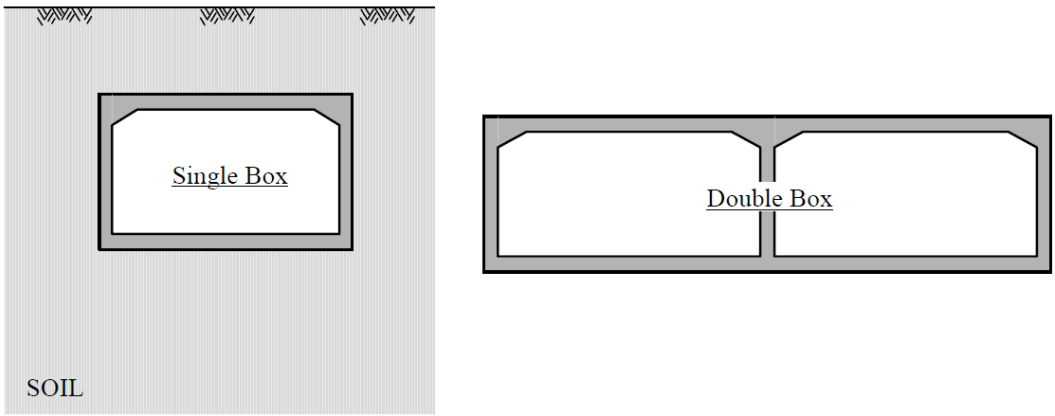

Figure 12 Typical box structures (Hashash,2010)

The analysis results were presented as in Figure 13.

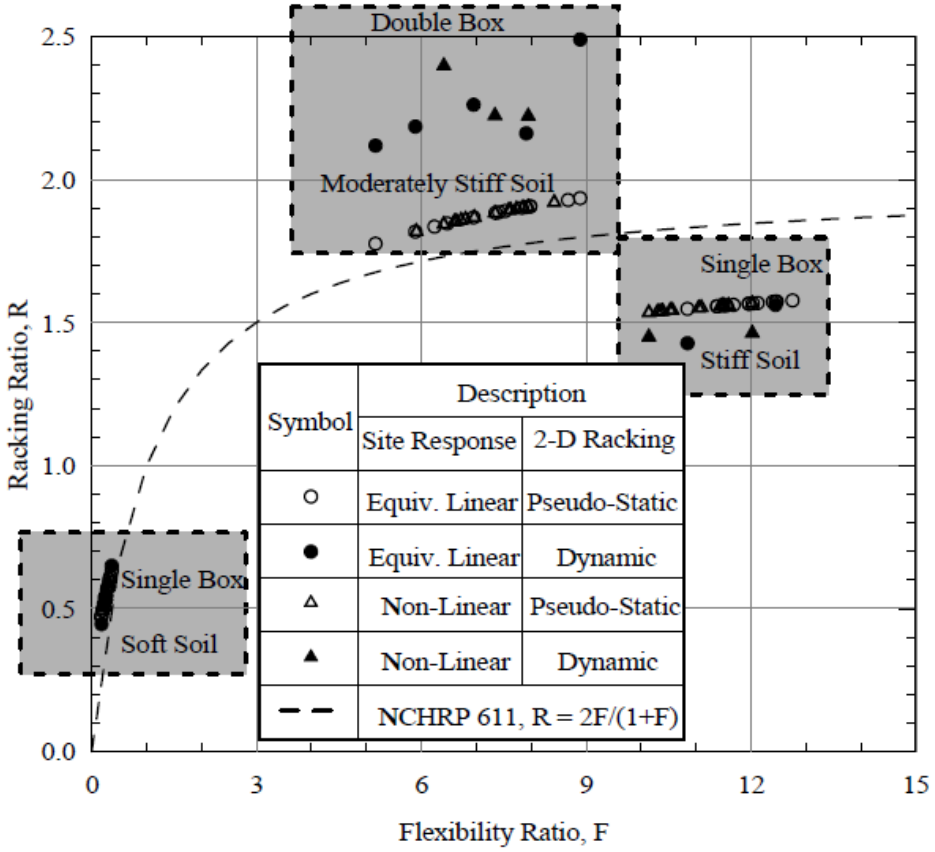

Figure 13 Pseudo static and dynamic analysis results (Hashash, 2010)

As a result of this study, the following results were obtained.

- For F<1, the racking stiffness of the soil is smaller than that of the structure.
- For the structure in soil 4<F<9 (moderately stiff soil), like the structure in soft soil.
- For the structure in soil 10<F<13 (stiff soil), the pseudo-static and dynamic racking ratios are less than those for NCHRP 611. Dynamic analyses result in slightly lower racking ratios than pseudo-static analyses.

Bobet (2010) investigated the seismic behavior of embedded rectangular structures under undrained and drained situations by conducting a parametric study using the finite element method in ABAQUS for no-slip or full slip conditions at between the soil and structure interface.

The flexibility ratio of the structure, F^w, is used that proposed by Wang (1993).

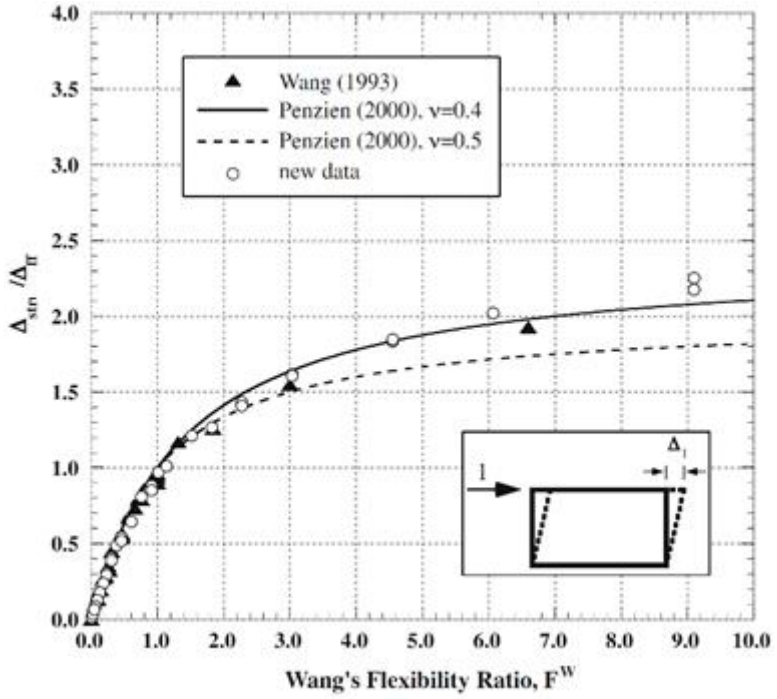

Figure 14 Normalized distortion of structure, from Penzien (2000) and Wang (1993), and this study-new data (Bobet,2010)

As can be seen, Figure 14 present results from Wang (1993), Penzien (2000) and Bobet (2010) who used the ABAQUS (FEM) to develop the distortion of deep rectangular structures with several flexibility ratios as well as different shape ratio (a/b) of 1, 2 and 3. The Bobet (2010) results are consistent with results of Wang (1993). Although the differences are small, the data of structures that have the same F^w do not consistent the same normalized distortion.

In addition to this, Bobet (2010) conducted the study considering different conditions such as:

- No-slip condition between the structure and soil and dry soil
- Full-slip condition between the structure and the soil and dry soil
- No-slip condition and saturated soil (undrained or short-term analysis)
- Full-slip condition between the structure and the soil and saturated soil

Figure 15 shows the results of analyzes under these conditions.

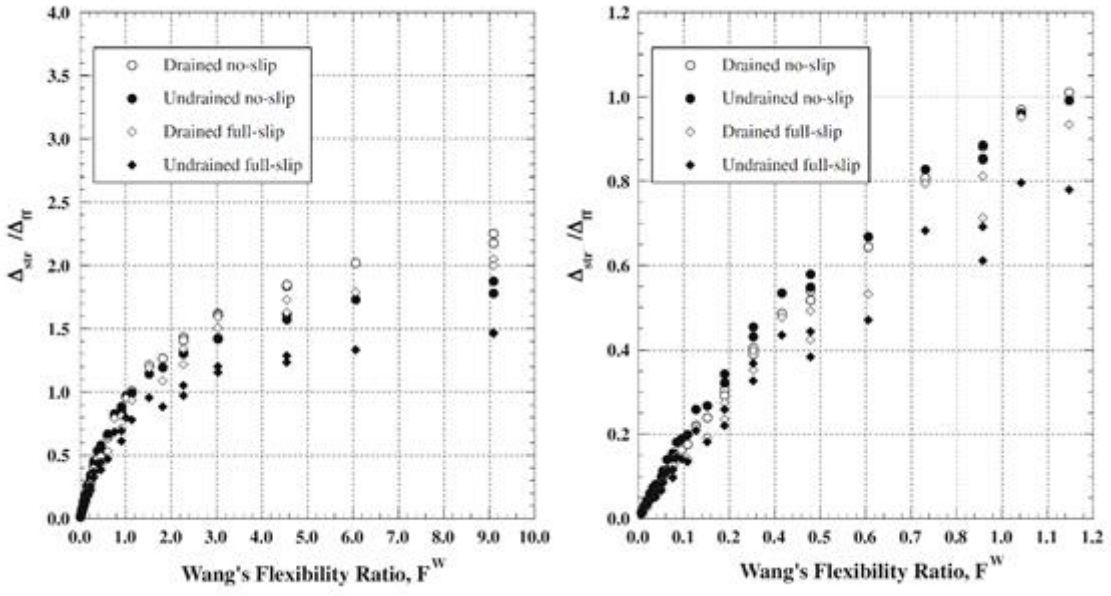

Figure 15 Deeply buried rectangular structure in the infinite medium with undrained - drained analysis, full-slip condition and no-slip condition and interactions between the liner and the soil

As can be seen in Figure 15, racking distortions with full-slip conditions between the structure and the soil are smaller than conditions with no-slip for the same flexibility ratio of Wang (F^W) and the same type of analysis. Also, the racking distortions under undrained analysis with full-slip conditions (structure and soil) are smaller than under drained analysis.

Undrained analyses exhibit large racking distortions when $F^W < 1$, and slightly smaller distortions when $F^W > 1$. This case is not observed to no-slip conditions, in which racking distortions are larger for undrained analyses than drained analyses (Bobet, 2010).

Cilingir and Madabhushi (2011) researched the depth effects and ground motion effects on seismic response of square structure in dry sand performing centrifuge model tests.

The flexural stiffness of the soil with respect to the tunnel was defined by (Wang,1993):

$$F_{square} = \frac{G}{12}\left(\frac{W^3}{E_1 I}\right)$$

where

G is the shear modulus of the soil

W is the tunnel width

E_1 is the Young's modulus of the lining material

I is the lining moment of inertia (per unit width)

In this study, dynamic centrifuge tests were carried upon a total of 4 models at different burial depth to examine the seismic response of shallow tunnels in sand with dry condition. The aim of centrifuge test is to get in-situ stress and strain relationships by increasing body forces through the high centrifugal acceleration application in small-scale models (Cilingir and Madabhushi, 2011). Properties of input motion and centrifuge models are given in Table 1.

Table 1 Properties of input motion and centrifuge models

Test ID	**Model Depth (m)**	**Lining Thickness (m)**	**Maximum Base Acceleration (%g)**	**Tunnel Depth (m)**	**Depth to Width Ratio (H/W)**	**Flexibility Ratio**
UC04	14	0.15	27.0	5	1.0	14
UC06	18	0.15	24.0	9	1.8	20
UC10	18	0.06	21.8	9	1.8	330
UC11	14	0.06	25.0	5	1.0	247

Piezoelectric accelerometers were utilized to measure accelerations around the tunnel. All of the centrifuge tests were carried out with an acceleration of centrifugal 50 g and an input motion frequency of 50 Hz in model scale (1.0 Hz in prototype).

In this test series, the deformation of the model was obtained from a high-speed camera image with having high resolution. Recorded images were analyzed using Particle Image Velocimetry (PIV) technique (Figure 16.). Using cross-correlation functions, this method divided the image into small patches and determined where those patches were in consecutive images (Cilingir and Madabhushi, 2011).

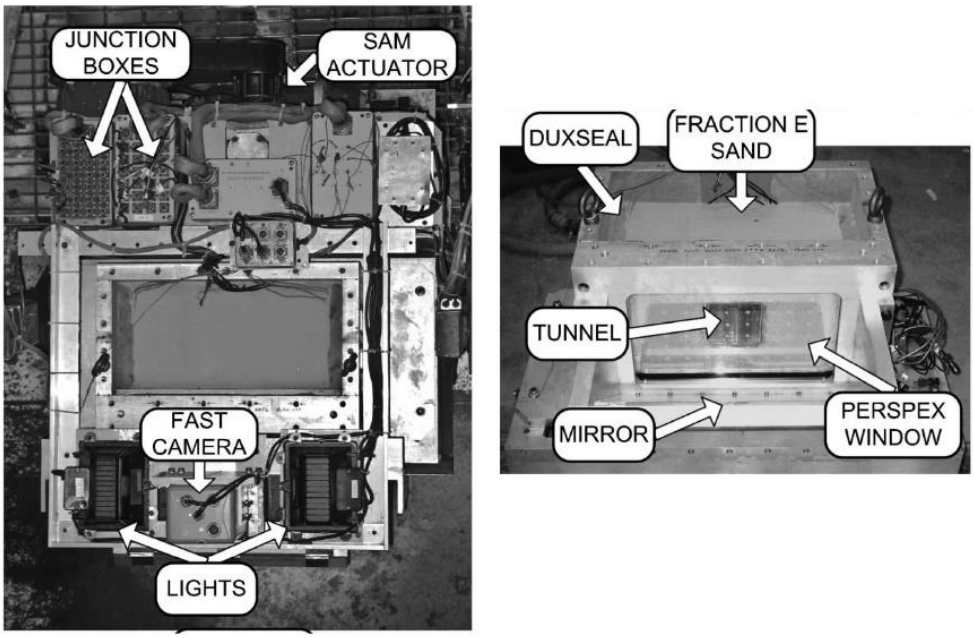

Figure 16 Centrifuge package and model container (Cilingir and Madabhushi, 2011)

An example of the square tunnel model is present in Figure 17.

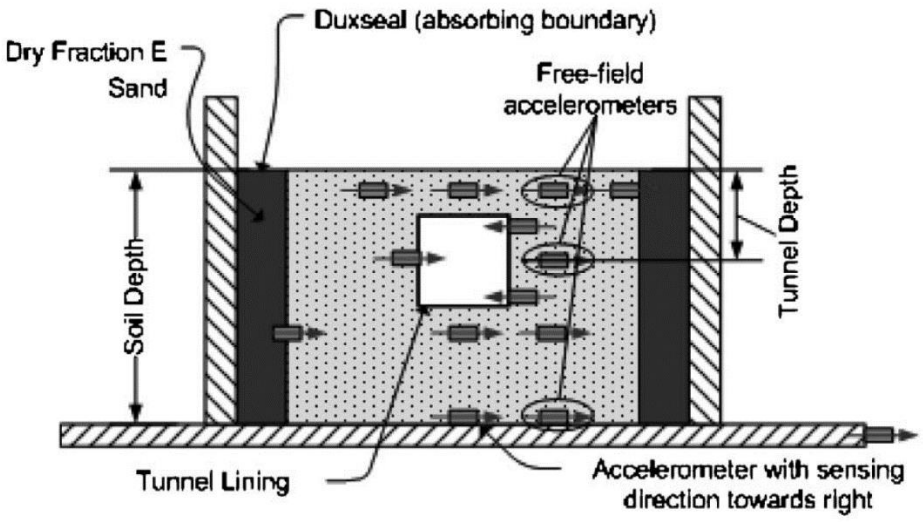

Figure 17 Centrifuge model container in the sand (Cilingir and Madabhushi, 2011)

Figure 18 presents soil deformations and tunnel lining from PIV analyses for shallow and deep depth for relatively flexible tunnel models UC10 and UC11. The crown of the deeper tunnel (UC10) deforms more than the crown of the shallow tunnel model (UC11). Also, deformations of the soil are amplified from bottom to top of the tunnel (Cilingir and Madabhushi, 2011).

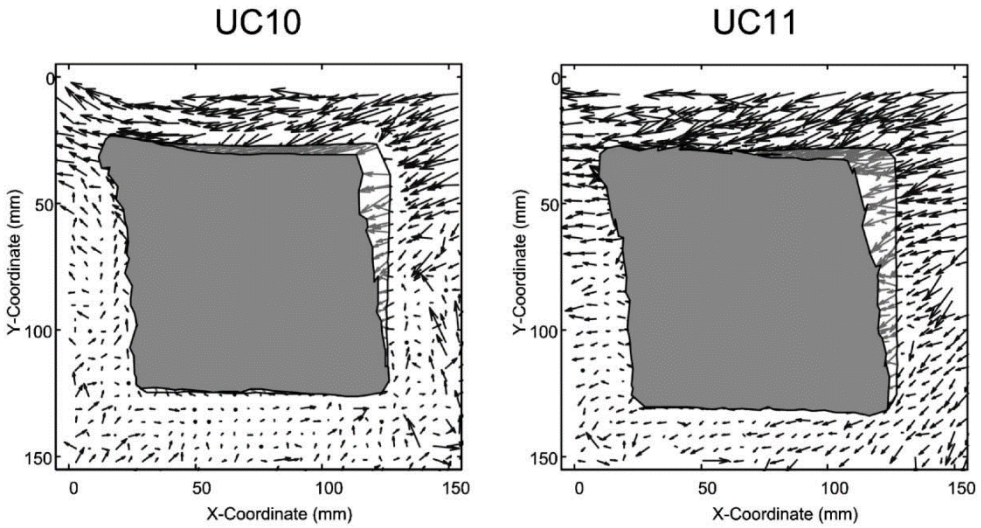

Figure 18 Tunnel and soil deformations measured using the PIV technique during the acceleration phase from zero to maximum (Cilingir and Madabhushi, 2011)

Debiasi et al. (2013) investigated the effect of seismic of shallow-buried rectangular structures. This analysis is using conducted finite element analyses with pseudo – static approach to investigate the structure geometry effects and the overburden depth, the interface friction condition between soil and box structure and aspect ratio on the shallow buried rectangular structures.

In Figure 19, the structure aspect ratio is defined as L/H (vary from 4 to 1/2 in this analysis) and the overburden depth ratio is specified as D_0/L. For aspect ratio of 2 or more, vertical walls are used in a manner that unsupported span length is no greater than height of the rectangular structure.

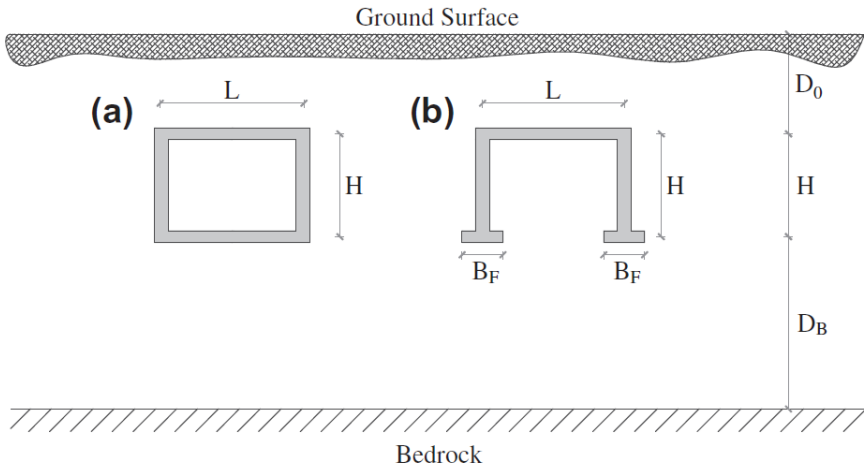

Figure 19 Geometric quantities of rectangular structures

where,

L: rectangular structure width

H: rectangular structure height

D_0: overburden depth

D_B: founded level above the bedrock

For all analyses, bedrock is assumed perfectly rigid and horizontal acceleration history is imposed on the bedrock in dynamic analyses. Distributed horizontal volume forces are used in the pseudo-static analysis (Figure 20).

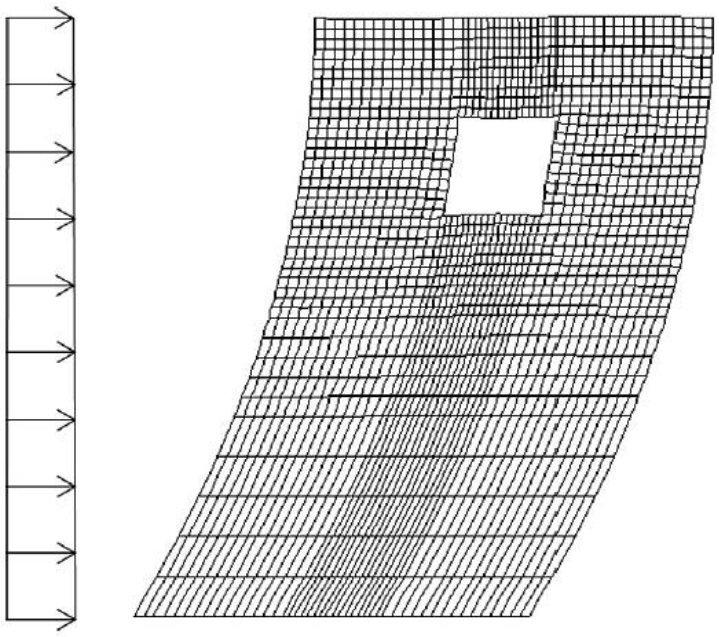

Figure 20 Distributed horizontal volume force illustration

Debiasi et al. (2013) chose to present the results of the study the same manner as in Wang (1993), by plotting the ratio of racking coefficient to flexibility.

Relative racking stiffness (racking coefficient) R is reported ratio of racking distortion of embedded box structure Δ_s to lateral shear deformation in free field condition Δ_{ff} .

$$R = \frac{\Delta_s}{\Delta_{ff}}$$

If the structure moves only in horizontal directions (no rocking), Δ_s is defined as the horizontal difference between the top elevation and bottom elevation of the structure (Figure 21).

For the involving movement of rocking case in structure behavior;

$\Delta_S = \Delta_{TOT} - \Delta_R$ where $\Delta_R = \gamma_R H$

The ratios are defined;

$$R_R = \frac{\Delta_R}{\Delta_{ff}} \text{ and } R_{TOT} = \frac{\Delta_{TOT}}{\Delta_{ff}}$$

The relationship between these equations is;

$$R = R_{TOT} - R_R$$

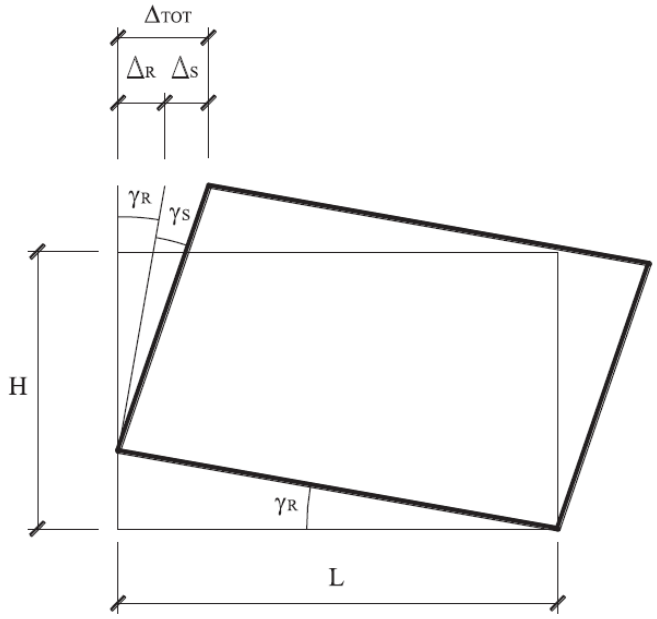

Figure 21 Relationship between shear distortion (γ_S), rocking distortion (γ_R) and total displacement

Generally, rocking (rigid rotation) is negligible in literature. Therefore R_{TOT} and R_R coincide.

According to Debiasi et al. (2013), the ratio of burial depth D_o/L does not affect the seismic behavior of structural beyond depth of critical D_{co} where there is no slip at the soil-structure interface. The results in Figure 22 show that difference in terms of R_{TOT} progressively changes from the case of deeply burial depth ($D_o/L = 1$) to case of null burial depth ($D_o/L = 0$). In addition to that the ratio of critical depth increases with an aspect ratio (L/H) and also decrease with an increase in flexibility ratio as shown Figure 23. This means stiff structures at shallow depths are more susceptible to nonlinearities than flexible structures.

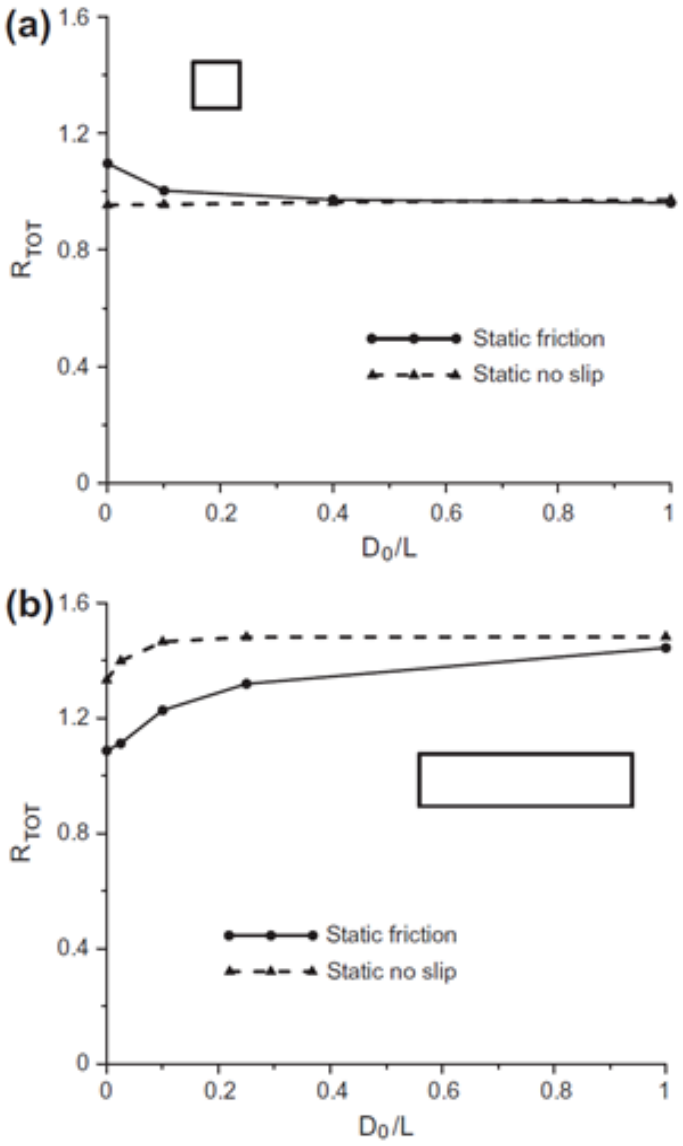

Figure 22 Racking coefficient R_{TOT} to flexibility ratio of shallow-buried structures (depth ratio between the range $D_o/L = 0$ and $D_o/L = 1$), where (a) F = 1 and L/H = 1 and (b) F = 3and L/H = 4

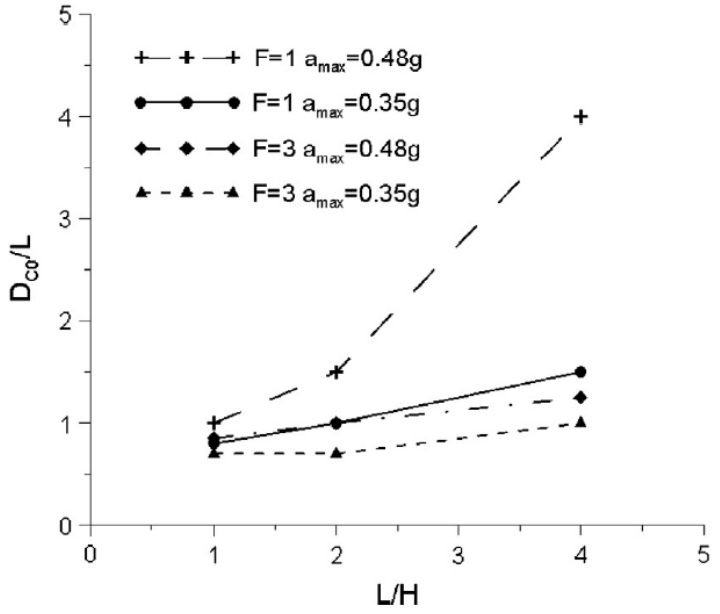

Figure 23 Critical depth ratio (D_{co}/L) to aspect ratio (L/H) with different PGA and flexibility ratio

The results are shown Figure 24 for shallow-buried rectangular structures with different aspect ratios. It is concluded that aspect ratio behaves almost the same for deep buried rectangular structures.

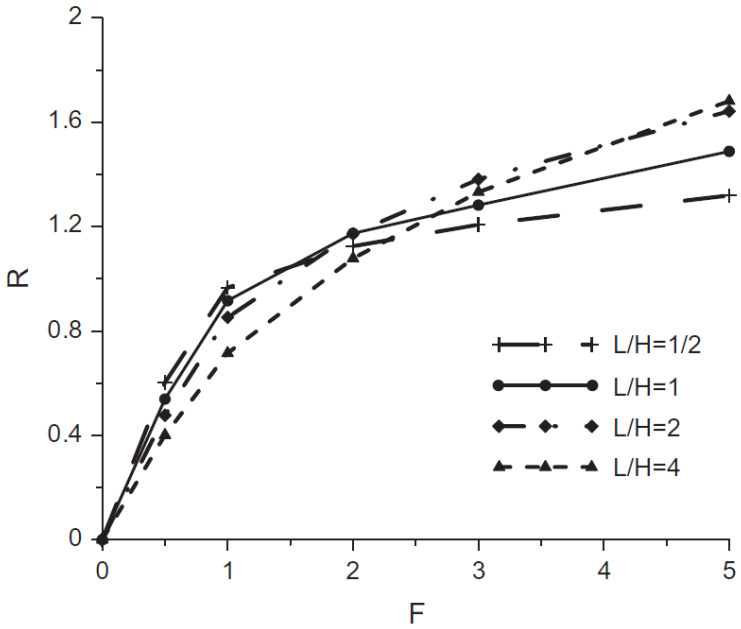

Figure 24 Racking coefficient to flexibility ratio for the case of shallow buried rectangular structure ($D_o/L = 0$)

Patil et al., (2018) performed a plain-strain numerical analysis in PLAXIS 2D AE.02 to investigate the effects of the interface condition between soil and tunnel and the tunnel embedment ratio (C/D).

Figure 25 shows the schematic illustration of deformed mesh (a) and a two-dimensional numerical model (b).

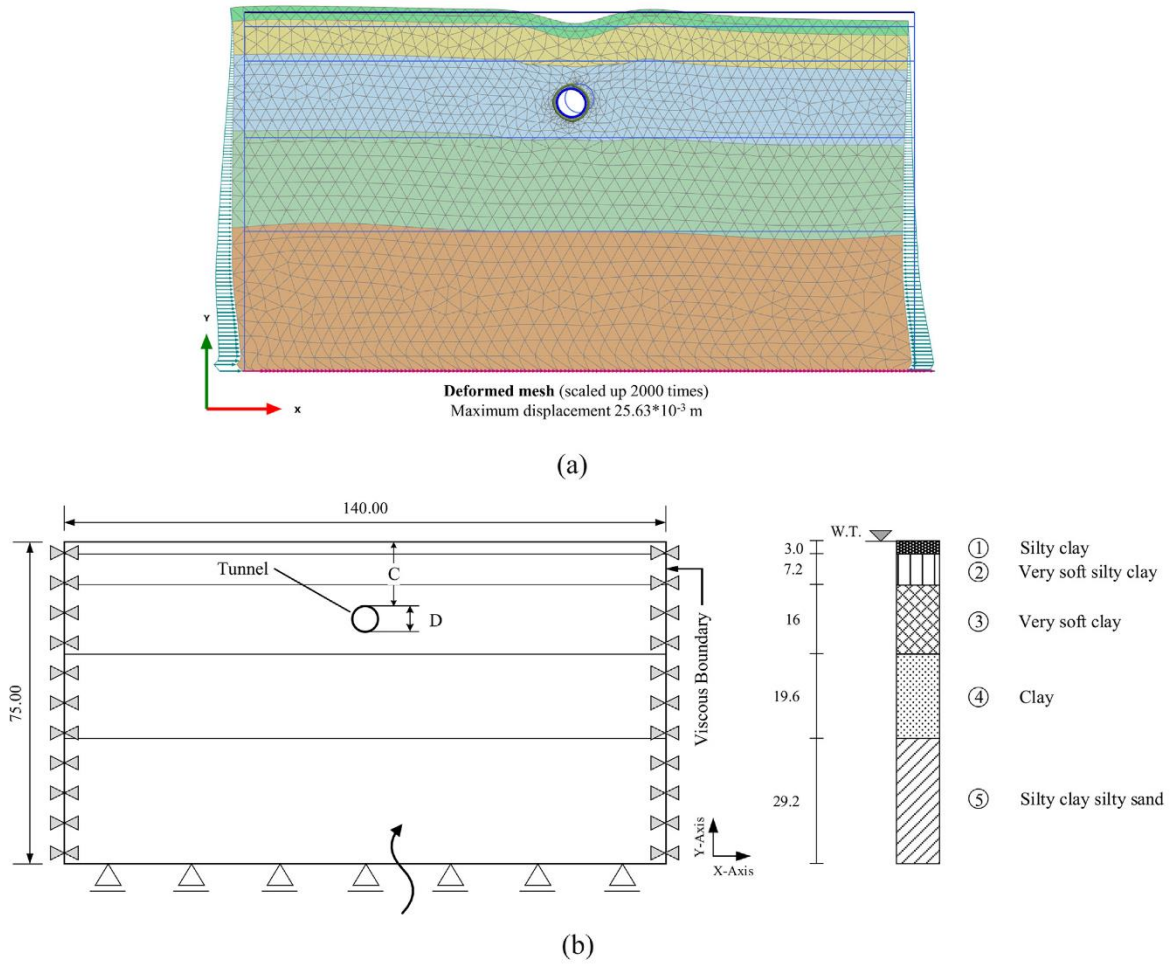

Figure 25 a) Example of deformed mesh (b) Schematic view of the model (unit: m)

The embedment depth effect on the seismic behavior of structures with square cross section was investigated by changing the embedment ratio of structure parameter between 0.5 and 3.0. The results revealed that for full-slip interface conditions, deeper depths tend to distort the tunnel's lining more than shallow depths (Figure 26). Additionally, the tunnel lining distortion will not be significantly affected by an increase in the rigid tunnel's embedment depth (Patil et al., 2018). The graph represents that the structure response substantially counts on the flexibility ratio and the embedment depth (Patil et al., 2018).

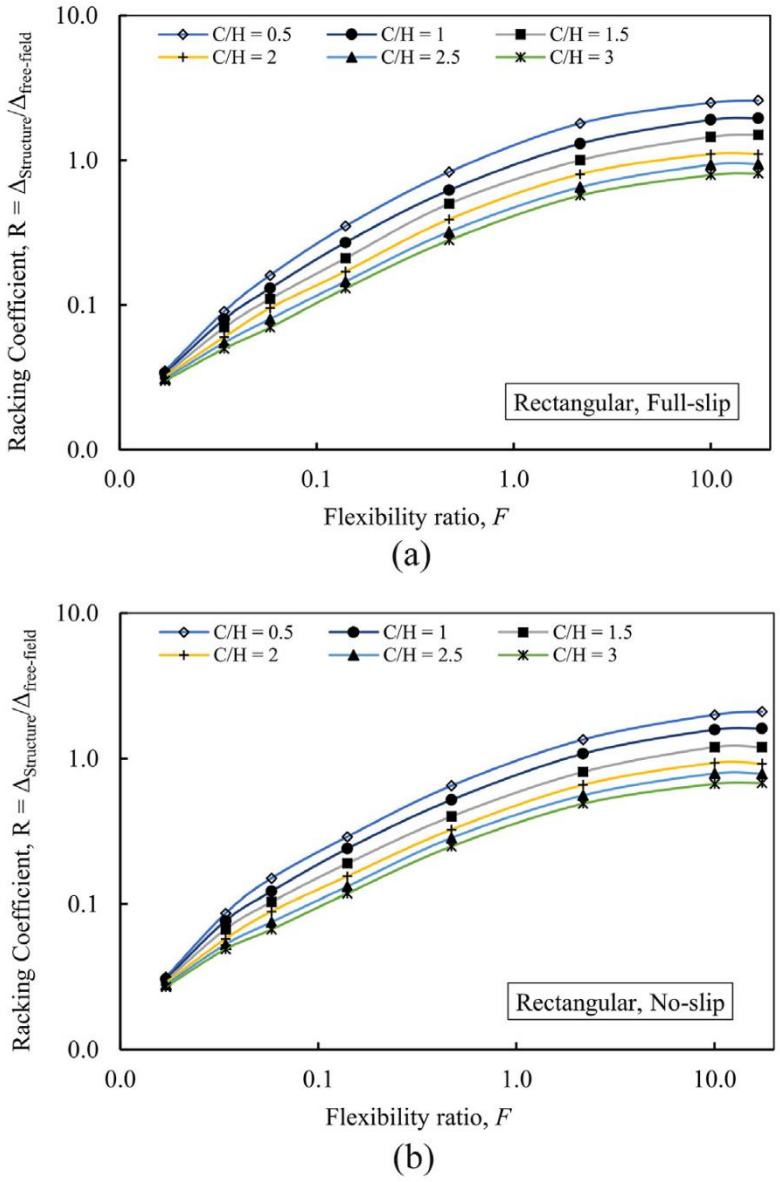

Figure 26 Rectangular tunnel response (PGA=0.4 g, H=5.3 m) for different embedment depth: (a) μ=0 for full-slip case between interface of the soil and the tunnel and (b) μ=1 for no-slip case between interface of the soil and the tunnel and

Tsinidis (2017) conducted numerical parametric analysis, aiming to investigate various parameters such as: tunnel-soil interface condition, the burial depth of the tunnel, the soil-tunnel relative stiffness, dimensions of the tunnel, and soil response and properties in embedded rectangular tunnels.

The sizes of structure and numerical model used in the analysis are shown in Figure 27.

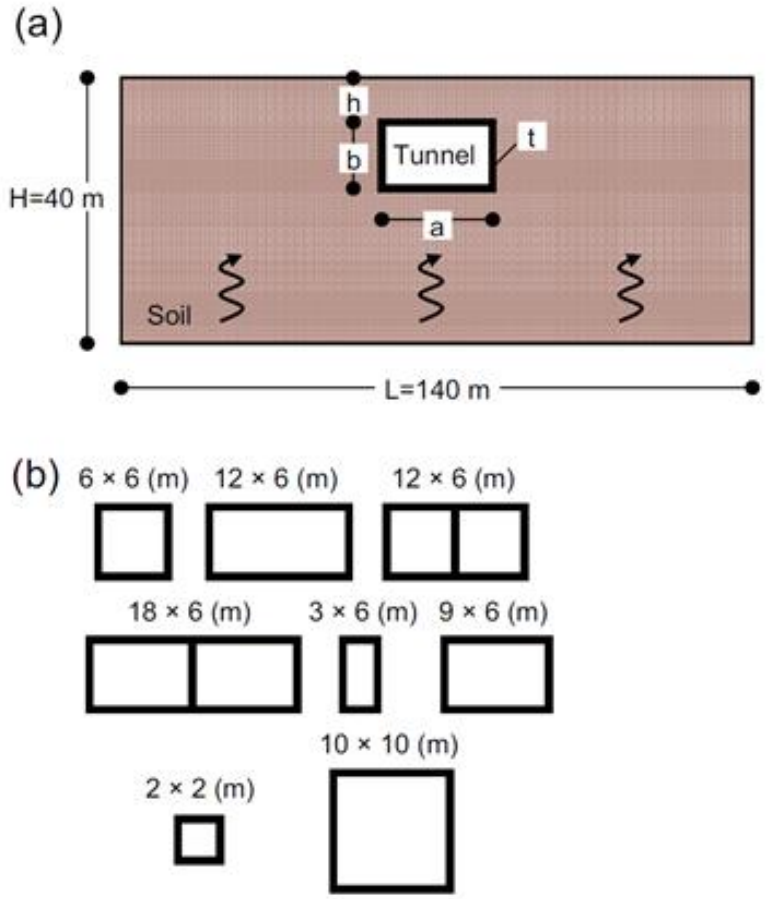

Figure 27 Illustration of (a) numerical model and (b) dimensions of structures

where;

h: burial depth of tunnel (ranged between 3 m and 12 m)

b: height of concrete rectangular tunnel (2 m -10 m)

a: width of concrete rectangular tunnel (2 m -18 m)

t: lining thickness

Aspect ratio λ is defined a/b (varied between 0.5 and 3.0) and overburden depth ratio is defined as h/a. When the aspect ratio is greater than 2, the internal column was considered to be more rational at the central of the span in tunnels.

Input motions and soil properties characteristics are shown in Table 2.

Table 2 Input motions and soil properties characteristics

	V_s (m/s)	EC8 soil class	Cohesion, c (kPa)	Poisson ratio, ν	Friction angle, ϕ (°)
B1 (sand)	400	B	10	0.3	44
B2 (clay)	400	B	50	0.3	27
C1 (sand)	250	C	1	0.3	36
C2 (clay)	250	C	10	0.3	25
Elastic Rock	1000	A	-	0.3	-

	Magnitude M_w	PGA (g)
EQ1	6.04	0.12
EQ2	6.4	0.34
EQ3	6.9	0.61

The analyses are conducted in two phases:

- Firstly, gravity loads were used in the static phase
- Secondly, the dynamic loads were applied in the implicit dynamic phase.

In addition to this, seismic loadings are introduced at the base boundary. According to shaking motion direction, the tunnels exhibit a rotation. For shaking motion toward left flexible (F>1) tunnels are subjected to counterclockwise whereas rigid tunnels (F <1) are subjected to clockwise (Figure 28).

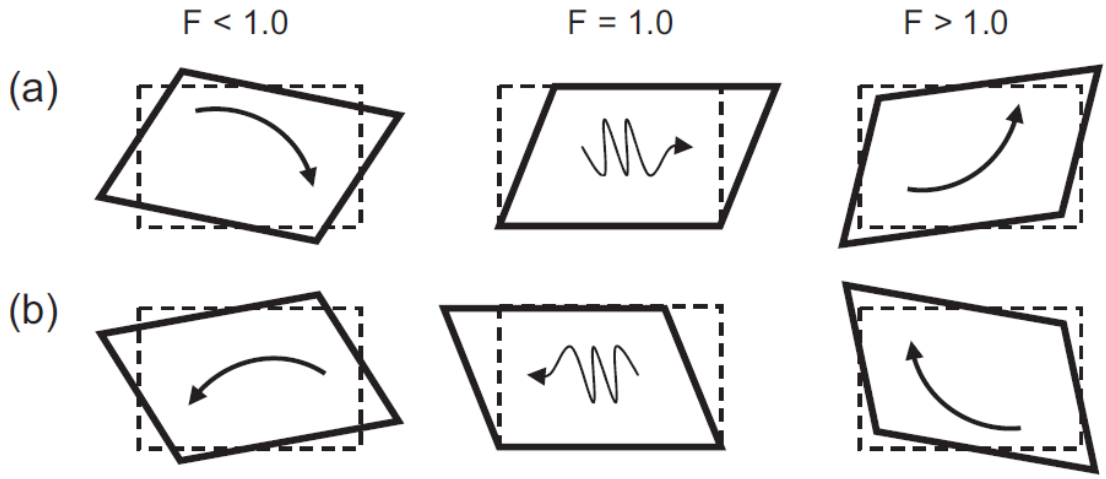

Figure 28 Illustration of deformed shapes of tunnels (a) motion towards the right (b) motion towards left (for full bonding condition)

For evaluation of flexibility ratio (F), the simplified frame analysis method of Wang (1993) is used. The analyses were conducted using ABAQUS in plane strain conditions, both no slip condition (full bonding) and full-slip interface conditions between interface of the soil and tunnel. An interface condition called full-slip occurs when the tunnel lining and soil are separated.

In this study to develop a numerical R-F relationship, R was calculated using horizontal deformations calculated directly from dynamic analysis, taking into account the maximum racking distortion of the tunnel section. As a result, the horizontal displacement (u_2 in Figure 29) effect of the tunnel section's rotation as well as the calculated racking ratio (R) are accounted for in the calculation.

$$R = \frac{\Delta_{st}}{\Delta_{ff}} = \frac{(u_C - u_D)}{(u_A - u_B)}$$

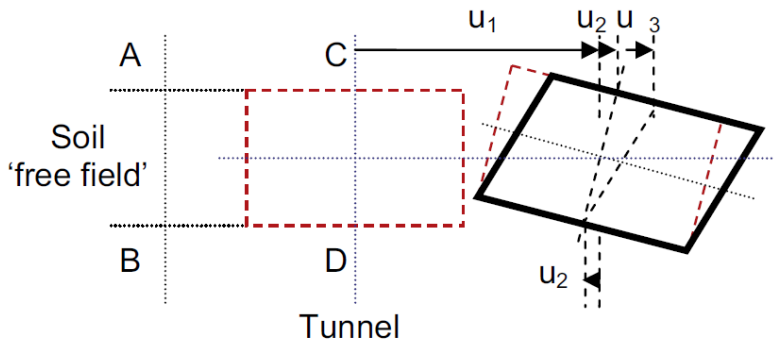

Figure 29 Simulation of the effect of rotation on the horizontal displacement of the tunnel section and calculation of the racking coefficient

where

u_1 = movement of the tunnel section′s rigid body

u_2 = displacement because of the rotation in section of the tunnel

u_3 = displacement because of the racking distortion

The R-F relationship is calculated for the condition of full bonding (no slip) between the soil and tunnel interface in the full bonding case. The effects of input motions and soil classes on the computed relations are shown in Figure 30. To determine how the other parameters affect the tunnels' racking response, a variety of earthquake motions were analyzed with the constant shear stiffness of soil.

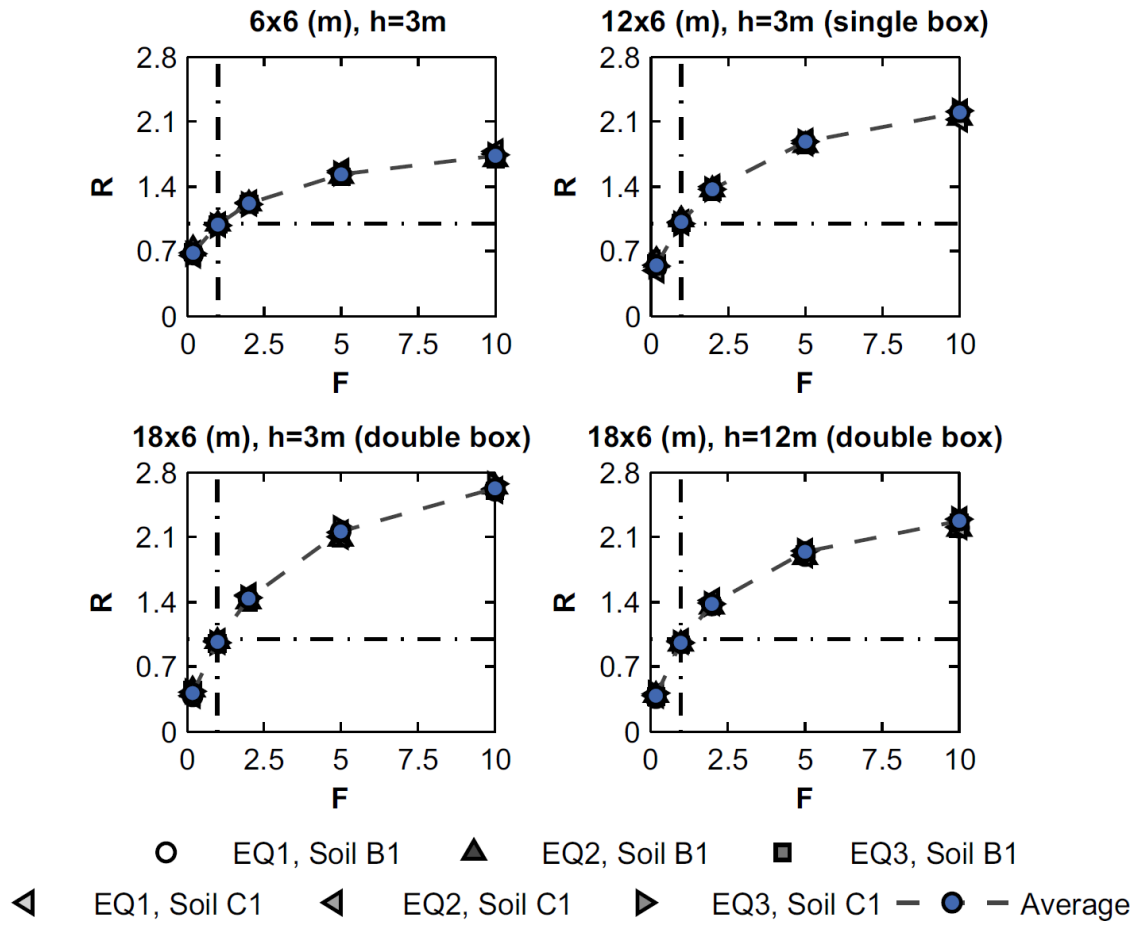

Figure 30 Relations of R-F for different earthquake, tunnel and soil parameters

In a more recent study, Tsinidis (2017) concluded that the racking coefficient increases when tunnel embedment decreases and aspect ratio (λ) increases.

In the analyzes to investigate the effect of the internal column, it was observed that there are many similarities between single and double box tunnels as shown in Figure 31. A double section tunnel had a thinner lining than a single barrel tunnel to achieve the desired flexibility ratio

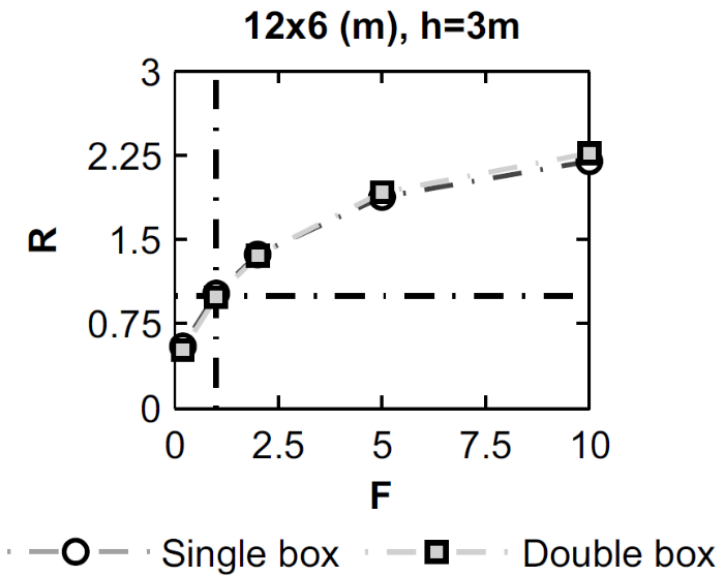

Figure 31 R-F relations for effect of the central column in elastic soil response

The results of analysis conducted to understand the effects of the aspect ratio is illustrated in Figure 32. According to burial depth, both the aspect ratio effects are illustrated and R-F relations is compared with existing empirical and analytical solutions.

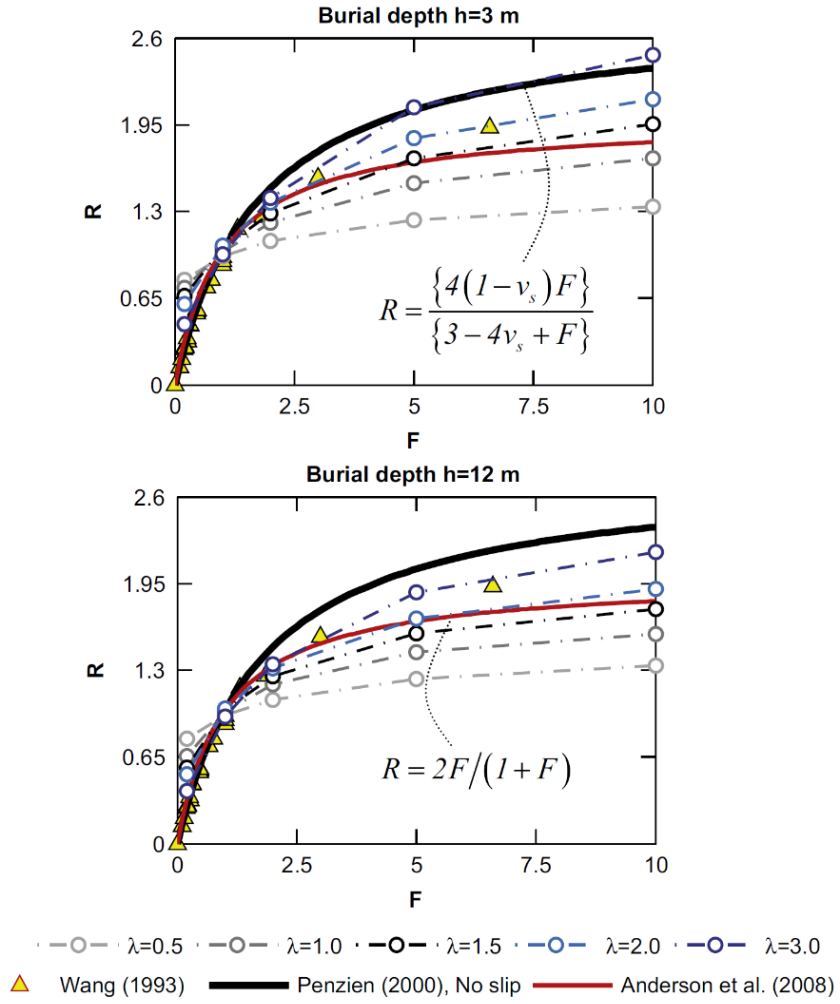

Figure 32 Comparison between numerical R-F relations computed and literature

Tsinidis and Pitilakis (2018) conducted dynamic analyses with related to racking coefficient flexibility ratio, structure aspect ratios $\lambda = a/b$, burial depths and Poisson's ratio for developing more accurate R-F relations. These analyses are taken into consideration the consolidated racking rocking deformation model for embedded structures with having rectangular cross section under transverse ground shaking.

Tsinidis and Pitilakis (2018) stated that can be obtain more realistic results for seismic racking distortion of rigid tunnels considering the horizontal displacement the rocking movement of the tunnel (Figure 33a). Also, horizontal displacement because of the rocking rotation is considered for flexible tunnels (Figure 33b) (Tsinidis and Pitilakis, 2018).

The new improved racking coefficient was defined by:

$$R = \frac{\delta_{str,a}}{\delta_{ff}}$$

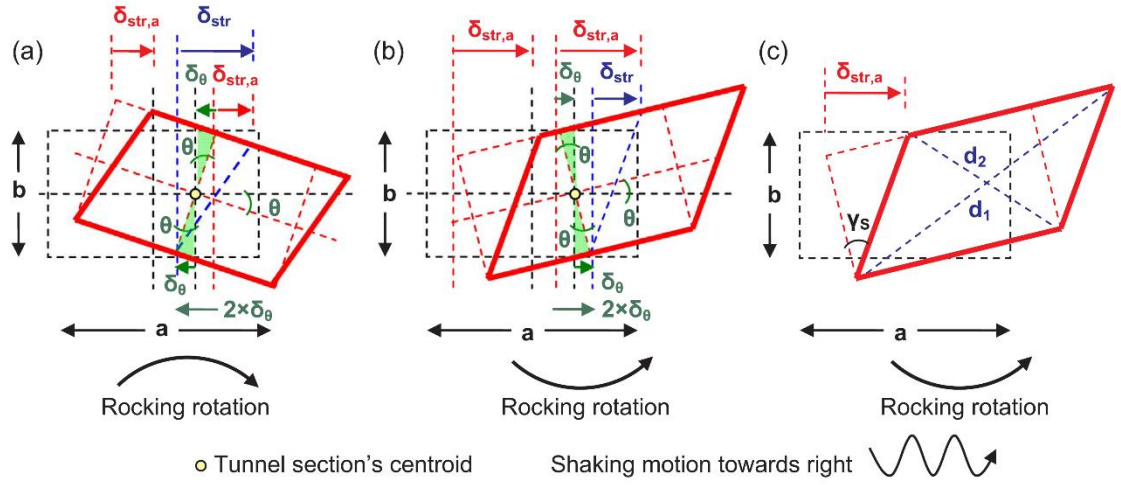

Figure 33 Error in the assessment of the actual seismic racking distortion $\delta_{str,a}$, because of the rocking response (Tsinidis and Pitilakis, 2018)

The numerically predicted structural distortions are used to determine the racking distortions of rectangular tunnels:

$$\delta_{str,a} \approx \begin{cases} \delta_{str} + 2 \times \delta_\theta = \delta_{str} + 2 \times \tan\theta \times b/2 \approx \delta_{str} + \theta \times b \ \text{ for } F > 1.0 \\ \delta_{str} - 2 \times \delta_\theta = \delta_{str} - 2 \times \tan\theta \times b/2 \approx \delta_{str} - \theta \times b \ \text{ for } F < 1.0 \end{cases}$$

where

δ_{str} is the tunnel racking distortion by numerically estimated

δ_θ is half of the horizontal displacement in the tunnel section is caused by rocking rotation

θ is the tunnel section rocking rotation

b is the tunnel section height

Also, racking distortions of rectangular tunnels are described according to the geometrical properties of the deformed tunnel cross section

$$\delta_{str,a} = \tan\gamma_s \times b \simeq \frac{(d_1^2 - d_2^2)}{4 \times a \times b} \times b = \frac{(d_1^2 - d_2^2)}{4 \times a}$$

where

γ_s is the average of racking angle in the tunnel

d_1 and d_2 are lengths of diagonals in the deformed tunnel (Figure 33c)

In rectangular tunnels, rocking behavior decreases with depth, so R_n and R racking coefficients decrease as well (Tsinidis and Pitilakis, 2018). These graphs are shown in Figure 34.

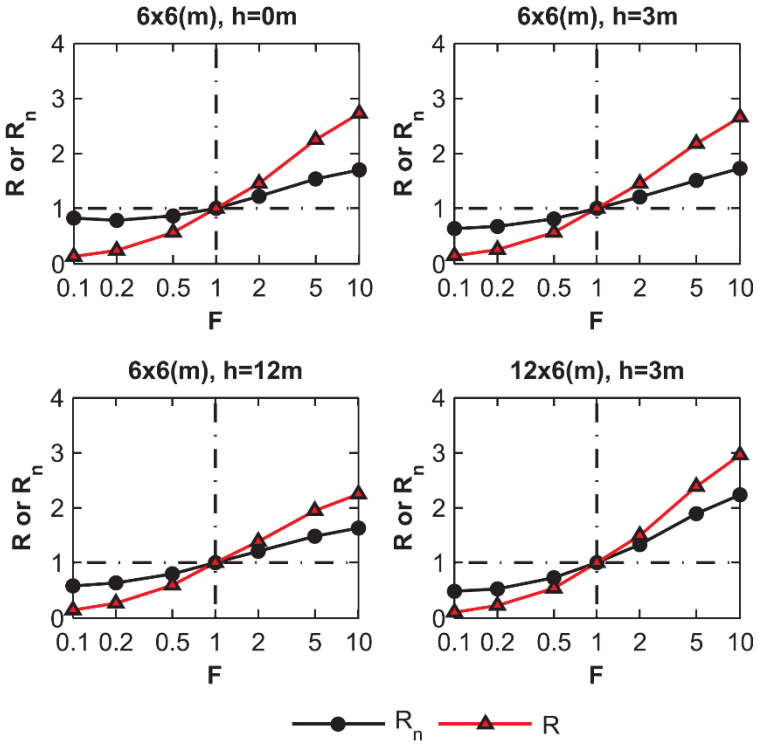

Figure 34 Relationships between R_n-F and R-F estimated based on different tunnel sections for different depths (Tsinidis and Pitilakis, 2018)

Recently, Gordo-Monsó et al. (2019) proposed a new methodology from obtained by a closed-form solution in the literature for the racking coefficient for buried structures with having rectangular geometry. In addition to this, these solutions from given the new methodology are compared with the finite element analyses and it is shown that these comparisons are consistent. A new method is proposed for the rocking rotation and the racking deformation of the rectangular structure at various distances.

Exterior perimeter of the surrounding soil is exposed to a pure shear stress (Gordo-Monsó et al., 2019). Therefore, to calculate the strain field in the surrounding soil and the structure was aimed.

In this study, rectangular structures are modelled with having width (defines as b) and depth (defines as d) as can be seen in Figure 35. Also, in this situation aspect ratio is defines as λ=b/d and a surrounding soil have arbitrary size (of depth H and width L) with the underground structure.

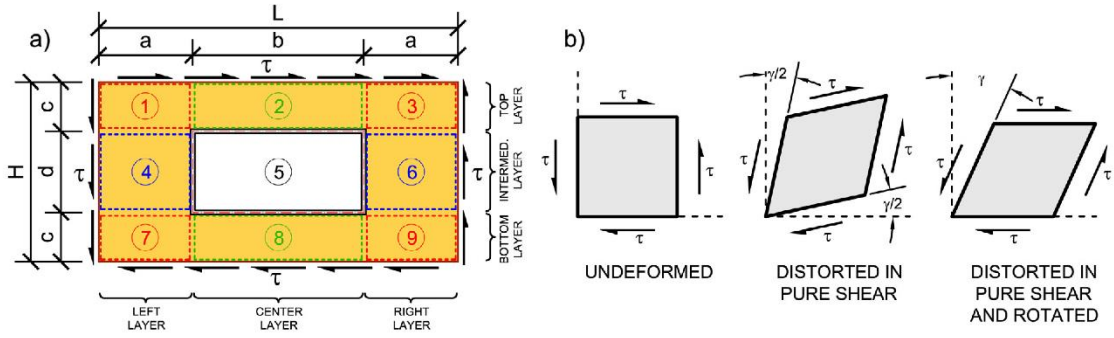

Figure 35 (a) Block scheme of the soil-structure interaction system. (b) Illustration of pure shear distortion for a splitted block.

In determining the strain field, firstly the soil-structure system was separated in rectangular blocks (see Figure 36). In a homogeneous, isotropic and elastic medium, the elasticity equation (γ=τ/G) identifies each rectangular block's shear stiffness during deformation in a pure shear only (Gordo-Monsó et al., 2019). The corners dislocate equally in both directions vertically and horizontally.

Gordo-Monsó et al. (2019) assumed that within the separated blocks shear strains and stresses are constant throughout all depth or width, especially in the boundaries.

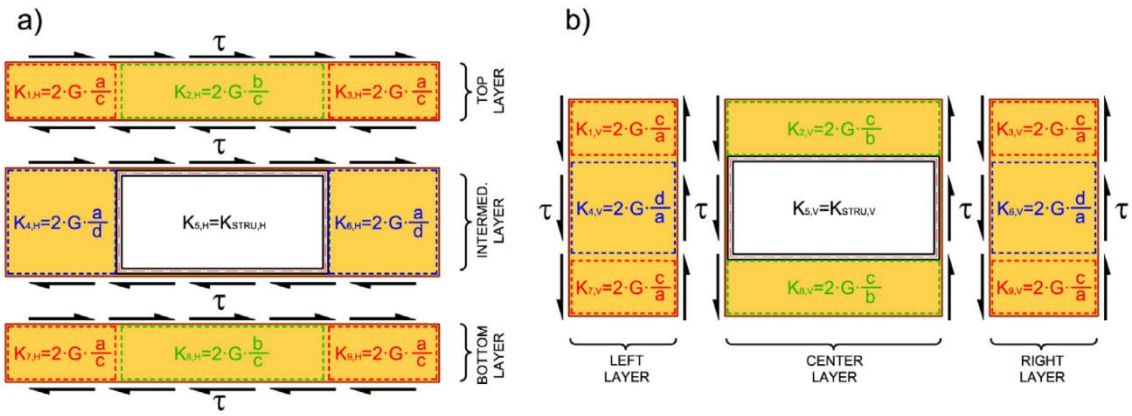

Figure 36 (a) Separated block and layers with horizontal shear stiffness, (b) Separated block and layers with vertical shear stiffness (Gordo-Monsó et al., 2019)

The shear stiffness of separated block K_H (for a horizontal force) is defined by

$$K_{1,H} = K_{3,H} = K_{7,H} = K_{9,H} = 2\,G\,\frac{a}{c}$$

$$K_{2,H} = K_{8,H} = 2\,G\,\frac{b}{c}$$

$$K_{4,H} = K_{6,H} = 2\,G\,\frac{a}{d}$$

$$K_{5,H} = K_{STRU,H} = 2\,\frac{G\frac{b}{d}}{F}$$

F is flexibility ratio proposed by Wang (1993) and defined by

$$F = \frac{K_{SOIL}}{K_{STRU}} = \frac{G \cdot \frac{b}{d}}{\frac{1}{\frac{d^2 \cdot b}{24 \cdot E \cdot I_b} + \frac{d^3}{24 \cdot E \cdot I_w}}}$$

For single barrel rectangular structure:

b = width

d=depth

I_w= slab bending inertia

I_b= wall bending inertia

The stiffness of each block K_v (for a vertical force) is defined by

$$K_{1,V} = K_{3,V} = K_{7,V} = K_{9,V} = 2\,G\,\frac{c}{a}$$

$$K_{2,V} = K_{8,V} = 2\,G\,\frac{c}{b}$$

$$K_{4,V} = K_{6,V} = 2\,G\,\frac{d}{a}$$

$$K_{5,V} = K_{STRU,V} = 2\,\frac{G\frac{d}{b}}{F}$$

The shear stiffness of horizontal layer (K_{BOT} for the bottom, K_{INT} for the intermediate and K_{TOP} for the top) is defined as a sum of stiffness in parallel direction because of the compatibility of shear strain between blocks that are horizontally adjacent (Gordo-Monsó et al., 2019).

$$K_{TOP,H} = K_{BOT,H} = K_{1,H} + K_{2,H} + K_{3,H} = K_{7,H} + K_{8,H} + K_{9,H} = 2\,G\,\frac{a+b+a}{c}$$

$$= 2\,G\,\frac{L}{c}$$

$$K_{INT,H} = K_{4,H} + K_{5,H} + K_{6,H} = 2\,G\,\frac{2a}{d} + K_{STRU,H}$$

Similarly, the shear stiffness of vertical layer (K_{RIGHT} for the right, K_{CENT} for the center and K_{LEFT} for the left) is calculated as follows;

$$K_{LEFT,V} = K_{RIGHT,V} = K_{7,V} + K_{4,V} + K_{1,V} = K_{9,V} + K_{5,V} + K_{3,V} = 2\,G\,\frac{c+d+c}{a}$$

$$= 2\,G\,\frac{H}{a}$$

$$K_{CENT,V} = K_{8,V} + K_{5,V} + K_{2,H} = 2\,G\,\frac{2c}{b} + K_{STRU,V}$$

The serial stiffness of each vertical layer was taken into consideration while calculating the average shear stiffness vertical ($K_{AVG,V}$) and horizontal ($K_{AVG,H}$) direction of the structure and soil.

Considering that it is subjected to a pure shear stress condition at the value τ of the external environment, racking coefficient is computed for the average soil shear distortion and the embedded structure shear distortion.

This racking coefficient is the ratio of the sum of strains and $\tilde{R}$ is defined by:

$$\tilde{R} = \frac{\gamma_{INT,H} + \gamma_{CENT,V}}{\gamma_{AVG,H} + \gamma_{AVG,V}} = \frac{\frac{\tau \cdot L/K_{INT,H}}{d} + \frac{\tau \cdot H/K_{CENT,V}}{b}}{\frac{\tau \cdot L/K_{AVG,H}}{H} + \frac{\tau \cdot H/K_{AVG,V}}{L}} = \frac{\frac{L}{d \cdot K_{INT,H}} + \frac{H}{b \cdot K_{CENT,V}}}{\frac{L}{H \cdot K_{AVG,H}} + \frac{H}{L \cdot K_{AVG,V}}}$$

and

For inner structure, shear distortion is $\gamma_{INN} = \gamma_{INT,H} + \gamma_{CENT,V}$

For the outer perimeter, shear distortion is $\gamma_{AVG} = \gamma_{AVG,H} + \gamma_{AVG,V}$

$\widetilde{R}$ is signified conditional and approximate to the block behavior of racking coefficient.

In this situation, racking coefficient is computed for between the structure and a perimeter of soil close enough to the structure. Also, Gordo-Monsó et al. (2019) supposed that when considering successive control perimeters of soil (perimeters i-1 and 1), individual racking coefficient. The shear distortion of the soil's successive perimeters could be used to estimate $\widetilde{R}_1$.

Also, Gordo-Monsó et al. (2019) supposed that when considering successive control perimeters of soil, individual racking coefficient could be estimated regarding the shear distortion for successive perimeters of soil. For geometrical parameters H_i, L_i, d_i, c_i, b_i, and a_i in any control perimeter (i) of soil (Figure 37), racking coefficient is described by

$$\widetilde{R}_1 = \frac{\gamma_{AVG,H,i-1} + \gamma_{AVG,V,i-1}}{\gamma_{AVG,H,i} + \gamma_{AVG,V,i}} = \frac{\frac{L_i}{d_i \cdot K_{INT,H,i-1}} + \frac{H_i}{b_i \cdot K_{CENT,V,i-1}}}{\frac{L_i}{H_i \cdot K_{AVG,H,i}} + \frac{H_i}{L_i \cdot K_{AVG,V,i}}}$$

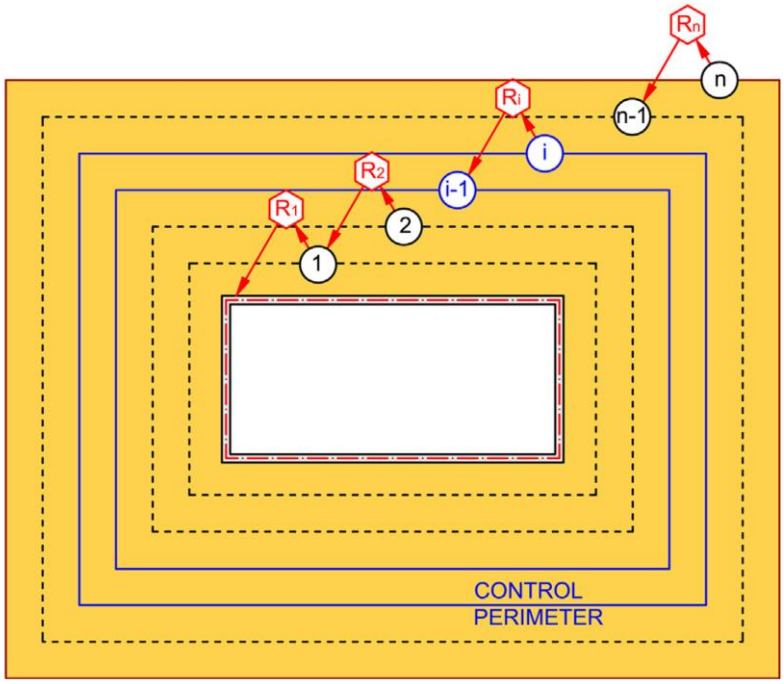

Figure 37 Series of control parameter between 1 and n. (Gordo-Monsó et al., 2019)

Total racking coefficient is composed of the structure shear distortion (γ_{STRU}) and free field distortion (γ_{FF}). According to Gordo-Monsó et al. (2019), when surrounding soil of the structure is sufficiently divided into fine discretization of control perimeters, racking coefficient of each soil portion is calculated as in the multiplicative:

$$R = \frac{\gamma_{STRU}}{\gamma_{FF}} \cong \prod_{i=1}^{i=n} \frac{\gamma_{i-1}}{\gamma_i} = \prod_{i=1}^{i=n} \widetilde{R_i}$$

To confirm the proposed closed-form solution, finite element analysis was conducted in OpenSEES (McKenna et al., 2010) for structure having different aspect ratios ranging between 1 and 3.

The soil boundaries were selected 50 m away vertically - horizontally from the rectangular structure for n =1000 closed form solutions and FEM analyses.

Figure 38 shows that comparison between FEM analyses and proposed multiplicative solution for different Poisson's ratio of the soil and aspect ratio of the structure.

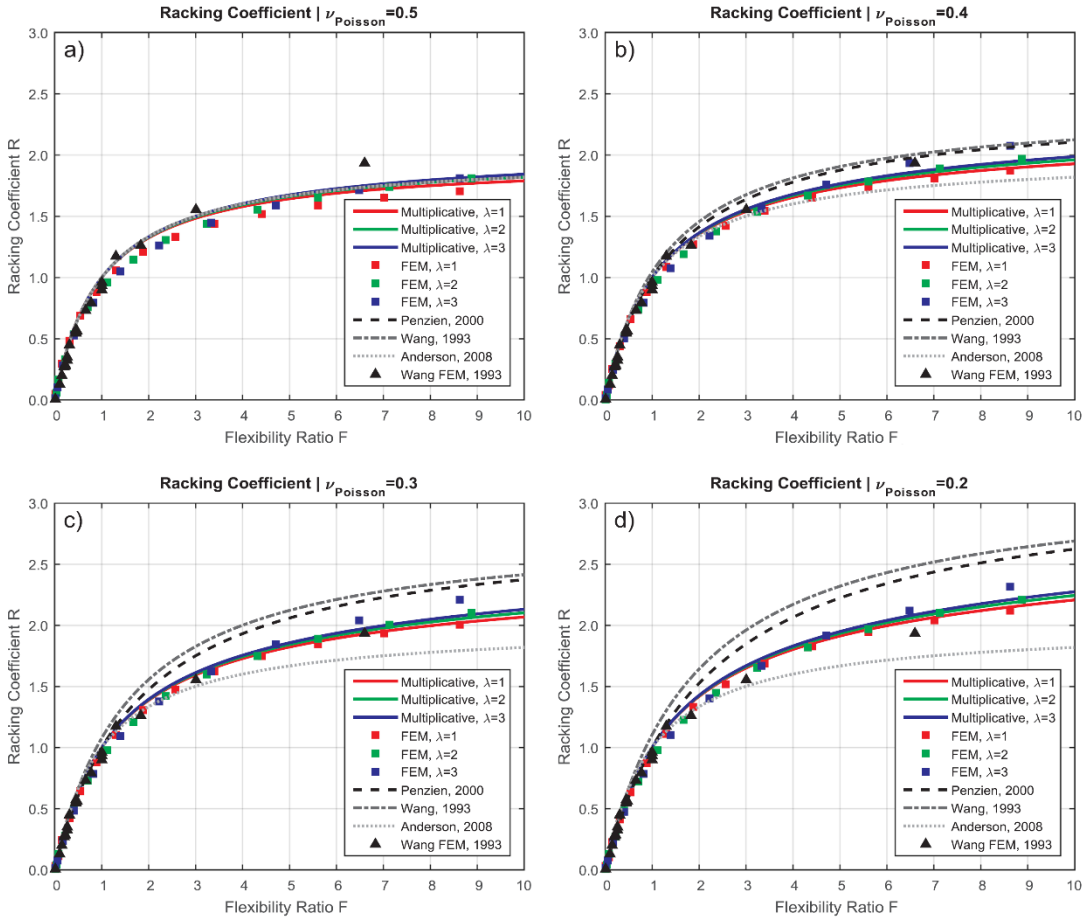

Figure 38 Comparison between closed-form solutions proposed by Anderson (2008), Penzien (2000), Wang (1993), and provided by Gordo-Monsó et al. (2019) and finite element results provided by Wang (1993) and provided by Gordo-Monsó et al. (2019) for different Poisson ratio values

It can be seen in Figure 38 that proposed multiplicative solution closely fit with the finite element analyses for all the studied cases as well as for the analyses in which the Poisson's ratio is equal to 0.5 (Gordo-Monsó et al., 2019).

After mentioned in the previous study, Gordo-Mons´o et. al. (2021) considered that the simplified analysis methodology currently used for rectangular underground structures imposed to seismic excitation give inaccurate results from the point of internal forces according to as compared with experimental measures and numerical analyses, particularly, for structures that are more flexible with regard to surrounding ground such as large underground cavity. In this study, an improved simple method was presented for estimating the internal forces imposed by earthquake for rectangular underground structures that are deeply or shallowly buried.

Gordo-Mons´o et. al. (2021) investigated the burial depth effect on the racking coefficient and the effect of surface proximity on structure deformation.

Analyzes were conducted from the soil surface to the deeply buried (up to 20 m) where burial depth Z, Poisson's ratio of soil ν and aspect ratio of the structure (Figure 39a). In addition to constant horizontal acceleration was imposed to soil profile, the lateral boundaries were also subjected to triangular shear stress and the bottom boundary was subjected to horizontal shear stress to balance the loading condition (Figure 39a and Figure 39b). As Gordo-Mons´o et. al. (2021) noted, in shallow buried structures, soil's surface does not correspond to a state of pure shear stress, because it is shear-free boundary (Figure 39c and Figure 39d).

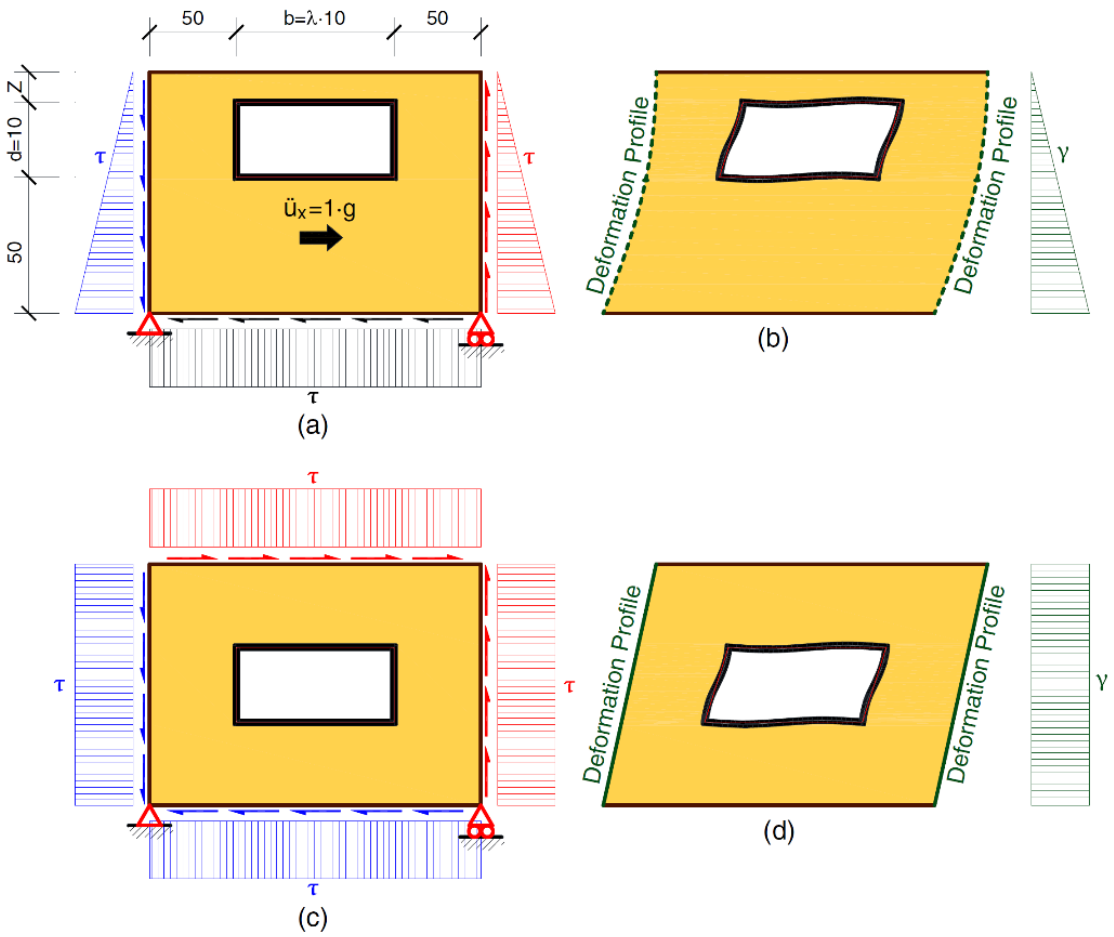

Figure 39 (a) Loading situation in shallowly buried; (b) deformation pattern in shallowly buried; (c) loading condition in deeply buried; and (d) deformation condition in deeply buried (Gordo-Mons´o et. al., 2021)

In a deeply buried condition, the racking coefficient ratio R_Z is described with respect to the racking coefficient R_{Deep}, but this dependence is small (see Figure 39b).

Gordo-Mons´o et. al. (2021) proposed correction coefficient for considering decrease or increase for shallow buried structures with respect to deep buried structures, Z=d is the relationship between the burial depth and the structure's depth. This correction coefficient depends on numerical parameters such as α and β and defined by:

$$\frac{R_Z}{R_{Deep}} = \begin{cases} \alpha\,\mathrm{Ln}(F) + \beta & \text{if } \frac{Z}{d} < 2 \\ 1 & \text{if } \frac{Z}{d} \geq 2 \end{cases}$$

where

$$\alpha = -0.04\left(\frac{Z}{d}\right) + 0.08$$

$$\beta = 0.035\left(\frac{Z}{d}\right) + 0.93$$

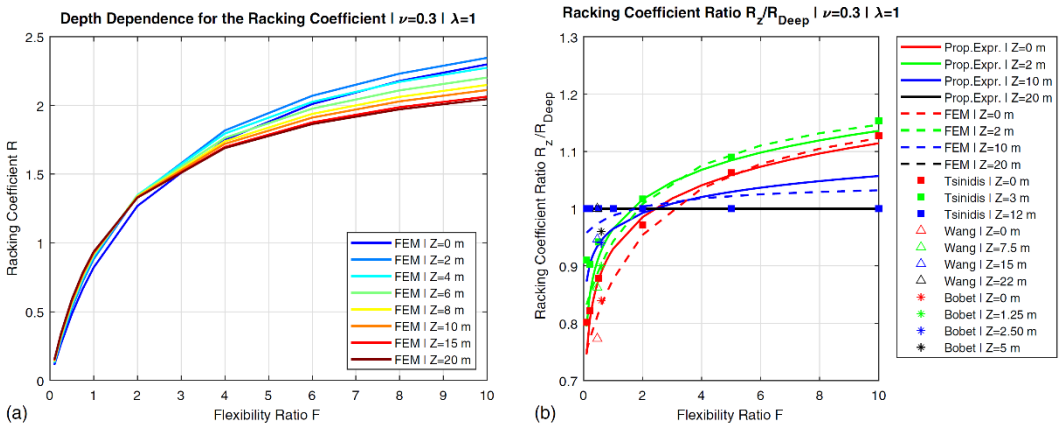

Figure 40 (a) Racking coefficient for shallow and deep buried structures depend on results of the FEM analyses; and (b) racking coefficient ratio R_Z=R_{Deep} for shallow buried respective to deep buried conditions and results by FEM analyses from Tsinidis and Pitilakis (2018), Wang (1993), and Bobet (2010) (Gordo-Mons´o et. al., 2021)

The results obtained by analysis seem consistent with other literature study (Figure 40). For shallow buried structures, racking coefficient can be up to 20% rely upon flexibility ratio and the burial depth (Z): more flexible structures tend to distort more closer to the soil surface (R_Z=R_{Deep} > 1), while structures that are stiff tend to distort less due to their closer proximity to the soil surface (R_Z=R_{Deep} < 1) (Gordo-Mons´o et. al., 2021).

Racking coefficient is increasing with the increase of aspect ratio in flexible tunnels (F <1) whereas response of rigid tunnels (F>1) was observed opposite trend. The tunnel's burial depth is decreasing with increase of the racking coefficient.

Following results are obtained from comparisons of existing literature:

- R-F relationships overestimate the rigid tunnel racking responses based on the numerical results.

- Comparing the numerical results for flexible tunnels in NCHPR611 (Anderson et al., 2008), the relationship either underestimates or overestimates the racking response.
- The results comply with results of Wang (1993), Debiasi et al. (2013) and Hashash et al. (2010).
- Penzien (2000) R-F relations was found maximum envelope for the racking coefficient.

In the Turkish Highways and Railways Tunnels and Other Ground Structures Earthquake Code, which entry into force in 2020, it is suggested to use the simplified frame method and the following steps are suggested:

- One-dimensional free field site response analysis is performed based on the vertical propagation of S-wave and derived the maximum ground acceleration profile expressed as a function of depth.
- The two-dimensional finite element model is developed and also make sure the lateral extension of the model (the horizontal distance to the side boundaries) is sufficiently far to avoid boundary effects. The side boundary conditions of the model should be in case that all horizontal displacements at the side boundaries are free to move and vertical displacements are prevented. These side boundary conditions are considered adequate for reasonably horizontal layered soil model and vertically propagating shear waves (S- waves).
- For two-dimensional model, the strain-compatible shear modulus of the soil obtained from the one-dimensional site response analysis should be used.
- The maximum ground acceleration profile obtained from the one-dimensional site response analysis is imposed to the soil-structure system in the horizontal direction in a pseudo-static approach.

Similarly, it is also possible to perform this analysis by applying a static approach to the two-dimensional soil-structure model of the profile of the variation of the maximum relative horizontal soil displacement with respect to depth, which is obtained by conducting the one-dimensional free field site response analysis based on the vertical propagation of the S wave.

Within the scope of this thesis, these steps were followed by applying the maximum horizontal displacement to the soil profile and the results were evaluated.

3. SIMPLIFIED FRAME METHODOLOGY

3.1. Introduction

In this thesis, numerical analyses were carried on to investigate the behavior of buried rectangular structures during earthquakes. The effects of soil type, structural properties (such as the dimensions of the structure, lining thickness, the burial depth ratio and etc.), burial depth as well as earthquake excitation on this dynamic response have been studied. For this purpose, first of all, one-dimensional free field site response analyses have been conducted for different soil profiles under different earthquake excitations. For this purpose, the software DEEPSOIL was utilized which can perform equivalent linear analyses. After that, two-dimensional analyses were performed using PLAXIS 2D which is based upon finite element modeling of the soil and also the structures. In this chapter, the details of the models (soil types, structural models, earthquake properties) used in the analyses will be presented.

3.2. Model Parameters

The numerical analyses were carried out on 10 different soil profiles with 5 different structure types under 3 different earthquake excitations. The properties of soil profiles, structure models and earthquake excitations will be given in the following sections.

3.3. Soil Profiles

The soil profiles were considered as uniform (with a uniform soil stiffness modulus) sand or clay layers with a depth of 30 m.

The homogeneous soil profiles were divided to six layers which consists sand and clay deposits in DEEPSOIL as shown in Figure 41.

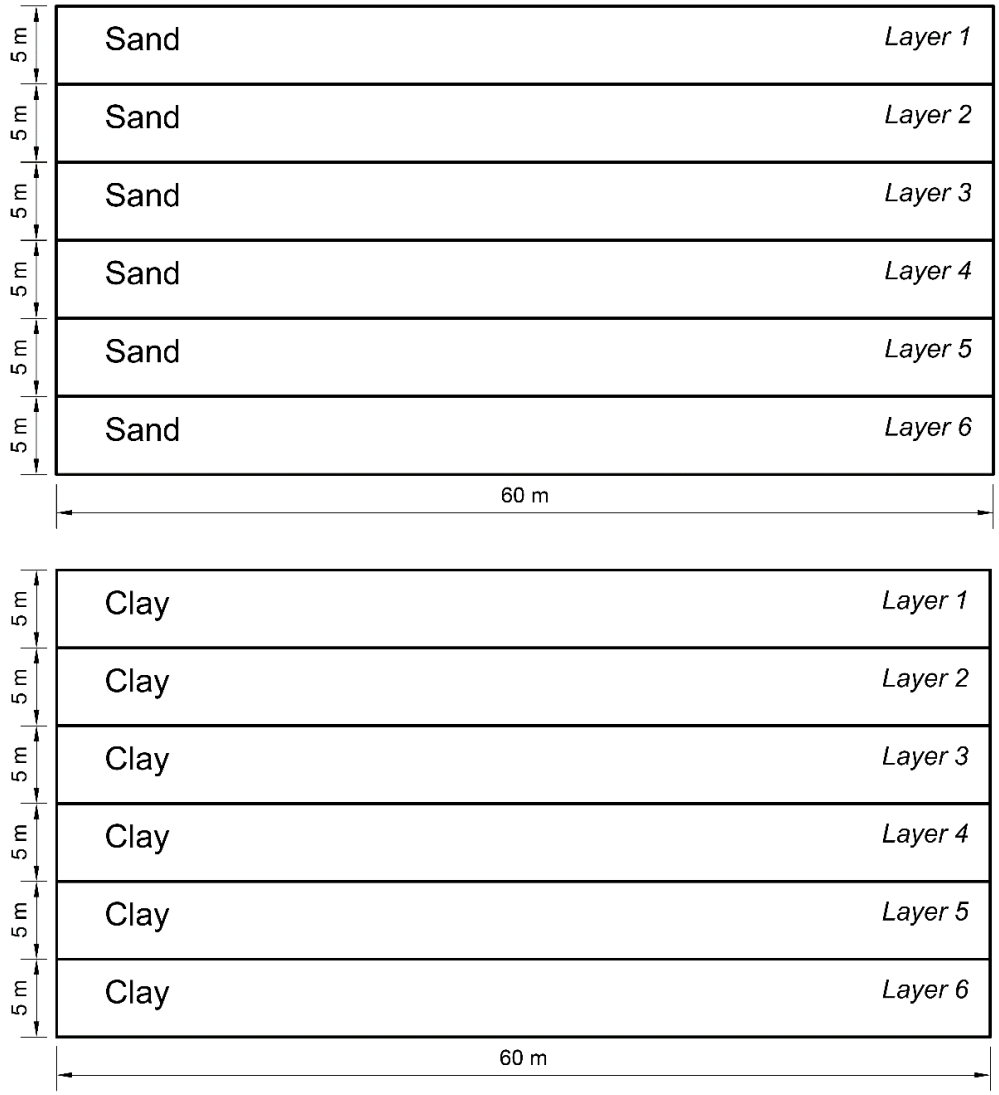

Figure 41 Soil layers of the Profile 1 (top) and Profile 2 (bottom) in this study

Soil Profile 1 in this study (Figure 41) was generated six layers thickness of 5 m consisting of sand. Likewise, soil layers from 1 to 6 were generated as clayey soils in Soil Profile 2. Underneath these layers, rigid bedrock was located. The groundwater table was not defined in soil profiles. The parameters of soil profiles that are used in the analyses were presented in Table 3.

Table 3 Soil parameters used in the analyses

Soil Profile No	Soil Type	Local Soil Class (TBEC, 2018)	Shear Wave Velocity (m/s)	Cohesion c (kPa)	Internal Friction Angle ϕ (°)	Plasticity Index PI	Dry Unit Weight γ_{unsat} (kN/m^3)
1	Sand	ZC	500	5	30	-	19
2	Sand	ZC	360	5	30	-	19
3	Sand	ZD	300	5	30	-	18
4	Sand	ZD	200	5	30	-	18
5	Sand	ZE	150	5	25	-	17
6	Sand	ZE	120	5	25	-	17
7	Clay	ZD	300	200	-	20	18
8	Clay	ZD	200	200	-	20	18
9	Clay	ZE	150	50	-	20	17
10	Clay	ZE	120	50	-	20	17

The shear wave velocity (V_s) values were selected for the six profiles ranges from 120 to 500 m/s according to soil class. Shear wave velocity of soil was defined between 120 m/s and 150 m/s based on site class ZE, between 200 m/s and 300 m/s based on site class ZD, between 360 m/s and 500 m/s based on site class ZC.

Shear modulus in defining properties of soil was evaluated using the following equation.

$$G = \rho V_s^2$$

where

G: Shear modulus of soil (kPa)

ρ: Unit mass of the soil (t/m^3)

V_s: Shear wave velocity (m/s)

3.4. Rectangular Buried Structures in the Model

Five types of rectangular box structures with having different flexibility ratios were taken into consideration in this study. The schematic views of these structures are presented in Figure 42. The wall and slab thickness for all box structures is 0.5 m and 1.0 m based on clear span distance. For Type V, an internal column was considered due to long span.

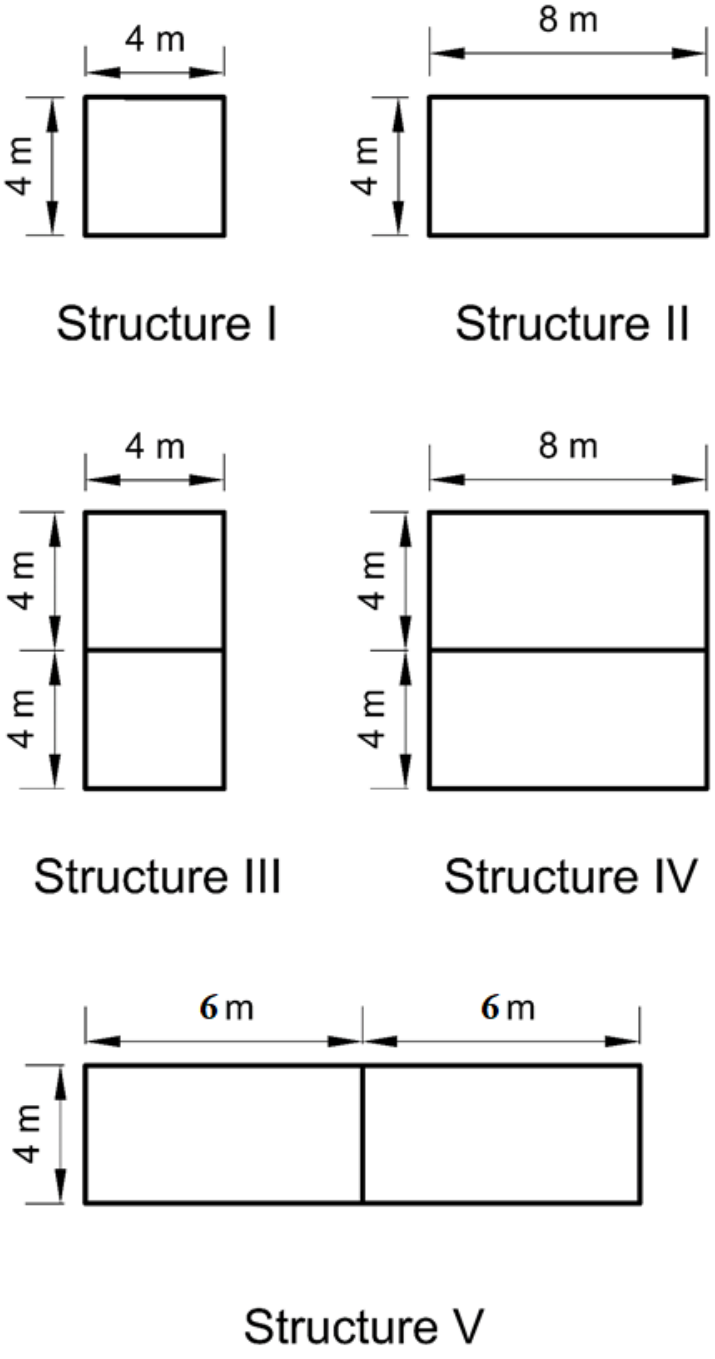

Figure 42 Buried structures with rectangular cross-section used in the study

For plate element, normal stiffness and flexural rigidity were calculated based on cross section properties of the member elements. Structure was defined as a plate element having an out-of-plane dimension of 1 m.

Table 4 presents the structural plate element properties that were used in the study for different plate thickness. The flexural rigidity EI and normal stiffness EA were calculated based on the properties of the materials of the plate. It should be noted that EA and EI are related to the stiffness per unit width of the plate member.

Table 4 Material properties of structural plates

Plate Thickness (m)	Parameters	Name	Value	Unit
0.5	Cross-Section	-	0.5 x 1.0	m x m
	Poisson's Ratio	ν	0.2	-
	Flexural rigidity	EI	312500	$kN/m^2/m$
	Normal stiffness	EA	15×10^6	kN/m
1.0	Cross-Section	-	1.0 x 1.0	m x m
	Poisson's Ratio	ν	0.2	-
	Flexural rigidity	EI	2.5×10^6	$kN/m^2/m$
	Normal stiffness	EA	30×10^6	kN/m

The concrete lining properties that were used in the study are shown in Table 5. The elastic parameters E (modulus of elasticity) and ν (Poisson's ratio) were based on the material properties of concrete.

Table 5 Material properties of concrete assigned in plates

Parameters	name	Value	Unit
Elasticity Modulus	E	30	GPa
Unit weight	γ_{unsat}	25	kN/m^3
Poisson's Ratio	ν	0.2	-

Another factor that is thought to be important in the behavior of buried structures is the burial depth ratio.

Several studies have been conducted on the burial depth effect on the racking coefficient. Wang (1993) conducted analyses to understand the effect on the normalized racking response for shallow embedment depth. The normalized racking distortion versus the dimensionless burial depth (embedment depth/height of the structure) indicated that the normalized racking distortion decreases so long as the burial depth of structure decreases for embedment depth is lower than 1.5 as seen in Figure 43.

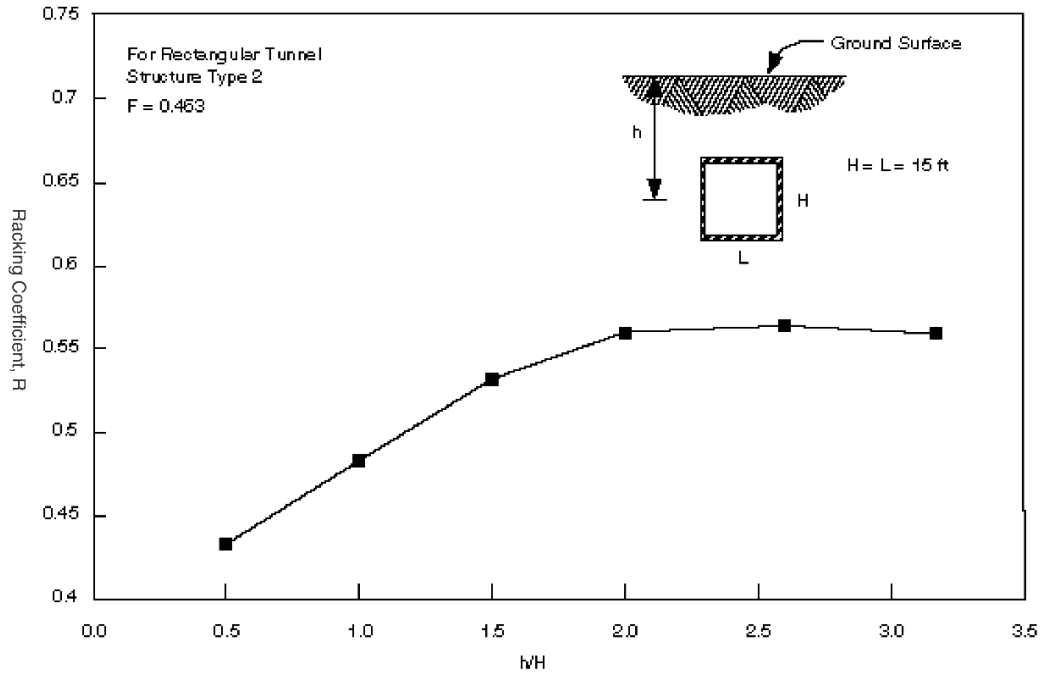

Figure 43 Effect of burial depth on racking response (Wang, 1993)

Debiasi et. al. (2013) analyzed the seismic behavior of buried rectangular structures accounting for the several effects such as overburden depth, aspect ratio and etc. For

different geometric cross-sections, overburden depths (deeply and zero buried) and different interface conditions, the relationship between flexibility ratio and racking coefficient R was revealed as shown in Figure 44.

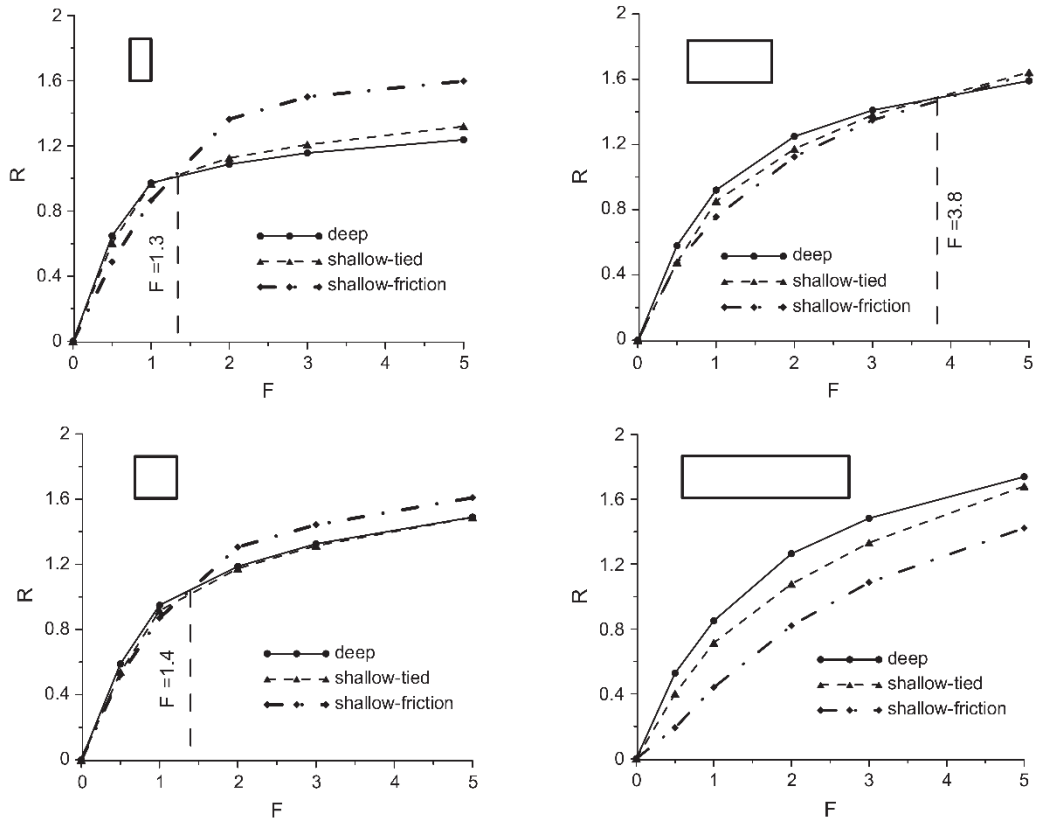

Figure 44 Racking coefficient to flexibility ratio for different geometrical conditions, burial depth (deeply buried or null overburden depth)

Tsinidis (2017) has chosen the burial depth of the structures ranged from 3 m to 12 m and aspect ratios (width of the structure/height of the structure) varied between 0.5 and 3.0 to investigate the behavior of deep and shallow tunnels. After analyses were conducted, Tsinidis (2017) found that as tunnels were buried deeper, the racking coefficient increased (Figure 45). Also, the racking coefficient increase with increasing of the aspect ratio in flexible tunnels.

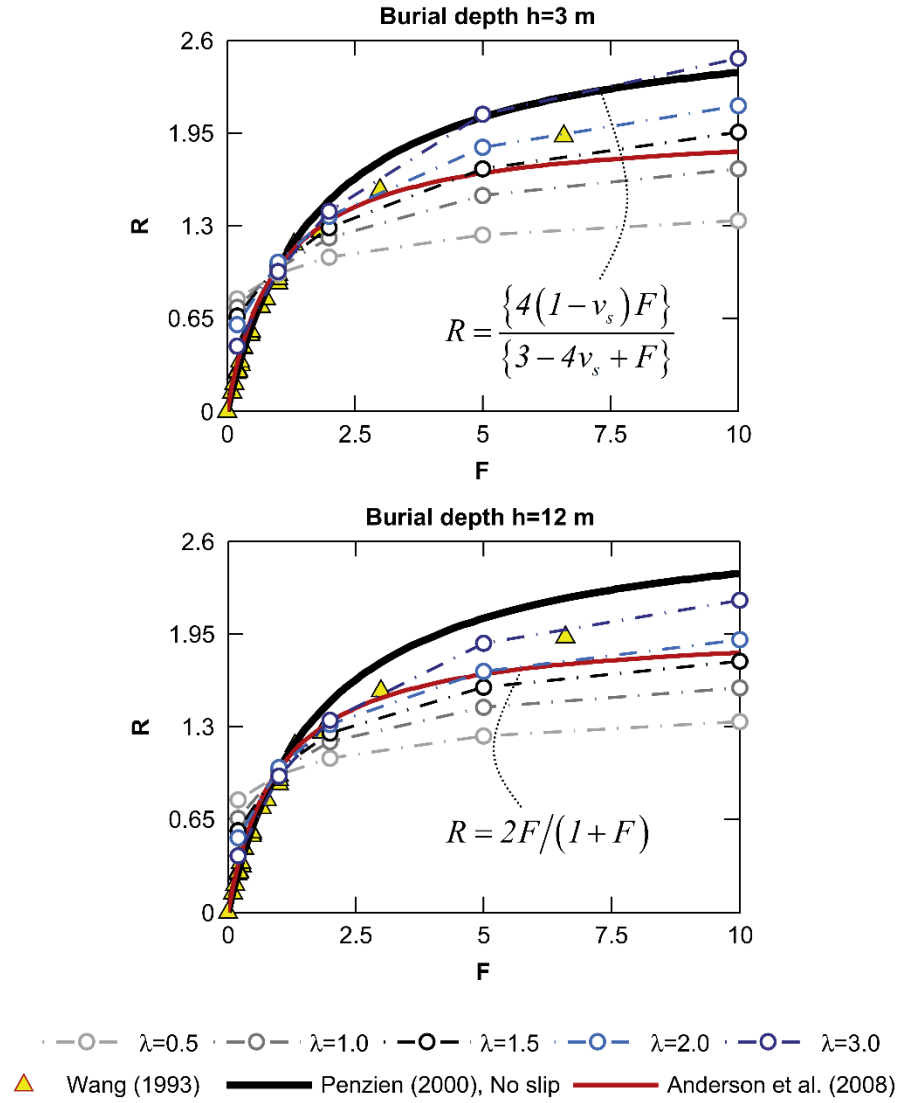

Figure 45 R - F relationships calculated for different burial depths and aspect ratios and comparison with existing literature (Tsinidis, 2017)

To investigate this effect, structures were modeled with having different geometric dimension and different stiffness.

This study was carried on to investigate the racking deformation of rectangular box structures with different burial depth ratio (h/a) and the horizontal displacement difference between top elevation and bottom elevation of the rectangular structures based on different soil types.

The burial depth ratio (h/a) considered as a ratio of buried depth (from the surface) of the structure (h) to structure width (a) as shown in Figure 46.

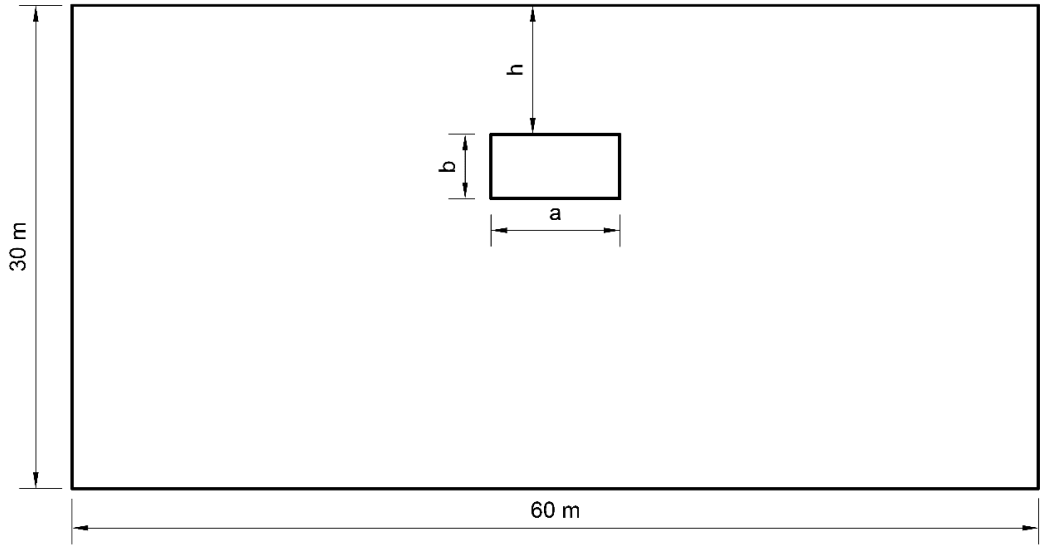

Figure 46 Soil model defined for analysis

3.5. The Earthquake Excitations Used

The earthquake records used in the analyses were selected from the Pacific Earthquake Engineering Research (PEER) Strong Motion Database (https://ngawest2.berkeley.edu, last accessed on June, 2020). Peak ground acceleration (PGA) was taken into account in the selection of earthquake records. PGA of input motion is varied from 0.11g to 0.70g and PGV values are between 0.16 m/s and 0.68 m/s. The earthquake record parameters which are used in the analyses were presented in Table 6.

Table 6 Earthquake data used in the analyses

Earthquake No	Event	Year	PGA (g)	PGV (m/s)	Magnitude	R_{jb} (km)	R_{rup} (km)	V_{s30} (m/s)
EQ-1	Chi-Chi, Taiwan	1999	0.11	0.16	7.62	66.64	66.64	200.86
EQ-2	Chuetsu-oki, Japan	2007	0.45	0.48	6.8	13.68	16.86	561.59
EQ-3	Kobe, Japan	1995	0.70	0.68	6.9	-	0.27	312.00

In addition to properties of selected earthquake, acceleration, velocity and displacement with respect to time graphs were presented in Figure 47, Figure 48 and Figure 49 for Chi-Chi, Chuetsu-oki and Kobe earthquake motions selected from the Pacific Earthquake

Engineering Research Center (PEER) Ground Motion Database, respectively. These input motion graphs are obtained from DEEPSOIL Software (Hashash et al.,2016).

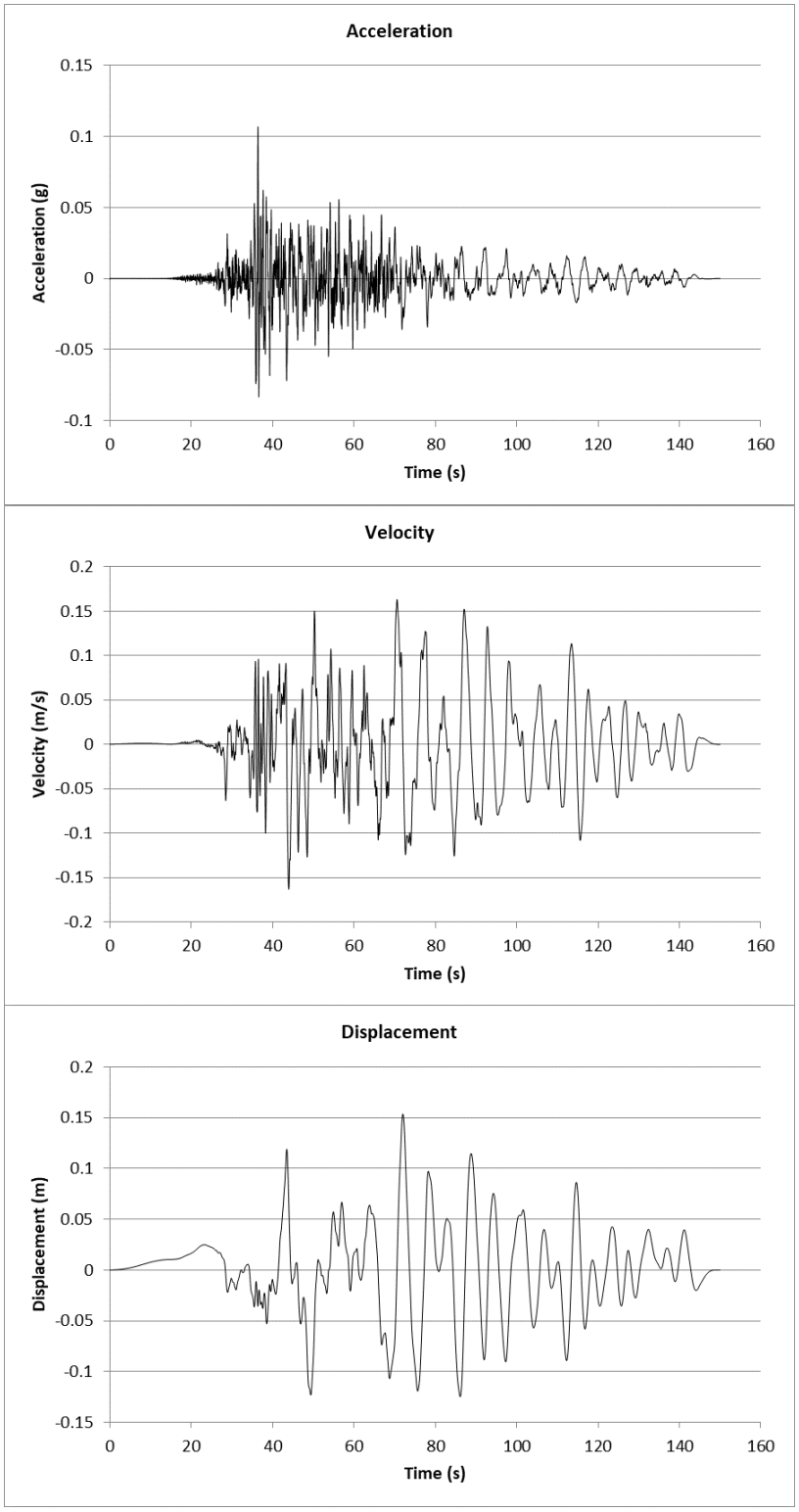

Figure 47 The acceleration, velocity and displacement time histories for Chi-Chi earthquake (EQ-1)

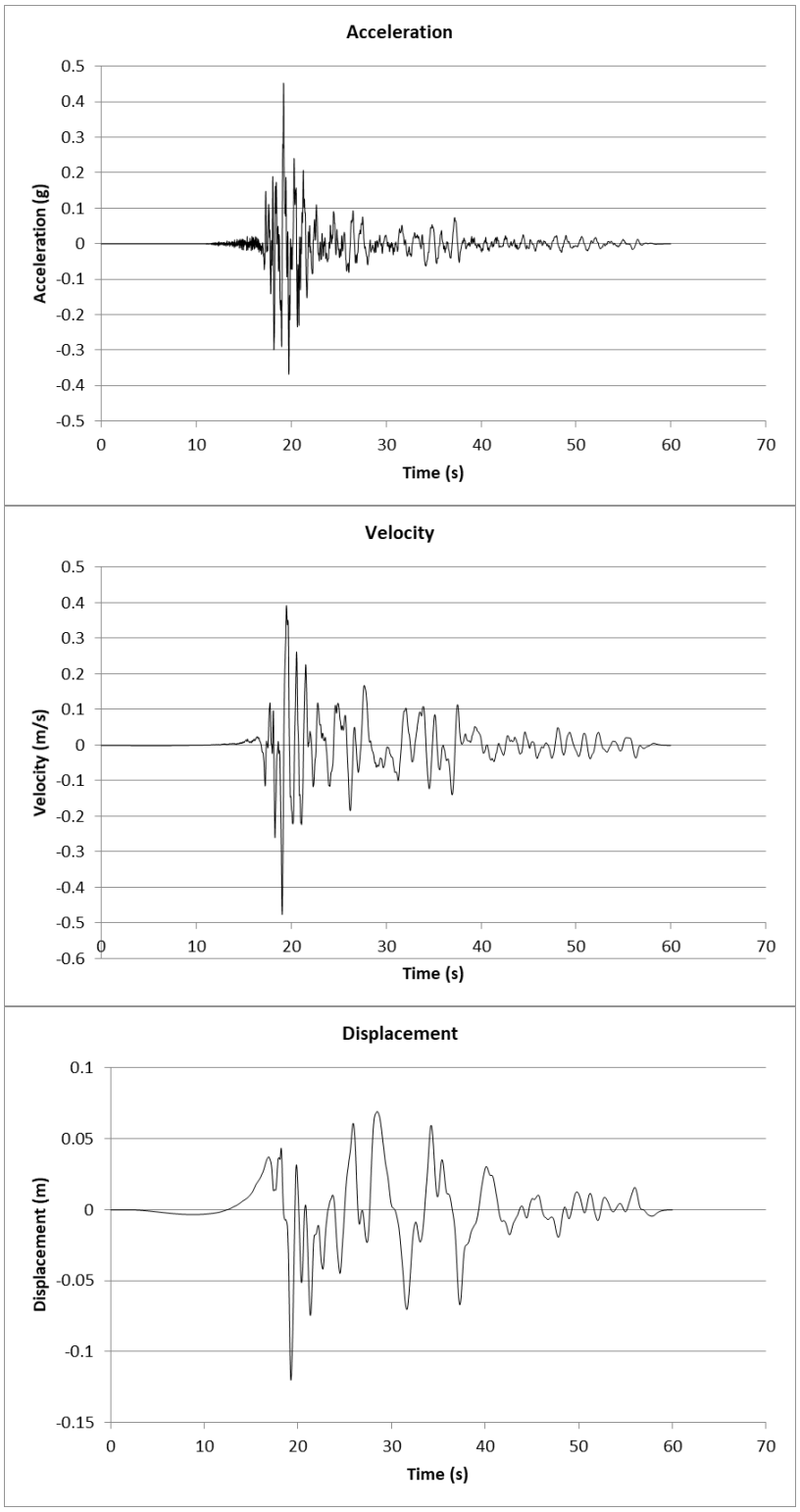

Figure 48 The acceleration, velocity and displacement time histories for Chuetsu-oki earthquake (EQ-2)

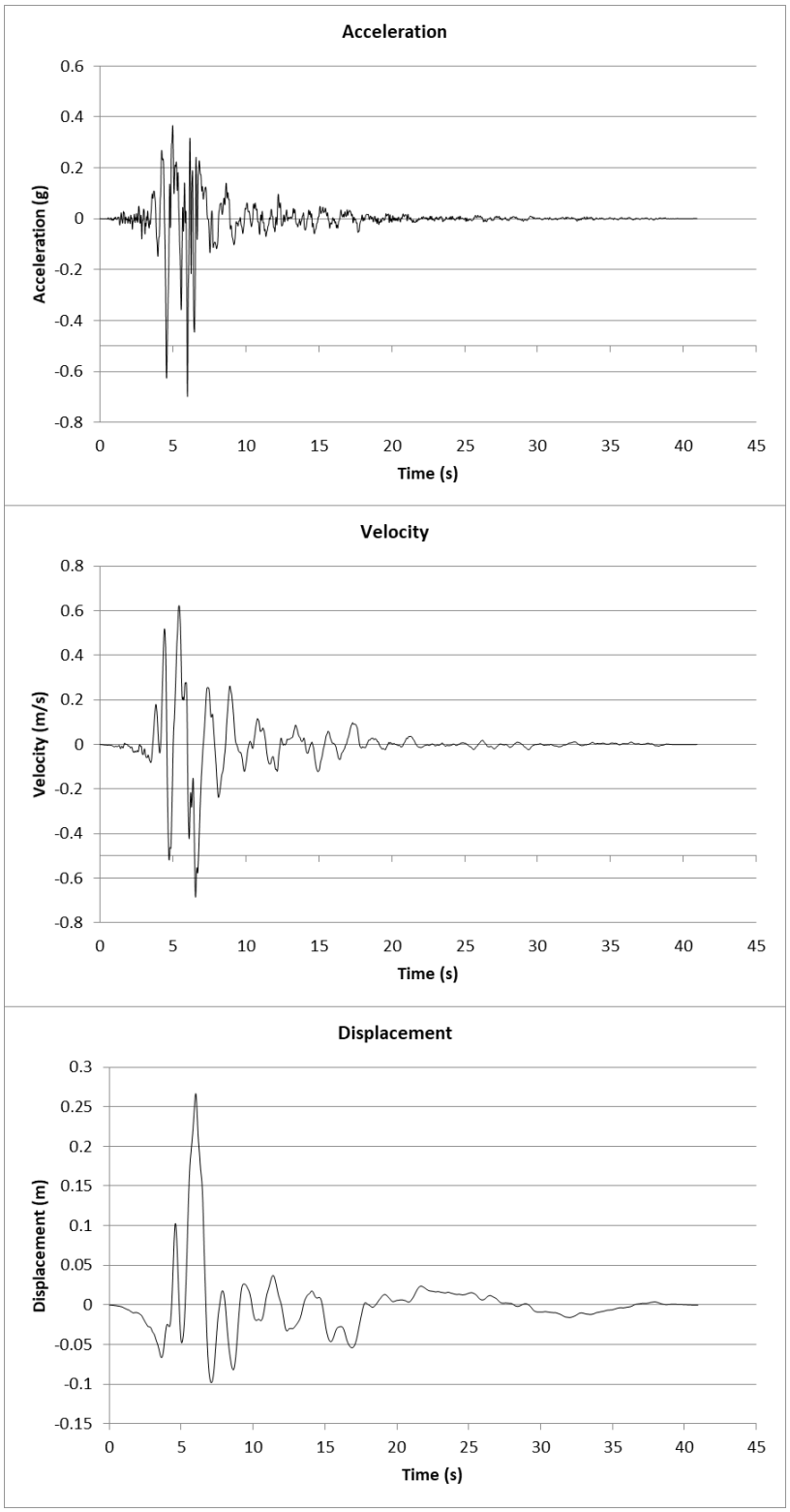

Figure 49 The acceleration, velocity and displacement time histories for Kobe earthquake (EQ-3)

3.6. One Dimensional Site Response Analysis

One-dimensional soil response analyzes to obtain the horizontal displacement values of the soil profile in free field conditions were performed using DEEPSOIL software. DEEPSOIL is a software for 1-D SRA (site response analysis) that can do the following:

- 1-D nonlinear analyses without and with generation of pore water pressure based on time-domain
- 1-D equivalent linear analyses with deconvolution and convolution based on frequency domain
- 1-D linear frequency and time domain analyses (Hashash et al.2020).

The equivalent linear method was used to carry out a 1-D site response analysis using Deepsoil software. This study consists of site response analyses having different soil profiles and seismic motions. Homogeneous soil profiles having depth of 30 m and rigid bedrock were generated.

Soil profiles were created in DEEPSOIL software considering soil characterization in Table 3, an example is given in Figure 50. Soil column was divided to six layers which are same depth to obtain horizontal displacement at surface and certain depths (5m, 10m, 15m, 20m, 25m).

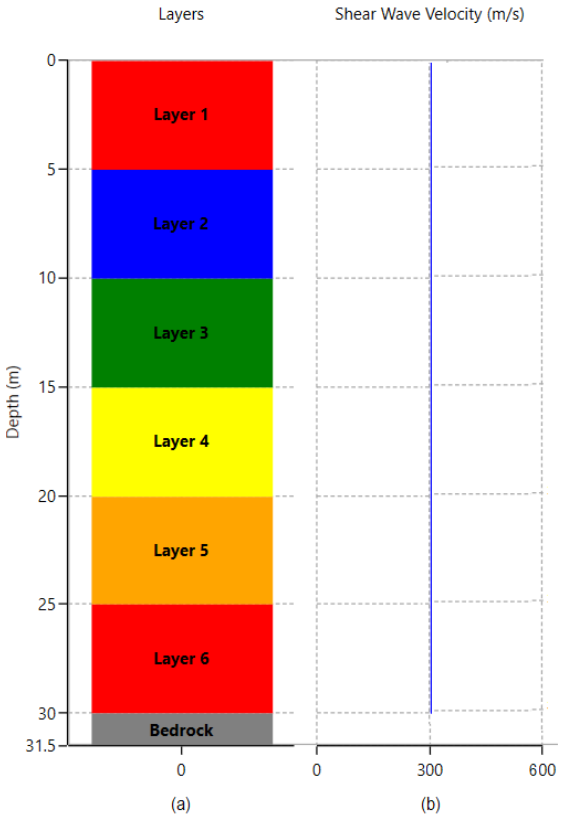

Figure 50 Example of the soil profile created in DEEPSOIL

Shear modulus degradation and damping ratio curves developed by Seed and Idriss (1970) and Vucetic and Dobry (1991) were used in the analyses for sand and clay soil layers, respectively.

Seed and Idriss (1970) indicated that the shear modulus are severely affected by relative density, effective confining pressure and strain amplitude. However, the shear modulus does not considerably influence by characteristics of grain size.

Vucetic and Dobry (1991) stated that the plasticity index is the principal property assessment the modulus reduction curves and damping ratio curves for a saturated soils varied from sands to clays.

In sands, the damping curve and shear modulus degradation curve are dependent on effective vertical stress. Modulus reduction and damping ratio curves referred by Seed and Idriss (1970) for different vertical effective stress ($\sigma' = 387.5$ kPa, $\sigma' = 212.5$ kPa, $\sigma' = 42.5$ kPa) are shown in Figure 51 and Figure 52, respectively. In clay, plasticity index

is defined to be the principal factor affecting the shear modulus reduction and damping curves. Modulus degradation and damping ratio curves proposed by Vucetic and Dobry (1991) were specified based on plasticity index of clay soils (PI=20) are shown in Figure 53 and Figure 54, respectively.

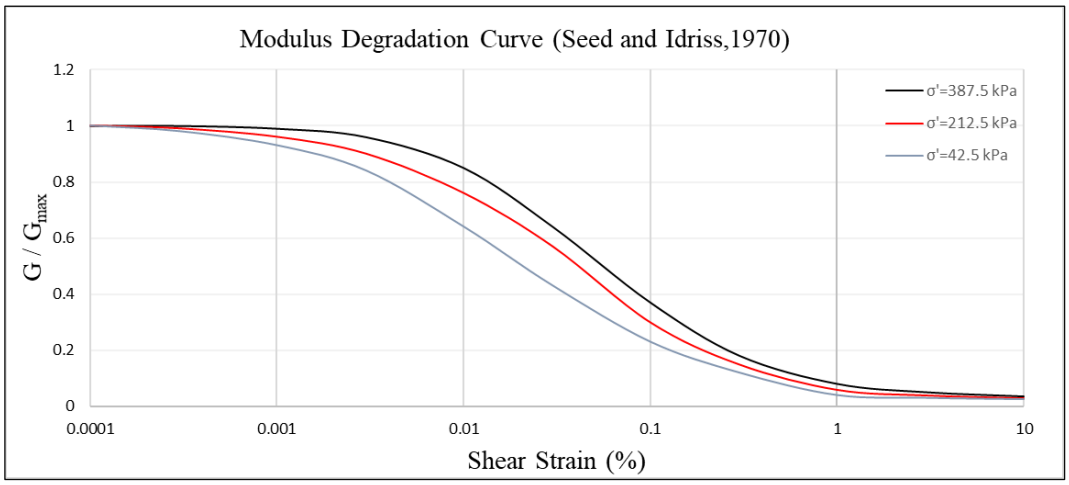

Figure 51 Modulus degradation curve developed by Seed and Idriss (1970) for sand soil

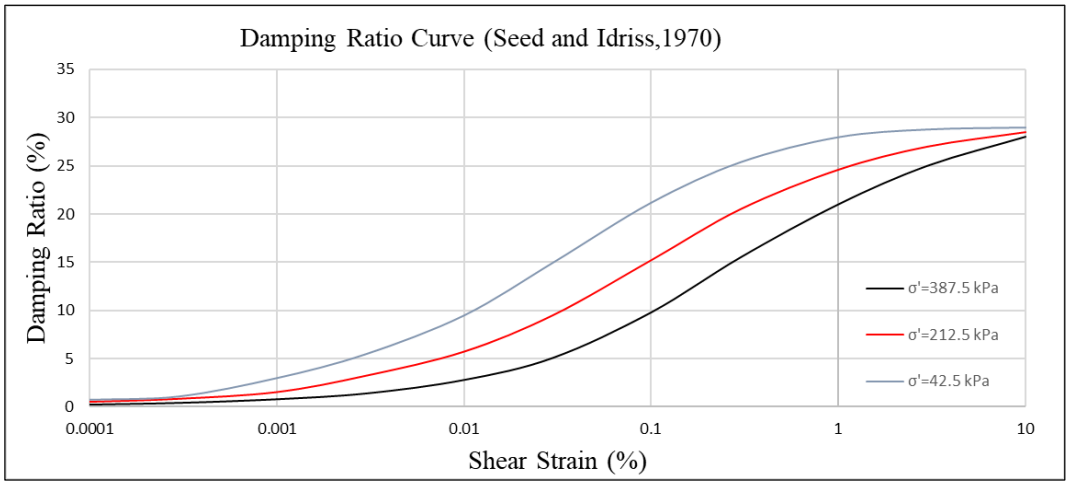

Figure 52 Damping ratio curve developed by Seed and Idriss (1970) for sand soil

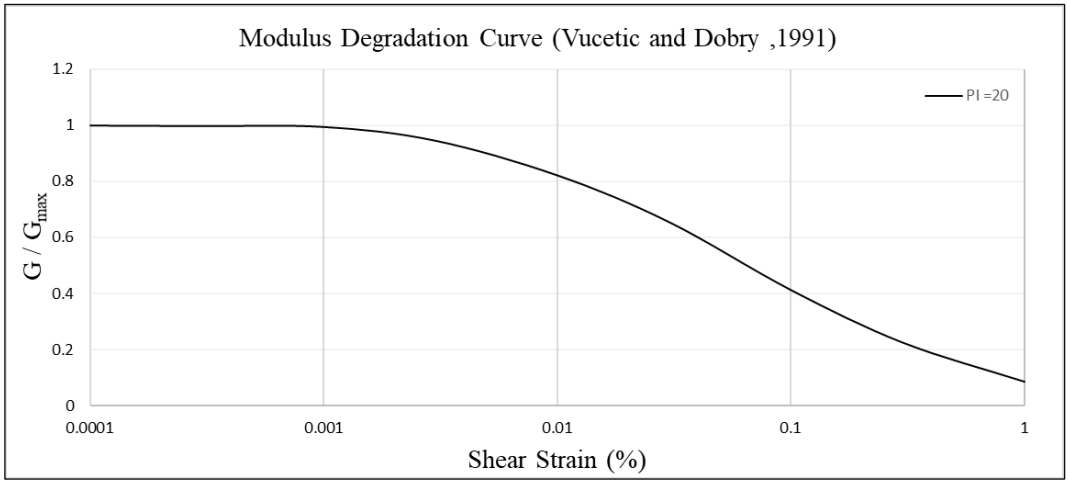

Figure 53 Modulus degradation curve developed by Vucetic and Dobry (1991) for clay soil (PI = 20)

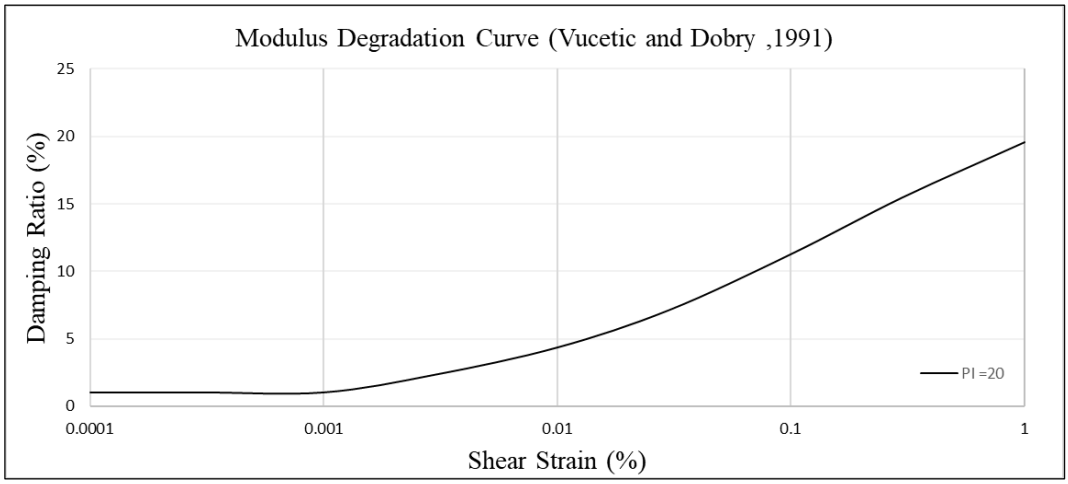

Figure 54 Damping ratio curve developed by Vucetic and Dobry (1991) for clay soil (PI = 20)

Soil profiles were analyzed by considering the ground motions in the equivalent linear analysis. Strong ground motions with different PGA values up to 0.70 g were selected from the Pacific Earthquake Engineering Research Center (PEER) Ground Motion Database.

From these analyzes, free field deformations of the soil profiles were obtained for each soil class. These displacements in free field conditions with respect to the depth are presented in Figure 55 and Figure 56.

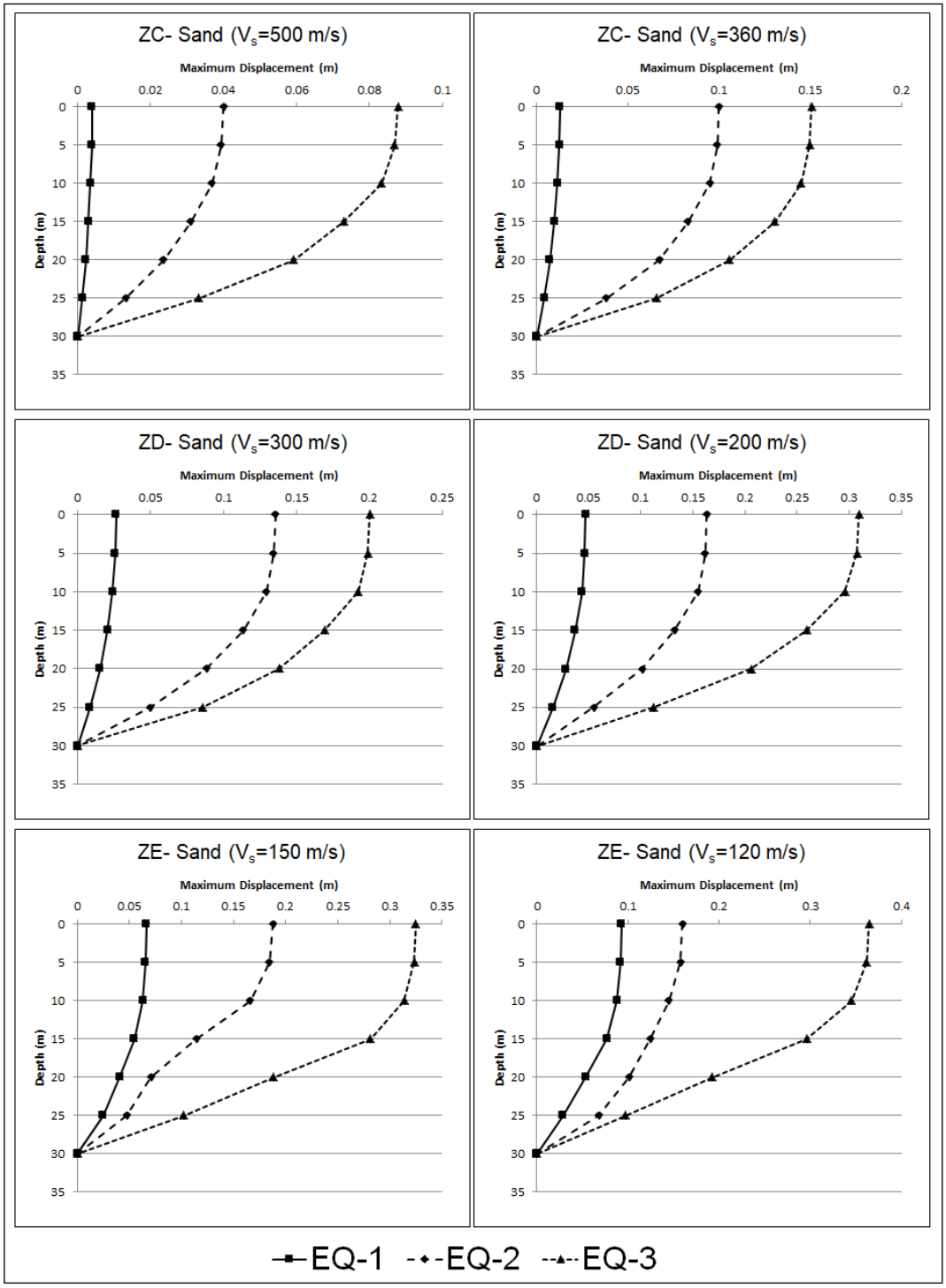

Figure 55 Soil displacement curves with the variation of the strong ground motions for all sand soil profiles analyzed

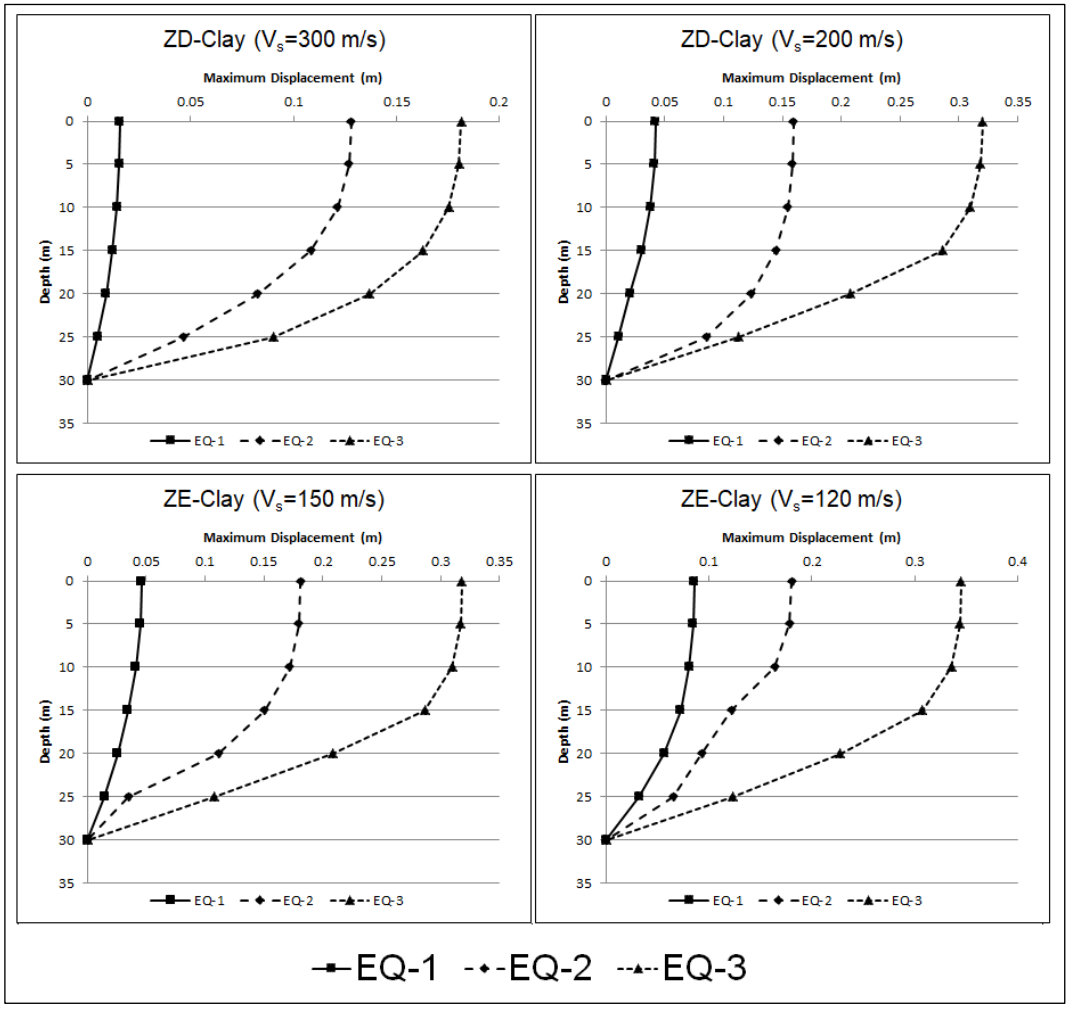

Figure 56 Soil displacement curves with the variation of the strong ground motions for all clay soil profiles analyzed

3.7. Two-Dimensional Finite Element Analysis

PLAXIS 2D is a finite element program developed for the analysis of deformation, groundwater flow and stability of the soil in geotechnical engineering.

Homogeneous sand and clay soil profiles were defined in all the analyses (Figure 57). Soil was modeled to be a Mohr-Coulomb material that has elastic-perfectly plastic behavior.

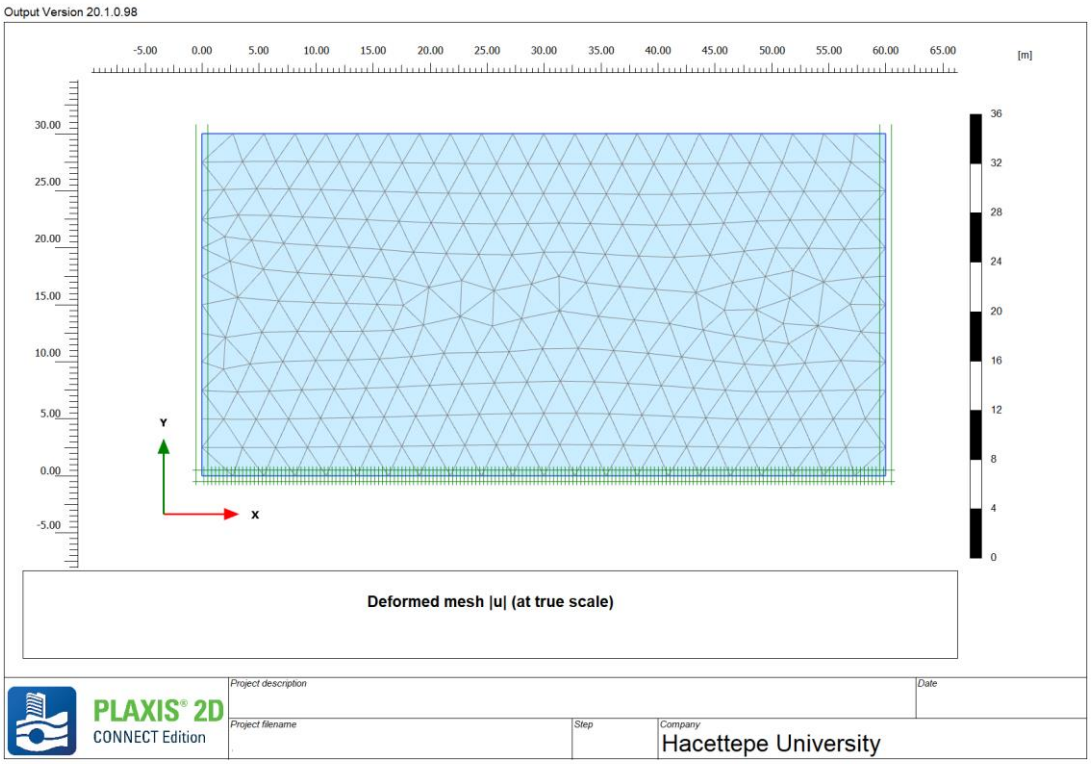

Figure 57 Geometric illustration of soil profile in PLAXIS 2D

Structure was modeled as a plate element having an out-of-plane dimension of 1 m. Structural material was defined as concrete having an elasticity modulus of 30.000 MPa.

Prescribed displacements are special condition tool that can be imposed to the soil model to control the displacements at certain locations.

In PLAXIS 2D analyses, firstly prescribed displacements were imposed on the soil profiles at the initial stage. After that, plastic calculation type was chosen and only weight of box structure and self-weight of soil were activated in Phase 1. In the final stage (Phase 2), all loads, weight of box structure and self-weight of soil and displacement of the boundary condition were activated to perform soil-structure interaction analysis. In addition to these, soil elements inside the rectangular box structure were deactivated in the Phase 1.

Step calculation procedure was performed during analyses as it is listed below and presented in Figure 58;

Phase 0: Initial phase K_0 procedure was used and prescribed displacement was applied to soil boundary

Phase 1: Plate element was activated and displacements were reset to zero

Phase 2: Plate element was activated, and again prescribed displacement was applied to soil boundary

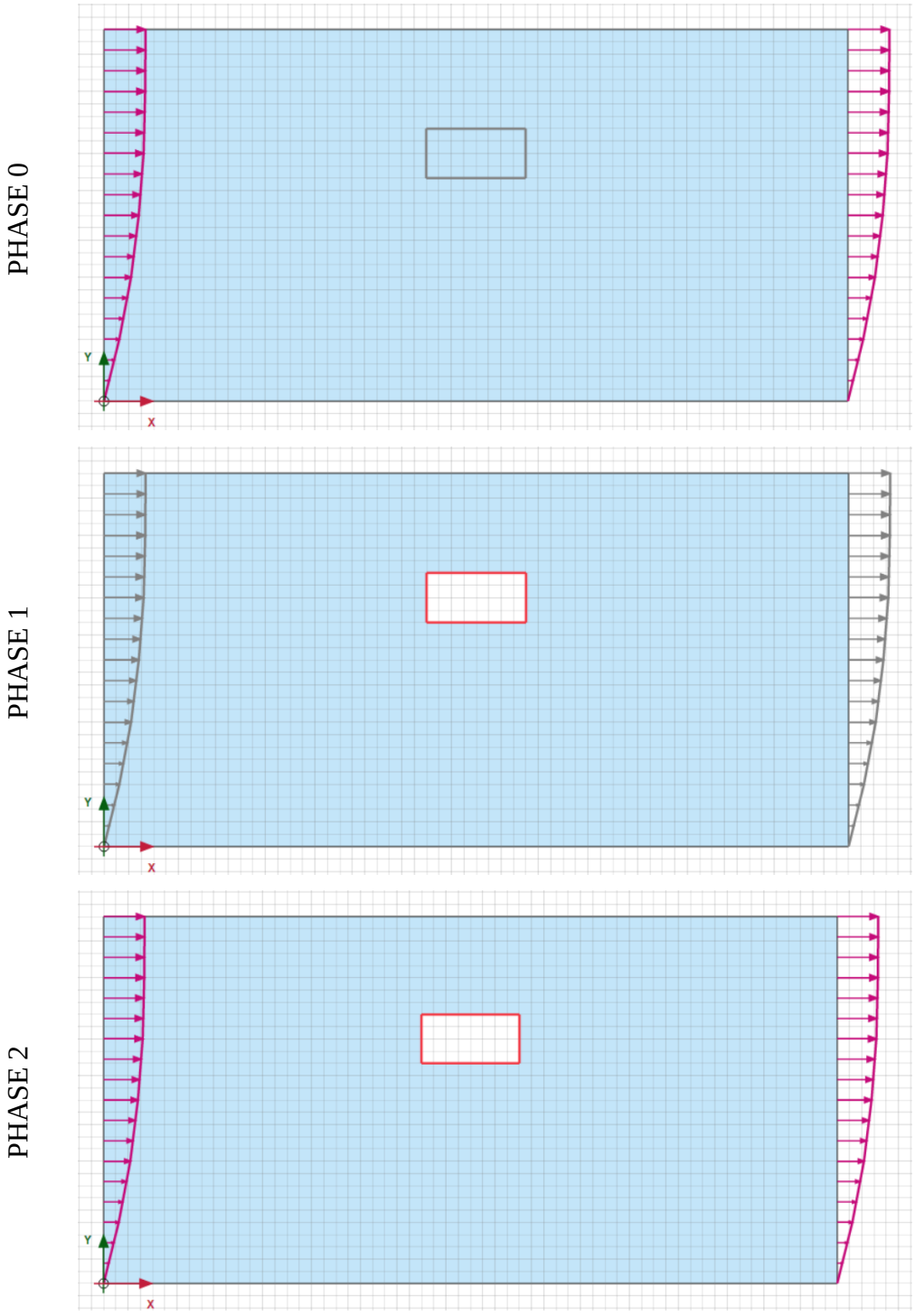

Figure 58 Step calculation procedure in PLAXIS 2D

The Poisson's ratio of soil should be 0.50 as the undrained behavior of the soil will be modeled. However, as the value of 0.50 results in some numerical instabilities, it was defined as 0.49 to be close to 0.5. No groundwater table was defined in the analyses.

The lateral displacements obtained at a specific point from one-dimensional DEEPSOIL analysis were imposed to the rectangular soil profile boundaries as prescribed displacement without having any structure and opening in the soil profile as shown in Figure 59. These boundary deformations are equal to free field deformations from the one-dimensional site response analysis. These displacements were obtained from a free-field site response analysis carried out in DEEPSOIL. In PLAXIS, the prescribed-displacements in horizontal direction were applied to 7 nodes on soil boundary.

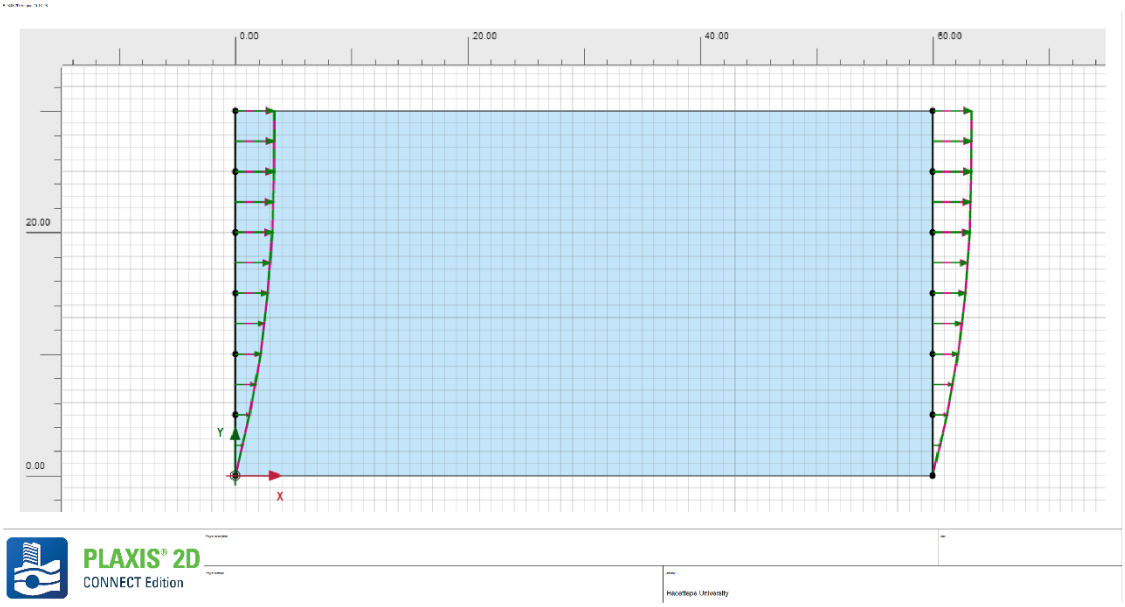

Figure 59 Boundaries of soil profile deformations in PLAXIS 2D

From these analyzes, the relative displacement values at the points where the structure is located were obtained. The displacement difference at the top (Point A) and the bottom points (Point B) of the structure was defined as free-field racking displacement (Δ_{ff}). (Figure 60)

$$\Delta_{ff} = u_A - u_B$$

where

Δ_{ff}= free-field racking displacement

u_A= lateral displacement of soil at point A

u_B=lateral displacement of soil at point B

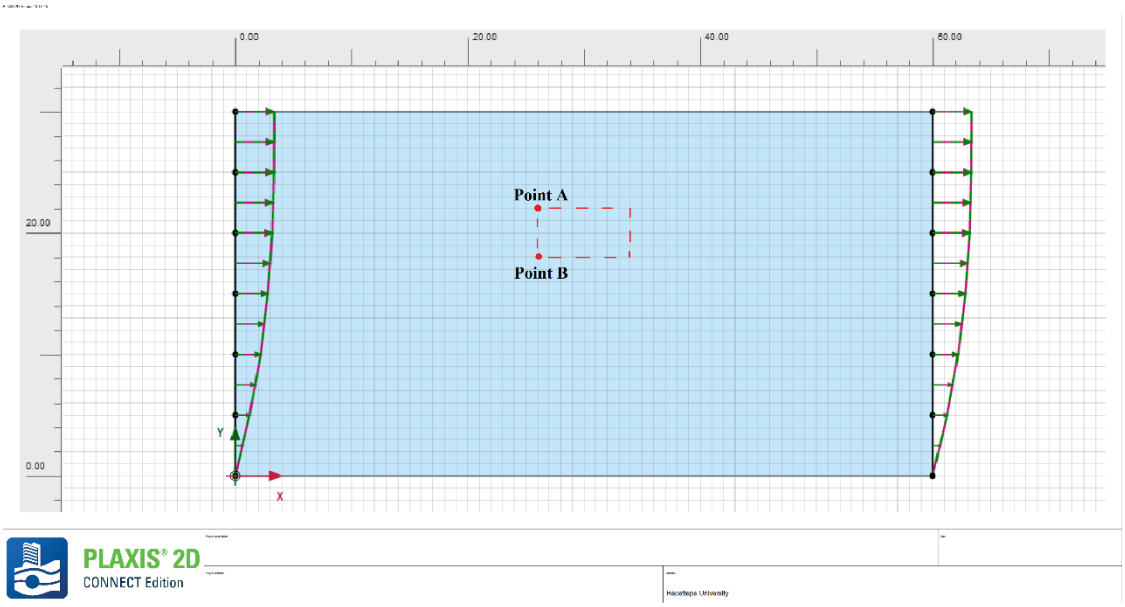

Figure 60 Free field deformation conditions

After the free-field racking displacement (Δ_{ff}) were determined, racking coefficient (R) and flexibility ratio (F) were calculated by using Wang (1993) method in the existing literature.

Racking coefficient are presented in Figure 61 and defined as follows by Wang (1993):

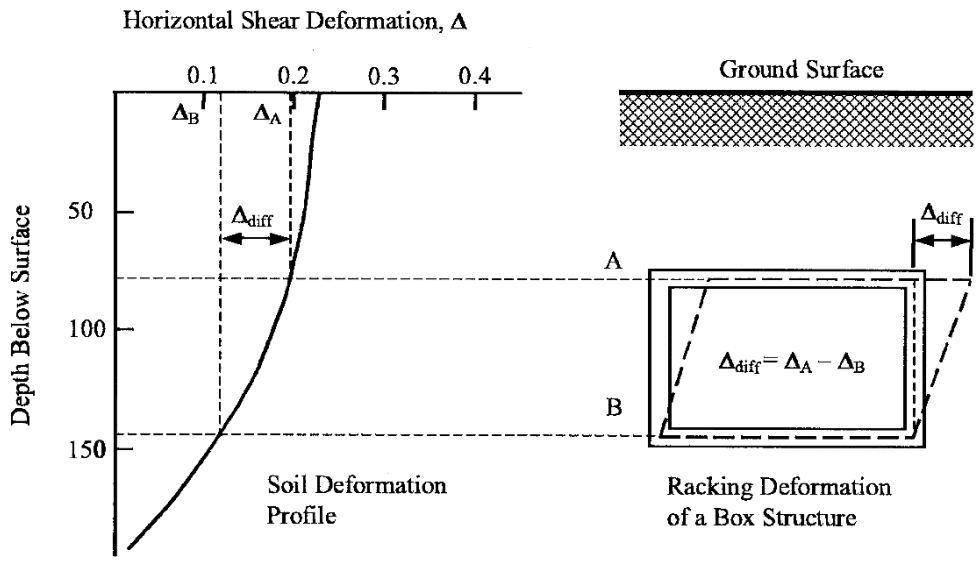

Figure 61 Free field racking deformation condition of the buried rectangular structure (after Wang, 1993) (Hashash et al., 2001)

The racking coefficient (or racking ratio) is:

$$R = \frac{\Delta_S}{\Delta_{ff}}$$

where

R is racking coefficient

Δ_S is racking distortion of the structure embedded in the soil,

Δ_{ff} is free-field racking displacement (or deformation)

The medium sized mesh was adapted to the overall model size in PLAXIS 2D. The generated mesh before analyses and after analysis are shown in Figure 62 and Figure 63, respectively.

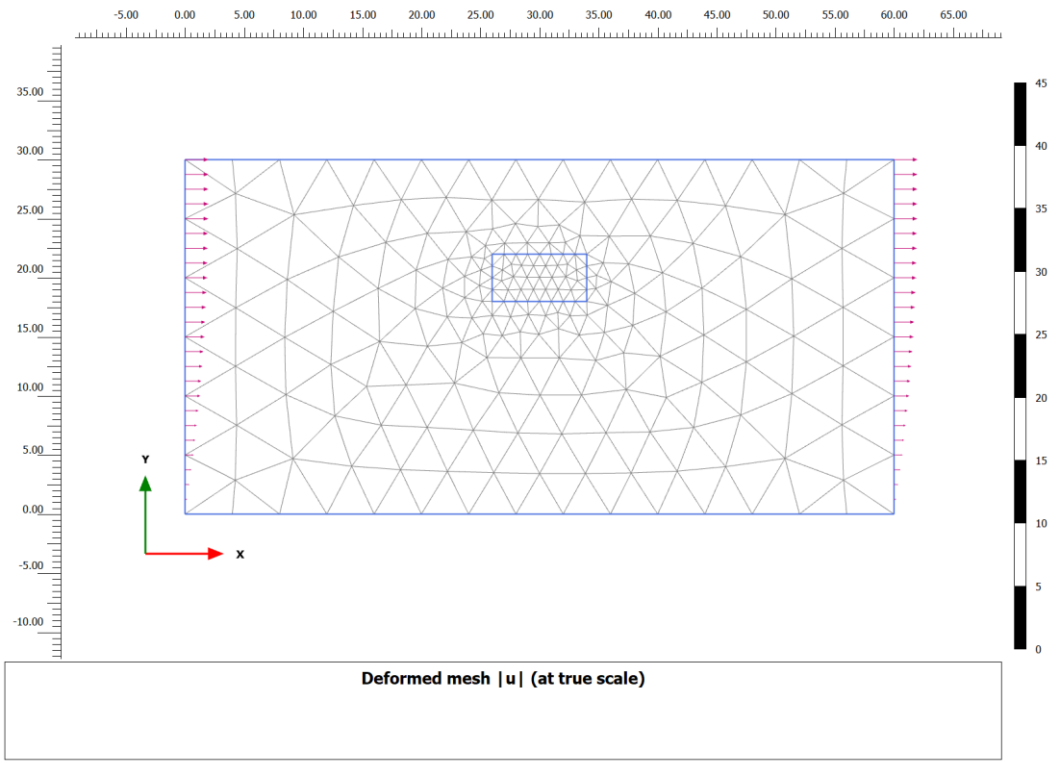

Figure 62 The mesh element

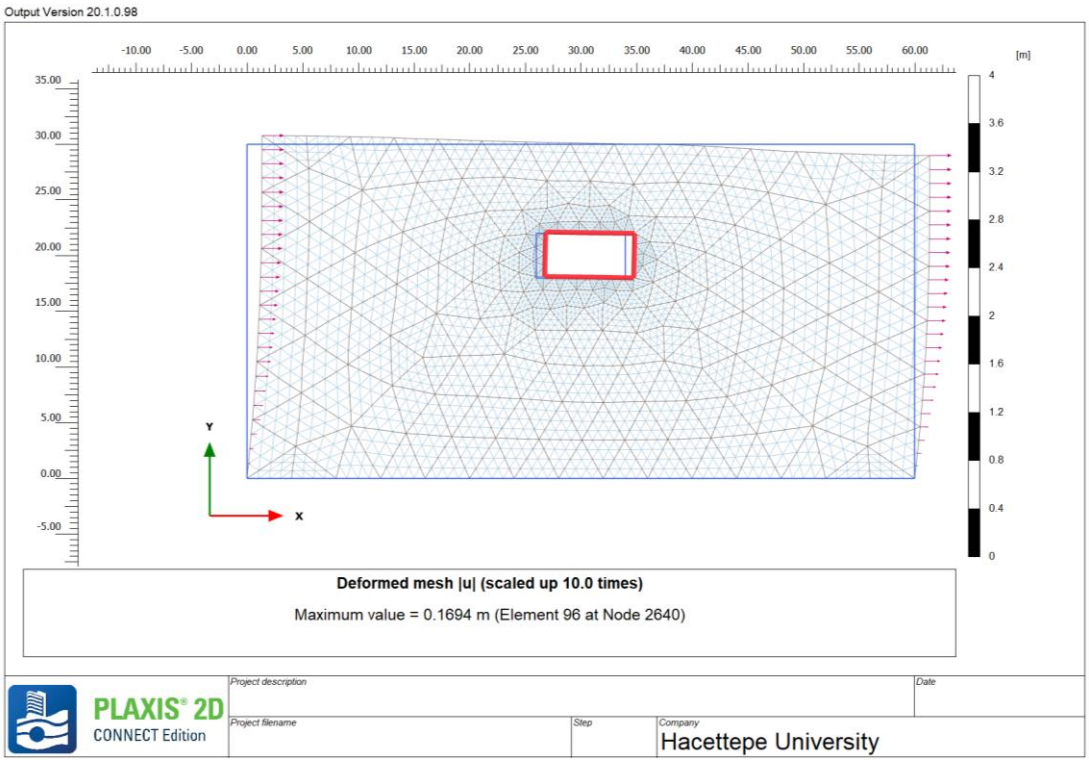

Figure 63 Deformed mesh after the analysis

The total displacement (u_x) distribution on the plate element is shown in Figure 65.

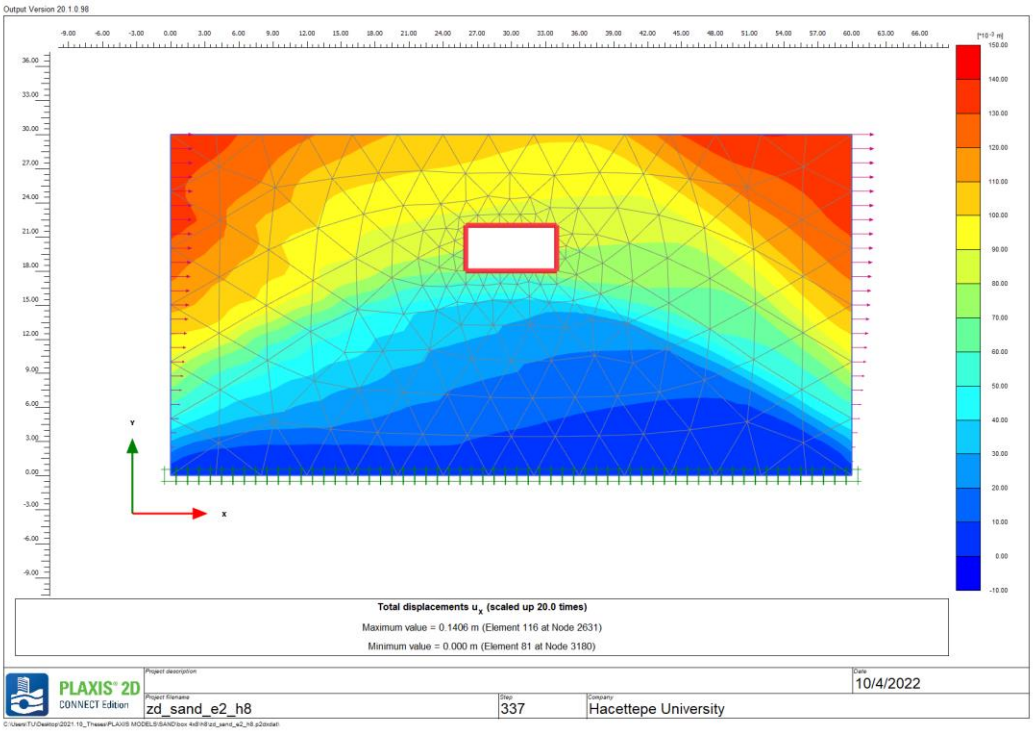

Figure 64 Total displacements distribution for the structure

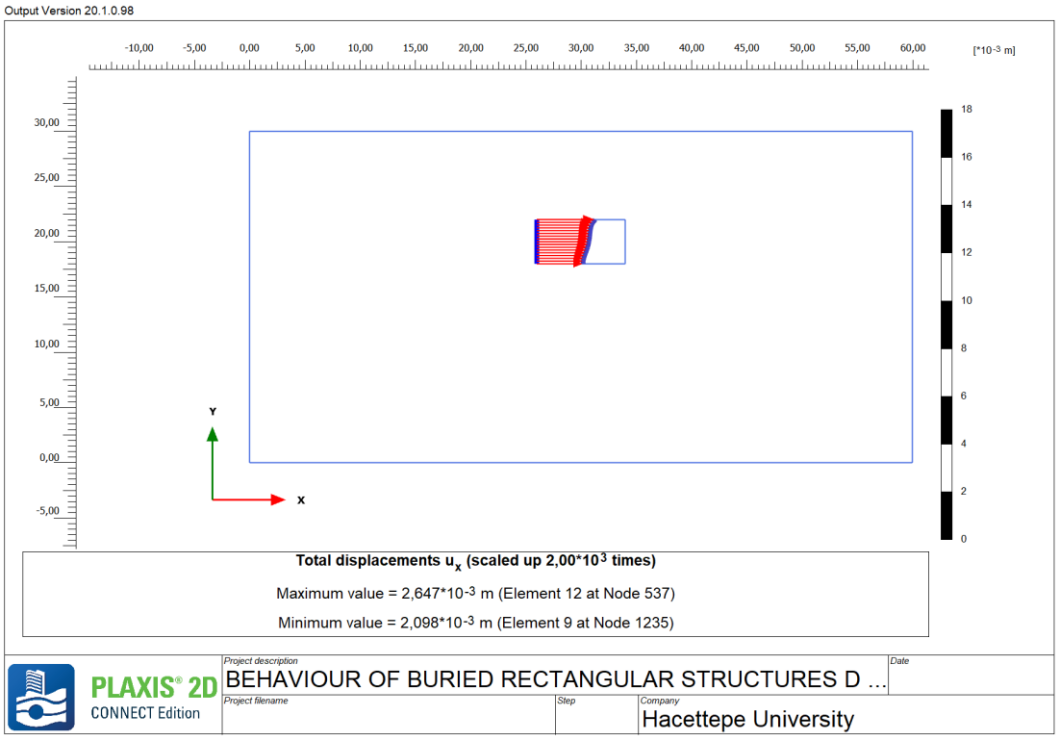

Figure 65 Total displacement (u_x) distribution on the plate element

According to Debiasi et. al. (2013), consider the structure's movement involves no rocking, as is typically the condition of deeply-buried structures, Δ_S obviously coincides

with the relative difference between the bottom and top horizontal displacements of the frame.
The racking coefficient (R) obtained from the all analyzes was presented in Appendix A.

The flexibility ratio of a rectangular structure is a measure of the shear stiffness of the surrounding soil with respect to that of the structure element (Wang, 1993). The flexibility ratio is predicted according to Wang (1993) as:

$$F = \frac{G_m \cdot W}{H \cdot K_s}$$

where
W is width of the structure,
H is height of the structure,
G_m is shear modulus of the surround soil and
K_s is the required concentrated force to induce a unit racking deflection of the top of the structure
Structural racking stiffness (K_s) is the ratio of the applied force to the resulting lateral displacement (NCHRP,2008). K_s can be calculated by use of a simple linear frame analysis (Debiasi et al.,2013). In conducting the structural frame analysis, appropriate moment of inertia values, consider the potential development of cracked section, should be used. (Kim et.al.,2016) (FHWA)

Wang (1993) highlighted that relationship flexibility ratio between surrounding soil and the embedded structure as stated below:

- $F \rightarrow 0.0$: The structure is rigid, so it will not rack regardless of the distortion of the ground (i.e. the structure must take the entire load)
- $F < 1.0$: The structure is considered stiff relative to the surrounding soil medium and will therefore exhibit lower deformation.
- $F = 1.0$: The structure and surrounding soil medium have equal stiffness, so that the structure will undergo approximately the same free-field distortions.
- $F > 1.0$: The racking distortion of the structure is amplified relative to the free field, though not because of dynamic amplification. Instead, the distortion is amplified because the soil medium now has a cavity, providing lower shear stiffness than the non-perforated ground in the free field.

- F $\rightarrow\infty$: The structure has no stiffness, so it will undergo deformations identical to the perforated ground.

The flexibility ratio obtained from the all analyzes are presented in Appendix B.

4. RESULTS

In this chapter, the results obtained from the analyses to present the behavior of buried rectangular structures on selected soil profiles during earthquakes were presented and discussed. To investigate the behavior of buried rectangular structures during earthquake excitation, analyses were conducted in PLAXIS using five different box structures (Two different thicknesses were used for Structure V.), five different soil types based on TBEC-2018 (ZC – Sand, ZD – Sand, ZE – Sand, ZD – Clay, ZE – Clay), three different earthquake excitations (PGA= 0.11g, PGA= 0.45g, PGA=0.70g) and two different burial depths (2m and 8m).

Simple homogenous soil profiles (with a uniform soil stiffness modulus) were proposed for simplicity in parametric analysis.

Two different embedment depth cases were modeled in PLAXIS 2D to investigate the effect of embedded depth ratio (as mentioned in Chapter 3.4 and given in Figure 46). As the thickness of the soil model is 30 m, analysis results were not seen realistic for very deeply-buried structures. So, embedment depth of box structures was chosen is 2 m and 8 m in this study.

The details of the analysis approach were explained by an example in the following sections of this chapter.

4.1. Sample Case

To obtain free field displacement results, one-dimensional (1-D) site response analyses were performed to evaluate the behavior of soil profile during earthquake in free field condition. As a result of these analyses, horizontal displacements of the soil profile in free field conditions were obtained. In DEEPSOIL V7, ten (10) different homogeneous soil profiles of 30 m depth with constant shear wave velocity were created. Properties of the soils used in these soil profiles were presented in Table 3. The soil profiles were subjected to three earthquakes loadings with different peak ground acceleration.

Horizontal relative free – field displacements (without any structure) corresponding to the bottom and top elevations of the rectangular box structures and the uniform soil profile used in DEEPSOIL V7 is illustrated in Figure 66.

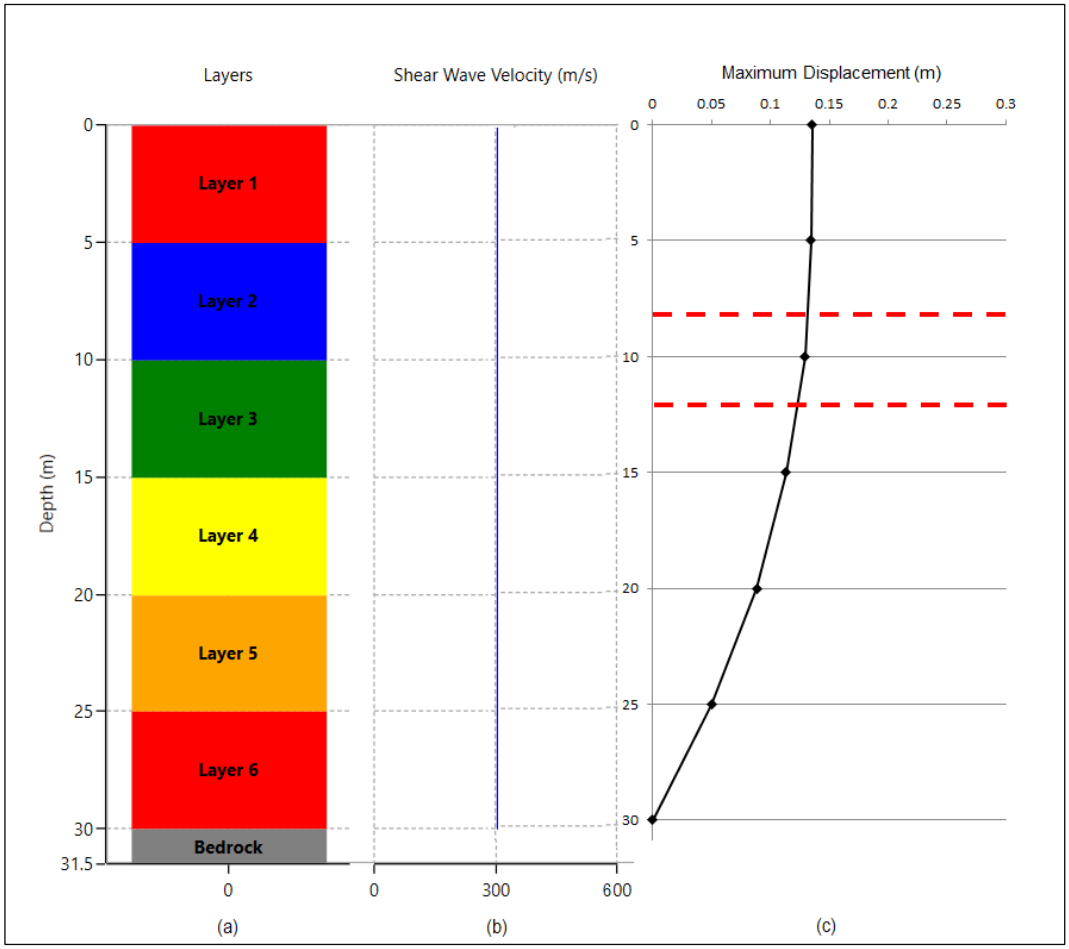

Figure 66 Soil profile used in the DEEPSOIL and horizontal relative free-field displacement graph

This soil profile (in Figure 66 - a) represents sandy soil and ZD soil class based on TBEC with a shear wave velocity of 300 m/s (Figure 66 – b). Figure 66 – c shows the results of equivalent linear site response analysis under Chuetsu-oki Earthquake. Horizontal relative free – field displacements (without any structure) corresponding to the bottom and top elevations of the rectangular box structures was delineated by red dashed line. The maximum horizontal displacement along the soil profiles were estimated in analysis as shown in Figure 55 and Figure 56 for different site class. After this stage, maximum displacement results were defined as prescribed displacement in PLAXIS 2D.

A representative soil model was generated with boundary conditions for pseudo-static analysis in PLAXIS 2D based on soil properties given in Table 3. The soil model and mesh used for this analysis is shown in Figure 67.

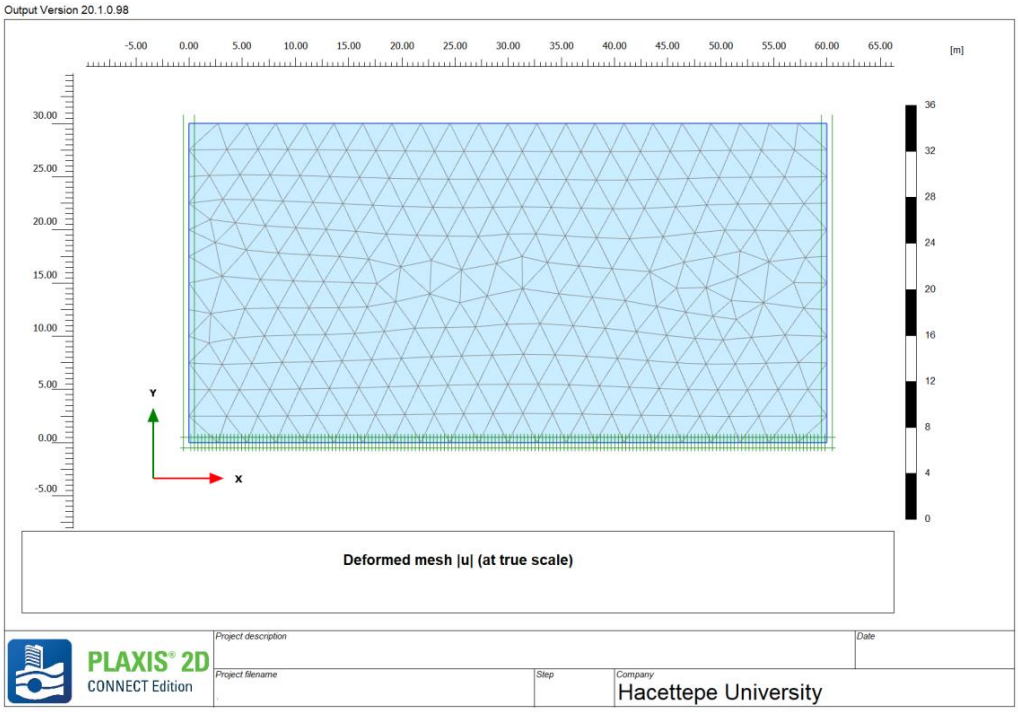

Figure 67 Finite element mesh used for sample case

Prescribed displacement values were assigned to be imposed to edge of the soil model at certain depth (0-, 5-, 10-, 15-, 20- and 25 m). Also, it should be noted that uniform deformation profile should be applied in left and right edge to the model boundaries (see Figure 68). Y direction of the prescribed displacement was chosen rotationally fixed.

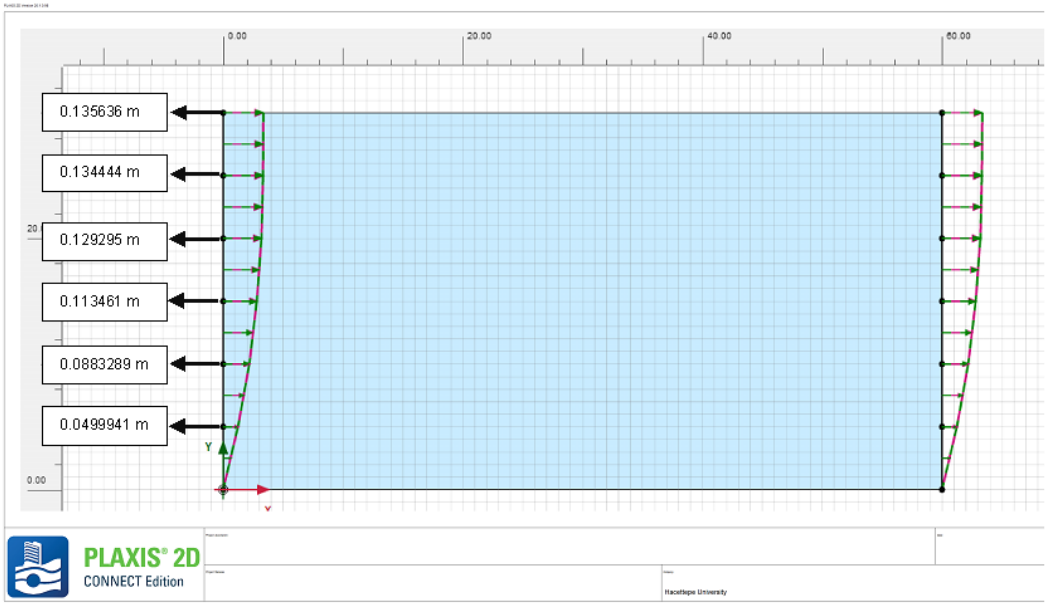

Figure 68 Schematic view of prescribed displacements applied on edge of the soil profile

The soil profile was simulated with Mohr – Coulomb model to obtain free field deformation in PLAXIS 2D. The purpose of this analysis is to estimate the response of the top (Point A) and bottom (Point B) elevation of the rectangular box structure in free field condition (see Figure 69).

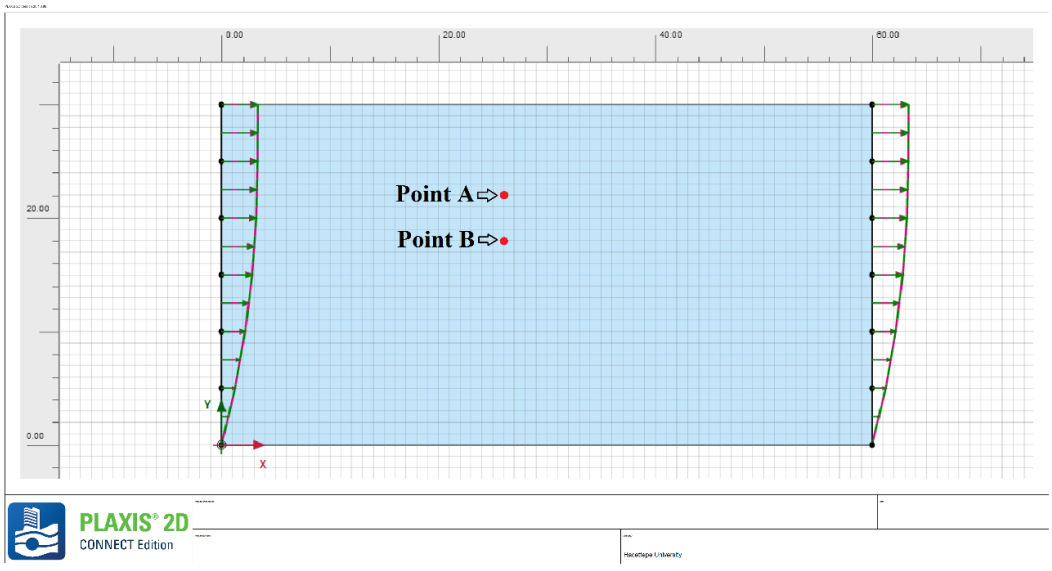

Figure 69 Free-field condition in PLAXIS 2D

The obtained results from PLAXIS 2D was presented in Table 7. As mentioned in the previous chapter, the differential deformation between the top and the bottom of the structure is defined as relative free field racking deformation (Δ_{ff}). of the box structure.

Table 7 Free field horizontal displacement of the soil

Soil Class and Type	PGA (g)	PGV (m/s)	Free Field Displacement of Top Elevation (Point A) (cm)	Free Field Displacement of Bottom Elevation (Point B) (cm)	Δ_{ff} (cm)
ZD Sand	0.45	0.48	9.23	8.21	1.02

According to this results, relative displacement between top and bottom elevation is 1.02 cm in free field condition.

The next step was to evaluate the relative displacement of the box structures based on the soil – structure interaction system. The soil-structure interaction can be described by the interaction between the surrounding soil and structure. Pseudo-static soil-structure interaction analyses was performed using finite element method in PLAXIS 2D. The buried rectangular structure was defined as a plate element and the thickness of the plate was taken as 100 cm. Considering the soil – structure interaction analysis, three stages were implemented in PLAXIS 2D. In the third (Phase 2) stage, all loads, weight of box structure and self-weight of soil were activated. Finite element meshing of 2D model used in the analysis is shown in Figure 70. In addition to this, the resulting contour of total displacement is indicated in Figure 71.

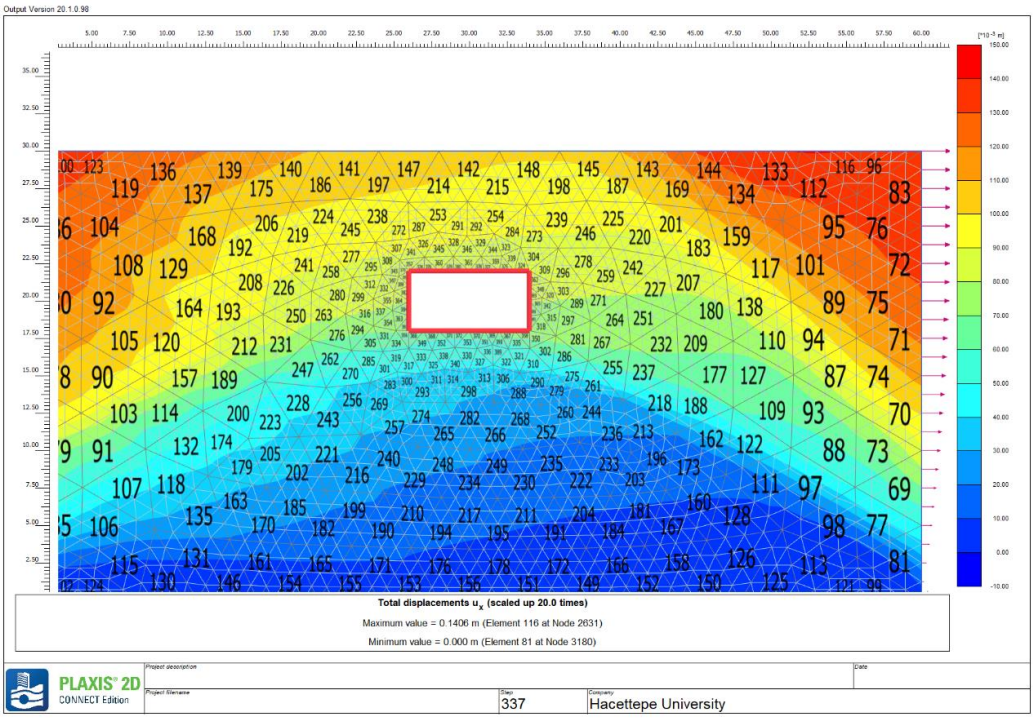

Figure 70 Last stage corresponding to the application of the displacement field with used mesh with element numbers

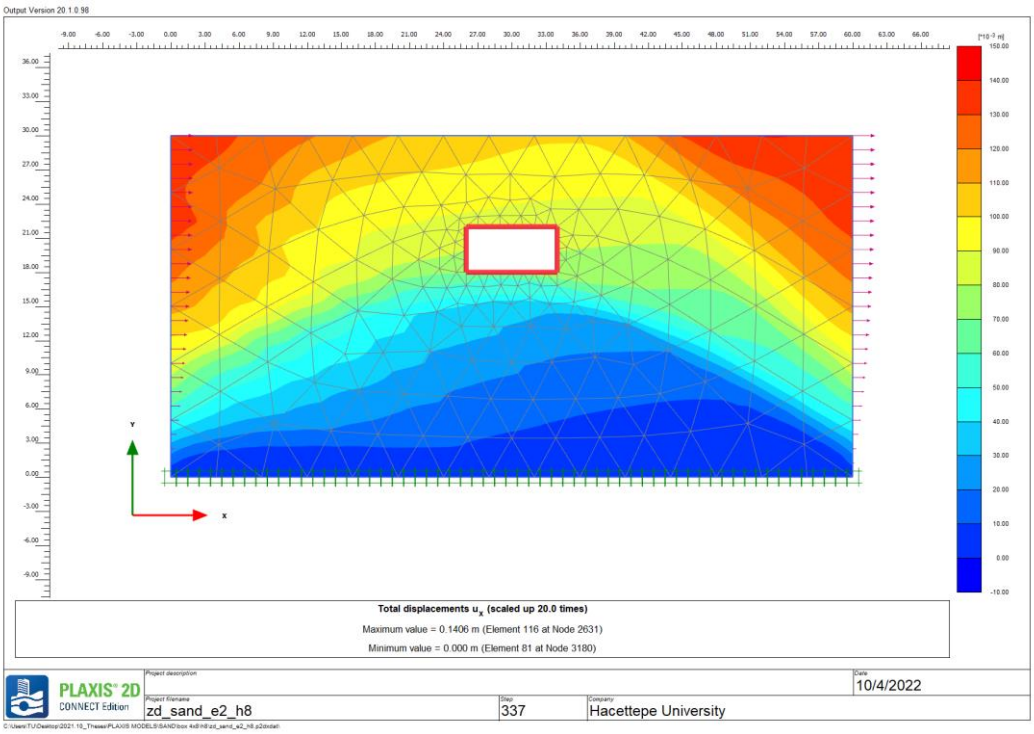

Figure 71 Contour of total displacements (u_x) for ZD sand model under Chuetsu-oki earthquake excitation in PLAXIS 2D

Nodes at the bottom of the mesh were constrained in all directions. The horizontal displacement behavior of rectangular box structure can be seen in Figure 72.

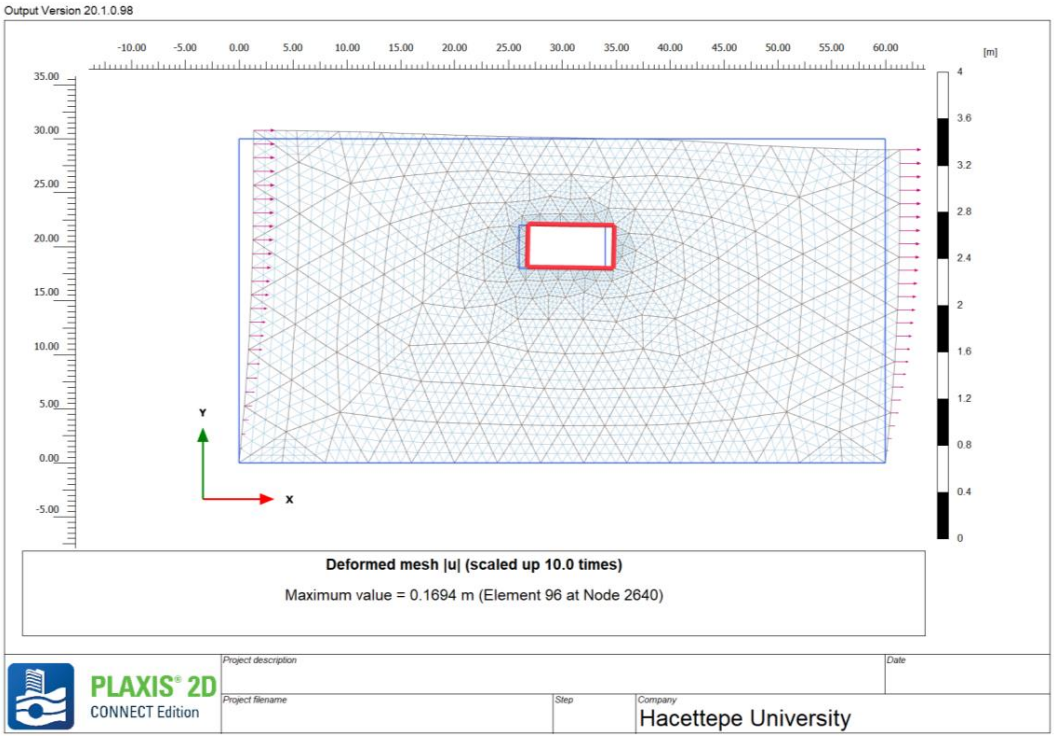

Figure 72 Configuration of the model for the final stage corresponding to the imposed of the displacement field

After the final stage, maximum horizontal displacements were calculated in PLAXIS 2D. The horizontal displacement of the plate at the top and the bottom point was shown in Table 8.

Table 8 Soil – structure interaction displacement of the plate

Soil Class and Type	PGA (g)	PGV (m/s)	SSI Displacement of Top Point of The Plate (Point A) (cm)	SSI Displacement of Bottom Point of The Plate (Point B) (cm)	Δ_S (cm)
ZD Sand	0.45	0.48	8.48	7.58	0.90

Based on these calculations, racking ratio was determined using following equation and presented in Table 9.

$$R = \frac{\Delta_s}{\Delta_{ff}}$$

Table 9 Racking coefficient result of the analysis

Δ_{ff} (cm)	Δ_s (cm)	Racking Coefficient (R)
1.02	0.90	0.88

The flexibility ratio is a measure of the relative racking stiffness of the surrounding soil to the racking stiffness of the structure (NCHRP, 2008). Flexibility ratio of the rectangular structure was calculated in the following equation.

$$F = \frac{G_m W}{K_s H}$$

The structural racking stiffness (Ks) was determined from structural frame analysis. In order to obtain the racking stiffness by using SAP2000, a unit lateral force was applied at the top level of the structure as depicted in Figure 73 and the resulting horizontal displacement was observed. While the bottom of the structure was restrained against translation, but with the joints free to rotate in these analyses. The material properties of the structural plates are given in Table 4 and Table 5 in the previous chapter.

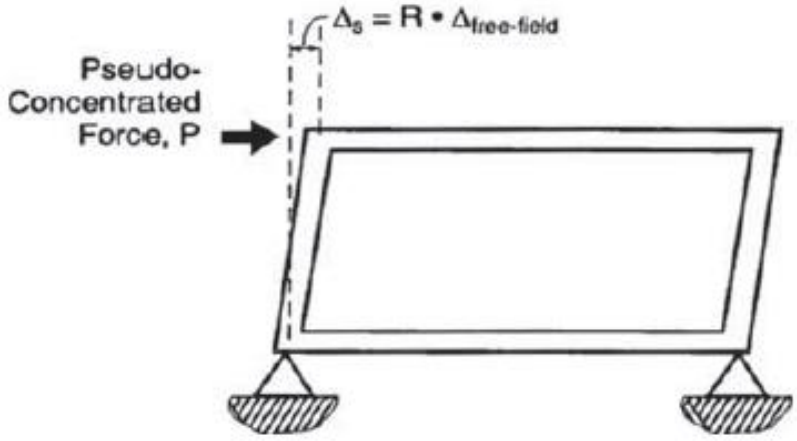

Figure 73 Simplified frame analysis of structural racking stiffness (NCHRP,2008)

Flexibility ratio of the rectangular box structure was calculated as 0.97 in this analysis.

Table 10 Racking coefficient and flexibility ratio of the sample case

Structure Type	Racking Coefficient	Flexibility Ratio
Type II	0.88	0.97

In Appendix A, the all results of flexibility ratio and racking coefficient were presented.

4.2. Flexibility Ratio – Racking Coefficient Graphs

This section is devoted to the demonstration of the results of the FE analysis conducted for the cases described in the previous chapter.

The effects of the flexibility ratio (varying between 0.3 and 5.5) for different case of the burial depth ratio h/a (varying between the two extreme cases of h/a = 0.17 and h/a = 2.0) on buried rectangular structures were examined.

Also, the effect of lining thickness on R-F was investigated. For this purpose, two different lining thicknesses were selected for Structure V.

Figure 74 shows the results of the analyses in terms of racking coefficient of the structures versus flexibility ratio for sand and clay soils based on different case and soil parameters.

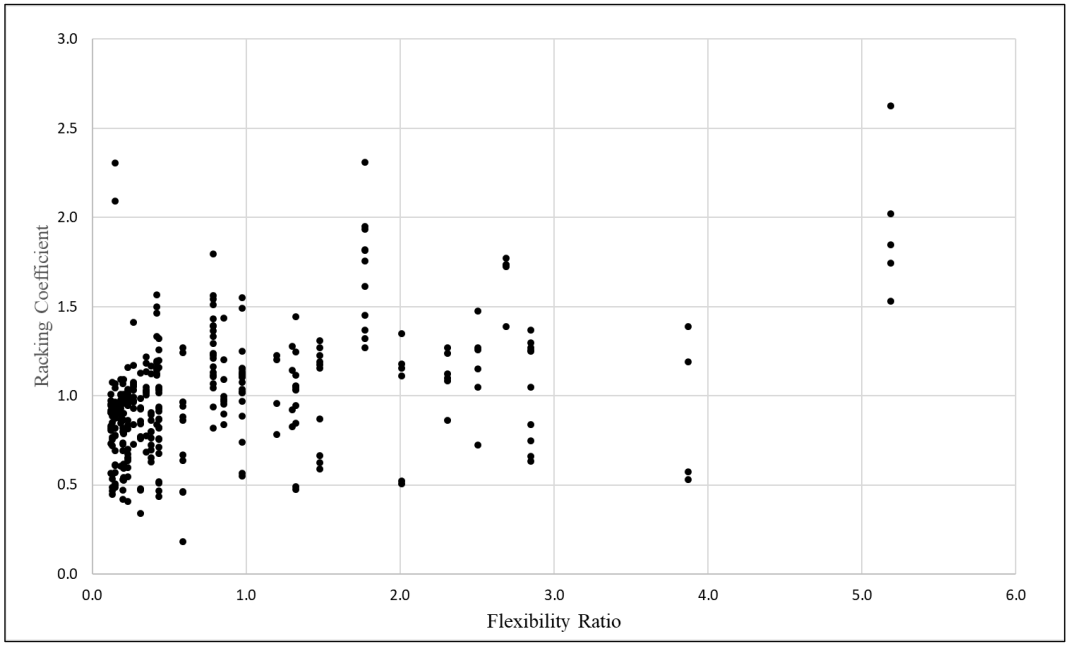

Figure 74 Flexibility ratio F versus racking ratio R for different soil types and structures

After the results obtained from these analyzes were separated according to different burial depth and soil type, the trend effect of the data was determined. For this purpose, the trend line equation was proposed for the sand and clay data. The trend data were calculated by using the trend line equation and the results for sand and clay soil are presented in Figure 75 and Figure 76, respectively.

The R-F relations computed for both thickness with 0.5m and 1.0 in Structure V given in Figure 77.

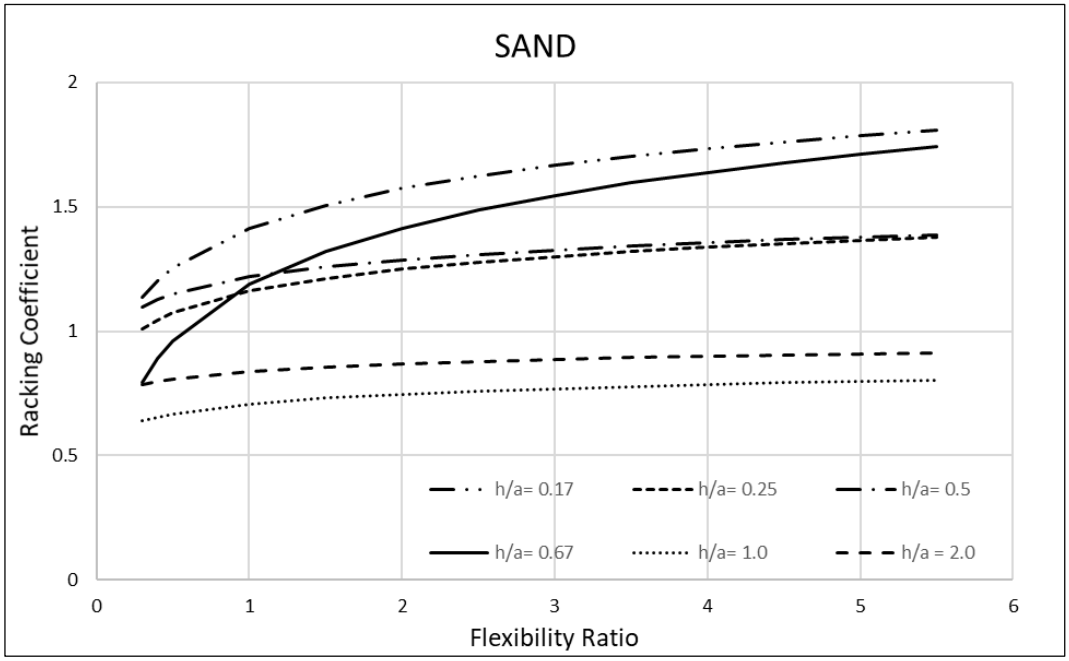

Figure 75 Flexibility ratio F versus racking ratio R for sand soils based on different burial depth ratio

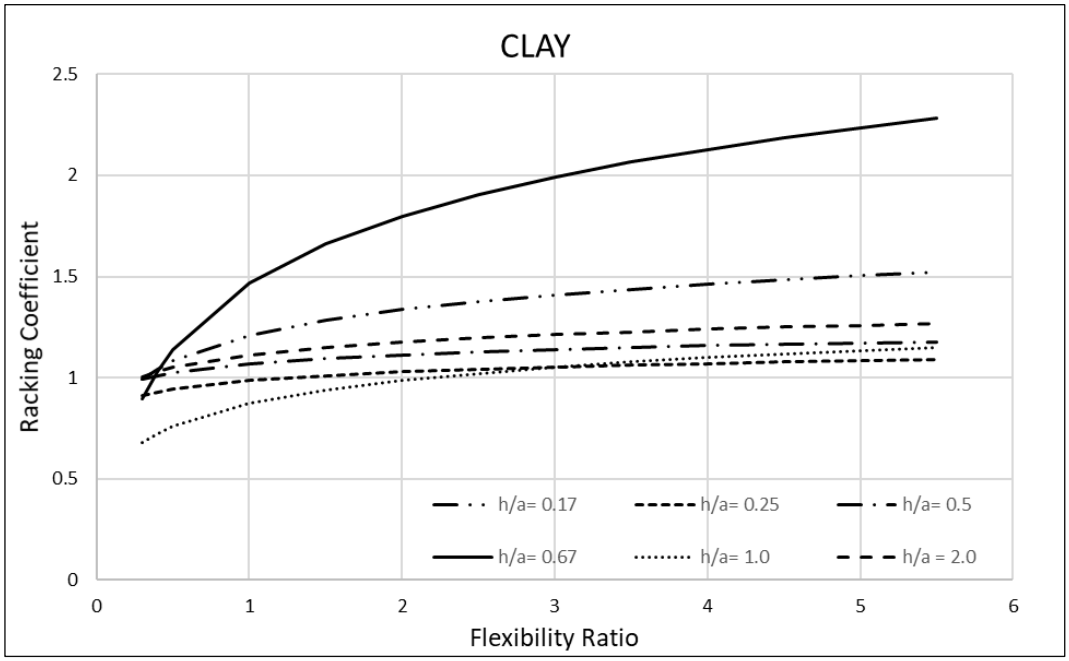

Figure 76 Flexibility ratio F versus racking ratio R for clay soils based on different burial depth ratio

The observation of the results is shown in Figure 75 is:

- The analyses performed for various types of structures for h/a ≤ 1 and for F <1, no proper trend was observed between the flexibility ratio and the racking coefficient. However, as expected, the racking coefficient increases as the flexibility ratio increases.
- For h/a ≥ 1, the h/a ratios also increase with increasing racking coefficient for a constant flexibility ratio.

The observation of the results is shown in Figure 76 is:

- For rectangular box structures having small depth ratio h/a, especially for h/a <1, flexibility ratio has no trends.

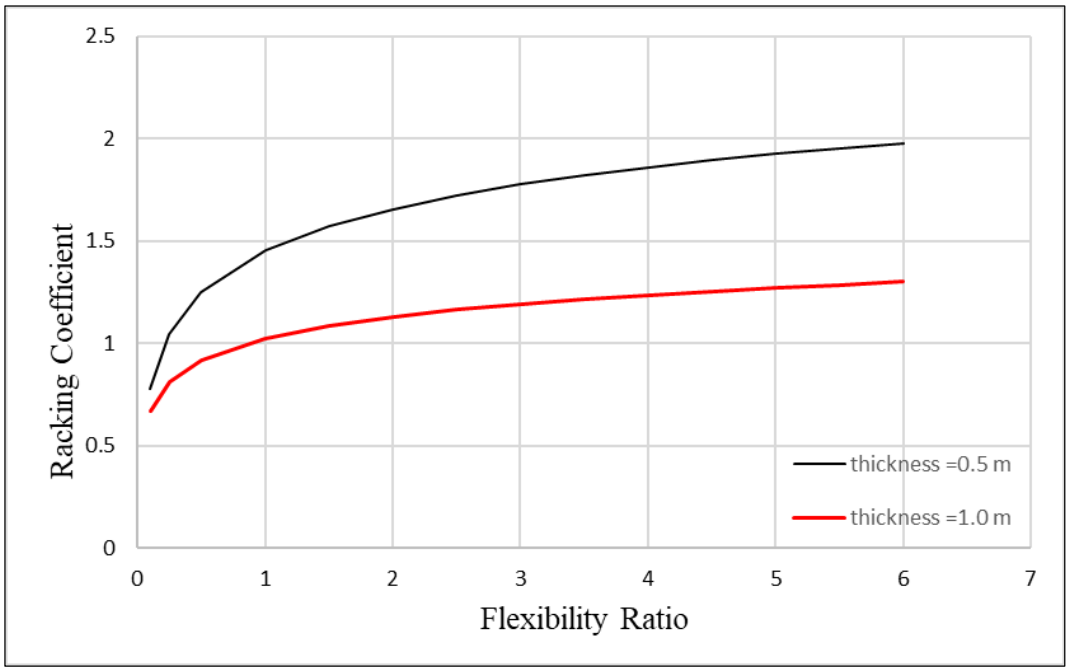

Figure 77 Flexibility ratio F versus racking coefficient R for Structure V based on different lining thickness

The comparison indicates the racking coefficient much more increase as the lining thickness for a constant flexibility ratio between two cases.

4.3. Proposed Equation

The next step is the development of a simplified empirical equation, which can be further used in assessing the horizontal deformation (or racking displacement based on soil-structure-interaction) of the rectangular structures during earthquake. Based on the results of the analyses, a simplified new equation incorporating soil-structure interaction for the racking deformation analysis of rectangular structures was proposed.

For this purpose, parameters affecting the displacement value have been determined. These parameters are: soil type, peak ground acceleration (PGA), peak ground velocity (PGV), shear wave velocity (Vs), flexibility ratio (F), racking coefficient (R), burial depth of the structure (h), width of the structure (a), height of the structure (b). Using all combinations of these parameters, various models have been tried. The most appropriate one which give the closest displacement value has been chosen among these parameters. For example, it was seen that the geometrical properties a, b, and burial depth of the structure h were seen to have nearly no effect if they are used without any further corrections. However, instead of using those values alone, using flexibility ratio values resulted in appropriate match with the values obtained from numerical analyses.

At the beginning, the proposed equation is correlated with the peak ground acceleration (PGA), shear wave velocity and flexibility ratio as they are found to be the most important parameters. Several parametric combinations were tried to find the best formulation of the parameters which gives the most suitable calculated FEM results.

A simplified equation for determining displacement difference of the box structure is proposed along with following equation:

$$\ln(\Delta) = \left[\frac{3.6 \times (\mathrm{F})^{0.02}}{0.057 \times \left(\ln\left(\frac{\mathrm{PGA}}{\mathrm{Vs}} \right) \right)^2} \right]^{1.6}$$

where

Δ	Displacement difference between the bottom and top elevations of the rectangular box structures (mm)
F	Flexibility ratio

PGA Peak ground acceleration (g)

V_s Shear wave velocity (m/s)

The purpose was to obtain a matching result between calculated and predicted results values and to propose new equation for displacement difference between top and bottom elevation of the structure.

It should be noted that sand and clay soils which are the same soil class have similar displacement response in conducted analysis. So, soil type is not considered in the proposed equation.

Displacement difference, which were calculated from the PLAXIS 2D and calculated by the proposed relations, are comparatively presented in Figure 78 through Figure 82.

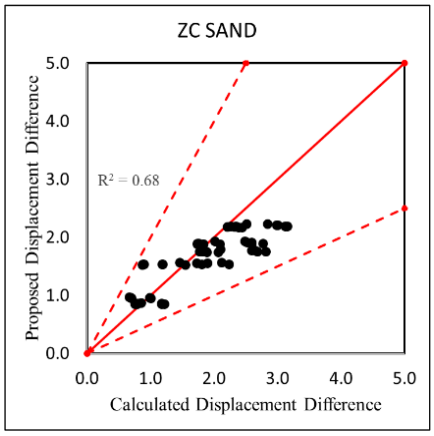

Figure 78 Comparison between the calculated and predicted top and bottom elevation of the box structure by the proposed methodology for ZC sand (based on PGA/Vs)

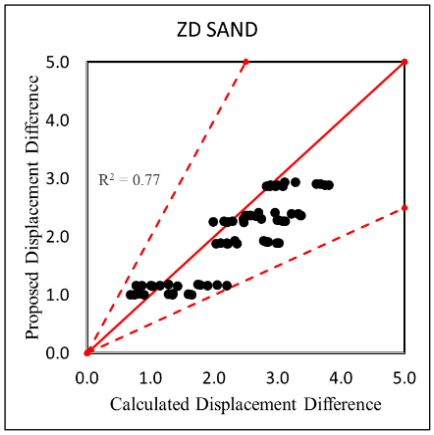

Figure 79 Comparison between the calculated and predicted top and bottom elevation of the box structure by the proposed methodology for ZD sand (based on PGA/Vs)

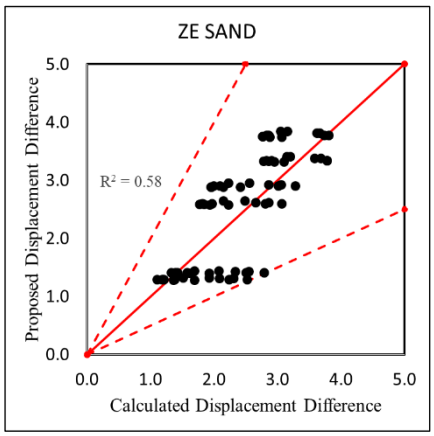

Figure 80 Comparison between the calculated and predicted top and bottom elevation of the box structure by the proposed methodology for ZE sand (based on PGA/Vs)

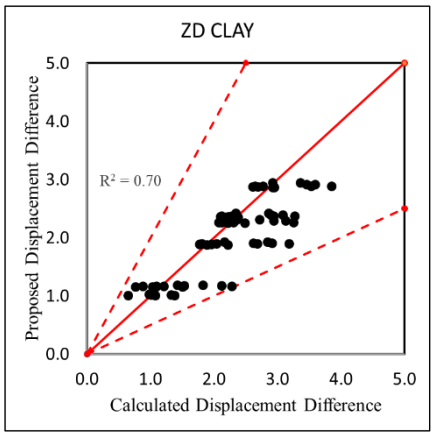

Figure 81 Comparison between the calculated and predicted top and bottom elevation of the box structure by the proposed methodology for ZD clay (based on PGA/Vs)

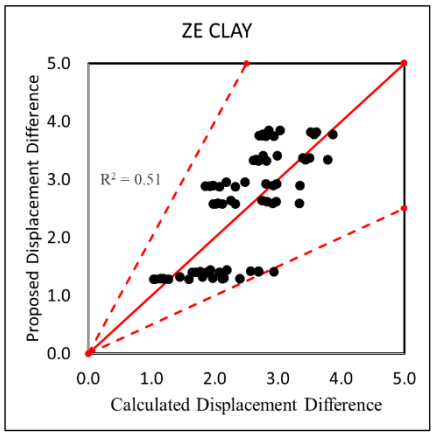

Figure 82 Comparison between the calculated and predicted top and bottom elevation of the box structure by the proposed methodology for ZE clay (based on PGA/Vs)

These figures present a good correlation between the values proposed equation and calculated ones as a consequence of numerical analyses. The solid red line is the diagonal line (1:1) and the dashed red lines show the border of 1:2 and 2:1. All of the data falls within 2:1 and 1:2 range.

However, trying the same form of equation with PGV/V_s which is presented in below, resulted in a better approximation as can be seen in Figure 83 through Figure 87.

$$\ln(\Delta) = \left[\frac{4 \times (F)^{0.048}}{0.5 \times \ln\left(\frac{PGV}{Vs}\right)}\right]^4$$

where

Δ	Displacement difference between the bottom and top elevations of the rectangular box structures (mm)
F	Flexibility ratio
PGV	Peak ground velocity (m/s)
V_s	Shear wave velocity (m/s)

As can be seen from these figures (Figure 83 - Figure 87), using PGV instead of PGA is more reliable results based on soil – structure interaction analysis.

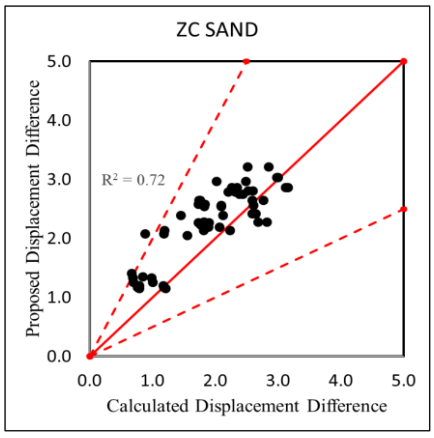

Figure 83 Comparison between the calculated and predicted top and bottom elevation of the box structure by the proposed methodology for ZC Sand (based on PGV/Vs)

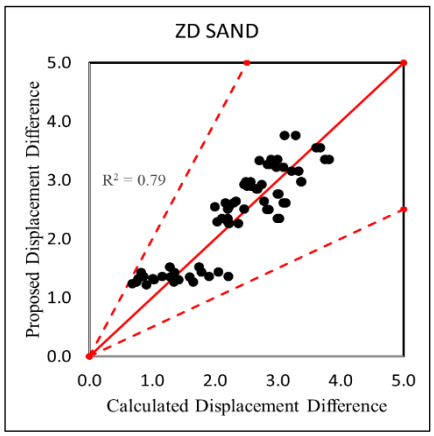

Figure 84 Comparison between the calculated and predicted top and bottom elevation of the box structure by the proposed methodology for ZD Sand (based on PGV/Vs)

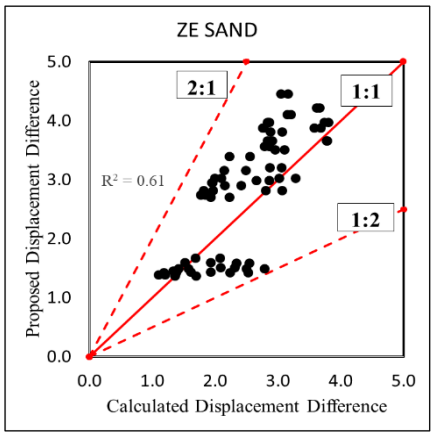

Figure 85 Comparison between the calculated and predicted top and bottom elevation of the box structure by the proposed methodology for ZE Sand (based on PGV/Vs)

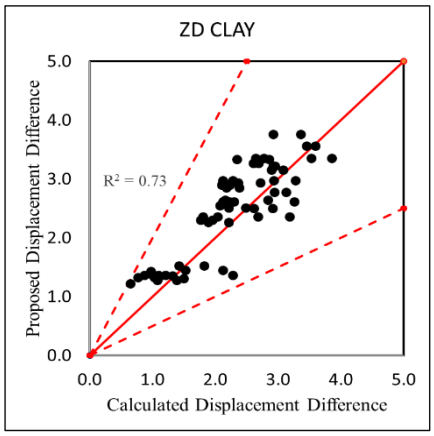

Figure 86 Comparison between the calculated and predicted top and bottom elevation of the box structure by the proposed methodology for ZD Clay (based on PGV/Vs)

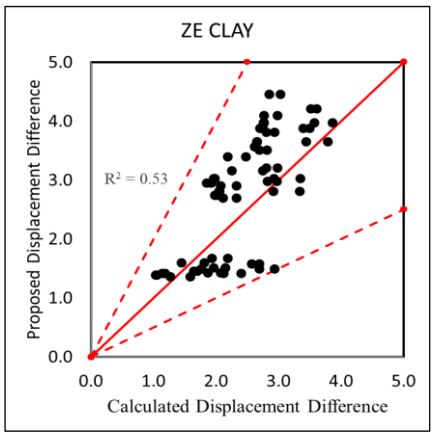

Figure 87 Comparison between the calculated and predicted top and bottom elevation of the box structure by the proposed methodology for ZE Clay (based on PGV/Vs)

As can be seen from these figures, although the results have been presented separately for different soil types, the equation is same for all of them. At the beginning, a different factor for sand and clay has been defined, however it was seen that these factors were very close to each other. For this reason, this factor has been eliminated to have a simpler form of equation. However, this does not mean that, there is no difference in soil response between sand and clay, but for the limited number of cases we use in these analyses, it was not possible to see the difference.

5. CONCLUSIONS

A comprehensive numerical study on the behavior of buried rectangular structures during earthquakes was presented. The simplified frame methodology is used to estimate seismic response in buried rectangular structures. Within this scope, pseudo-static finite element analyses were conducted accounting for the effects of the geometry of the box structure, the type of soil, the peak ground acceleration, the peak ground velocity and the burial depth. Based on the assessments presented in the previous chapters, the following conclusions can be derived:

1. The analyses performed for various types of structures for h/a <1 and for F <1, no proper trend was observed between the flexibility ratio and the racking coefficient in sand soil. However, as expected, the racking ratio increases as the flexibility ratio increases.
2. For h/a ≥ 1, the h/a ratios also increase with increasing racking coefficient for a constant flexibility ratio in sand soil. However, it is not true for other cases.
3. For rectangular box structures having small depth ratio h/a, especially for h/a <1, flexibility ratio has not any trend in clay soil.
4. The numerical results show that the displacement difference of top and bottom elevation of box structure are not exactly based on soil type. Sand and clay soils which are the same soil class have very similar response for this condition. For this reason, in addition to the soil type, other soil and structure parameters should also be considered in the analysis.
5. A simplified new equation was proposed considering several geotechnical and structural parameters based on soil-structure interaction for the racking deformation analysis of rectangular structures. The most appropriate parameters which give the closest results has been determined by combining and testing various parameters. As a result, flexibility ratio, shear wave velocity, peak ground velocity gives good matches with the finite element analysis results.
6. The results showed that the displacement difference of top and bottom elevation of box structure values from the numerical analysis are consistent with values from simplified proposed solutions. Moreover, it is noticed that the parameter of peak ground velocity gives more realistic results than the parameter of peak ground acceleration in proposed equation.

7. A simplified equation for predicting the displacement difference is proposed based on flexibility ratio, peak ground velocity and shear wave velocity:

$$\ln(\Delta) = \left[\frac{4 \times (\mathrm{F})^{0.048}}{0.5 \times \ln\left(\frac{\mathrm{PGV}}{\mathrm{Vs}}\right)}\right]^4$$

Although it is known that this equation does not cover a wide range, it can be seen that it predicts the displacement difference with a good accuracy, in the range of 1:2. However, it is recommended to use this simplified equation for only preliminary purposes as it has many limitations, i.e.: limited number of soil and structural properties, number of earthquake records used and etc.

In the future studies,

- Further analysis can be performed using different soil and structure parameters for more accurate results. In addition to pseudo-static analysis, a safe design can be revealed by comparing the results obtained by performing dynamic analyzes.
- For the confirmation of finite element analysis and proposed equation results, precise model test such as centrifuge modelling need to be conducted.
- In this study, groundwater effect is ignored but analysis can be performed considering this effect according to site-specific conditions. It should be considered that soil deformations and seismic triggering are affecting the pore pressure development and soil liquefaction can occur in saturated soils. This effect can be investigated in future studies.
- Any movement of the buried structure affects the surface settlement. For this purpose, this effect can be investigated considering soil-structure-interaction.
- In addition to racking behavior effect, rocking response of the section of the rectangular structure can be investigated during seismic excitation.
- The buried rectangular box structure response can be affected the presence of the temporary wall. Due to this reason, shoring wall can be added in construction stage phase in PLAXIS 2D.

.

6. REFERENCES

- Anderson, D.G., Martin, G.R., Lam, I., Wang, J.N., 2008. NCHRP 611 – Seismic Analysis and design of Retaining Walls, Buried Structures, Slopes, and Embankments. Washington, DC.
- Bobet, A., 2010. Drained and undrained response of deep tunnels subjected to far-field shear loading. Tunn. Undergr. Space Technol. 25 (1), 21–31.
- Brinkgreve R B J, Kumarswamy S, Swolfs W M, Zampich L and Manoj N R (2019). PLAXIS 2D Tutorial Manual CONNECT Edition V20. Plaxis
- Cilingir, U., Madabhushi, G., 2011a. Effect of depth on the seismic response of square tunnels. Soils Found. 51 (3), 449–457.
- Debiasi, E., Gajo, A., and Zonta, D.,2013. On the seismic response of shallow-buried rectangular structures. Tunnelling and Underground Space Technology, Vol. 38, pp. 99–113.
- FHWA., 2009. Technical Manual for Design and Construction of Road Tunnels — Civil Elements, U.S. Department of Transportation, Federal Highway Administration, Publication No. FHWA-NHI-10-034.
- Gordo-Monsó, C., González-Galindo, J., Olalla-Marañón, C., 2019. A closed-form solution for the seismic racking and rocking behavior of rectangular tunnels. Tunnel Underground Sp. Technol. 88, 87–97.
- Gordo-Monsó, C., González-Galindo, J., Olalla-Marañón, C., 2021. Enhanced Simplified Method for Pseudostatic Analysis of Seismic Internal Forces in Rectangular Underground Structures. Journal of Geotechnical and Geoenvironmental Engineering, Vol. 147, Issue 9.
- Hashash, Y.M.A., Hook, J.J., Schmidt, B., Yao, J.I.C., 2001. Seismic design and analysis of underground structures. Tunnel Underground Space Technol. 16 (4), 247–293.
- Hashash, Y. M. A., Karina, K., Koutsoftas, D., & O'Riordan, N. (2010). Seismic design considerations for underground box structures. In Earth Retention Conference 3 - Proceedings of the 2010 Earth Retention Conference (208 GSP ed., pp. 620-637). (Geotechnical Special Publication; Vol. 384, No. 208 GSP).
- Hashash, Y.M.A., Phillipes, C. & Groholski D. 2010. Recent Advances in Non-linear site response analysis. Fifth International Conference on Recent Advances

in Geotechnical Earthquake Engineering and Soil Dynamics, San Diego, California, 1-21.

- Hashash, Y.M.A., Dashti, S., Romero, M.I., Ghayoomi, M. & Musgrove M. 2015. Evaluation of 1-D seismic site response modeling of sand using centrifuge experiments. Soil Dynamics and Earthquake Engineering, 78, 19–31.
- Hashash, Y.M.A., Musgrove, M.I., Harmon, J.A., Groholski, D.R., Phillips, C.A., and Park, D. (2016). "DEEPSOIL 6.1, User Manual. Urbana, IL, Board of Trustees of University of Illinois at Urbana-Champaign
- Hashash, Y.M.A., Musgrove, M.I., Harmon, J.A., Okan, I., Xing, G., Numanoglu, O., Groholski, D.R., Phillips, C.A., and Park, D. (2020) "DEEPSOIL 7.0, User Manual". Urbana, IL, Board of Trustees of University of Illinois at Urbana-Champaign.
- Hendron, A. J., Jr., & Ferna´ndez, G. (1983). Dynamic and static design considerations for underground chambers. In Seismic Design of Embankments and Caverns, ASCE Symposium, Philadelphia, Pennsylvania (pp. 157–197).
- Huo, H., Bobet, A., Ramírez, J., 2005. Load transfer mechanisms between underground structure and surrounding ground: evaluation of the failure of the Daikai station. ASCE, J. Geotech. Geoenviron. Eng. 131 (12), 1522–1533.
- Huo, H., Bobet, A., Fernández, G., Ramírez, J., 2006. Analytical solution for deep rectangular structures subjected to far-field shear stresses. Tunn. Undergr. Space Technol. 21 (6), 613–625.
- Japan Society of Civil Engineers 1975. Seismic design of immersed tunnels. Tokyo
- McKenna, F., Scott, M.H., Fenves, G.L., 2010. Nonlinear finite-element analysis software architecture using object composition. J. Comput. Civ. Eng. 24, 95–107.
- Merritt, J. L., Monsees, J. E., & Hendron, A.J., Jr. (1985). Seismic design of underground structures. In Proc. rapid excavation and tunneling conference (Vol. 1, pp. 104 131). New York, New York.
- Owen, G. N. and Scholl, R. E. (1981). Earthquake engineering of large underground structures, Federal Highway Administration, Report No: FHWA/RD-80/195.
- Pacific Earthquake Engineering Research Center, 2005. PEER Strong Motion Database on Line. Berkley. https://peer.berkeley.edu/peer-strong-ground-motion-databases

- Patil, et al., 2018. Behavior of shallow tunnel in soft soil under seismic conditions. Tunn. Undergr. Space Technol. 82, 30–38.
- Penzien, J., 2000. Seismically induced racking of tunnel linings. J. Earthquake Eng. Struct. Dynam. 29, 683–691.
- Republic of Turkey Ministry of Transport and Infrastructure (2020). Turkish Highways and Railways Tunnels and Other Ground Structures Earthquake Code
- SAP 2000. Structural Software for Analysis and Design. Computers and Structures, Inc. Berkeley, California, USA.
- Seed, H.B. and Whitman, R.V. (1970). "Design of Earth Retaining Structures for Dynamic Loads," ASCE Specialty Conference, Lateral Stresses in the Ground and Design of Earth Retaining Structures, Cornell Univ., Ithaca, New York, 103–147.
- Seed H.B., Idriss I.M., 1970. Soil moduli and damping factors for dynamic response analysis, Report no. UCB/EERC-70/10, University of California, Berkeley.
- St. John, C.M., Zahrah, T.F., 1987. A seismic design of underground structures, Tunnel. Undergr. Space Technol., vol. 2, no. 2.
- Tsinidis, G., 2017. Response characteristics of rectangular tunnels in soft soil subjected to transversal ground shaking. Tunn. Undergr. Space Technol. 62, 1–22.
- Tsinidis, G., Pitilakis, K., 2018. Improved R-F relations for the transversal seismic analysis of rectangular tunnels. Soil Dyn. Earthquake Eng. 107, 48–65.
- TBEC. (2018). Turkish Seismic Earthquake Code. Retrieved from https://www.resmigazete.gov.tr/eskiler/2018/03/20180318M1-2-1.pdf
- Vucetic, M. and Dobry, R. 1991. Effect of soil plasticity on cyclic response. Journal of geotechnical engineering, 117, 89-107
- Wang, J.N., 1993. Seismic Design of Tunnels: A State-of-the-art approach, Monograph, monograph 7. Parsons, Brinckerhoff. Quade and Douglas Inc., New York.
- Wood, J.H., 1973. Earthquake Induced Soil Pressures on Structures, PhD Thesis, California Institute of Technology, Pasadena, CA.

APPENDICES

APPENDIX A – Racking coefficients values based on different structure types and soil classes

Structure Type	Soil Class	Soil Type	Shear Wave Velocity (m/s)	Embedment Depth (h)	Racking Coefficient
I	ZC	Sand	500	2	1.237
I	ZC	Sand	500	2	1.122
I	ZC	Sand	500	2	1.099
I	ZC	Sand	500	8	1.268
I	ZC	Sand	500	8	0.862
I	ZC	Sand	500	8	1.083
I	ZC	Sand	360	2	1.225
I	ZC	Sand	360	2	1.201
I	ZC	Sand	360	8	0.784
I	ZC	Sand	360	8	0.958
II	ZC	Sand	500	2	1.270
II	ZC	Sand	500	2	1.299
II	ZC	Sand	500	2	1.047
II	ZC	Sand	500	8	1.255
II	ZC	Sand	500	8	0.633
II	ZC	Sand	500	8	0.840
II	ZC	Sand	360	2	1.225
II	ZC	Sand	360	2	1.174
II	ZC	Sand	360	8	0.665
II	ZC	Sand	360	8	0.870
III	ZC	Sand	500	2	1.367
III	ZC	Sand	500	2	1.249
III	ZC	Sand	500	8	0.746
III	ZC	Sand	500	8	0.661
III	ZC	Sand	360	2	1.190
III	ZC	Sand	360	2	1.309
III	ZC	Sand	360	2	1.271
III	ZC	Sand	360	8	1.154
III	ZC	Sand	360	8	0.624
III	ZC	Sand	360	8	0.590
IV	ZC	Sand	500	2	1.386
IV	ZC	Sand	500	2	1.191
IV	ZC	Sand	500	8	0.532
IV	ZC	Sand	500	8	0.575
IV	ZC	Sand	360	2	1.180
IV	ZC	Sand	360	2	1.351
IV	ZC	Sand	360	2	1.155

Structure Type	Soil Class	Soil Type	Shear Wave Velocity (m/s)	Embedment Depth (h)	Racking Coefficient
IV	ZC	Sand	360	8	1.111
IV	ZC	Sand	360	8	0.508
IV	ZC	Sand	360	8	0.523
V (t=0.5 m)	ZC	Sand	500	2	1.744
V (t=0.5 m)	ZC	Sand	500	2	2.628
V (t=0.5 m)	ZC	Sand	500	2	1.530
V (t=0.5 m)	ZC	Sand	500	8	1.848
V (t=0.5 m)	ZC	Sand	500	8	2.020
V (t=0.5 m)	ZC	Sand	360	2	1.772
V (t=0.5 m)	ZC	Sand	360	2	1.390
V (t=0.5 m)	ZC	Sand	360	8	1.731
V (t=0.5 m)	ZC	Sand	360	8	1.725
V (t=0.5 m)	ZC	Sand	360	8	1.737
V (t=1.0 m)	ZC	Sand	500	2	1.256
V (t=1.0 m)	ZC	Sand	500	2	1.477
V (t=1.0 m)	ZC	Sand	500	2	1.153
V (t=1.0 m)	ZC	Sand	500	8	1.270
V (t=1.0 m)	ZC	Sand	500	8	0.723
V (t=1.0 m)	ZC	Sand	500	8	1.047
V (t=1.0 m)	ZC	Sand	360	2	1.278
V (t=1.0 m)	ZC	Sand	360	2	1.144
V (t=1.0 m)	ZC	Sand	360	8	0.828
V (t=1.0 m)	ZC	Sand	360	8	0.920
I	ZD	Sand	300	2	1.509
I	ZD	Sand	300	2	1.233
I	ZD	Sand	300	8	1.132
I	ZD	Sand	300	8	0.939
I	ZD	Sand	300	8	0.820
I	ZD	Sand	200	2	1.049
I	ZD	Sand	200	2	1.137
I	ZD	Sand	200	2	1.182
I	ZD	Sand	200	8	1.004
I	ZD	Sand	200	8	0.777
I	ZD	Sand	200	8	0.685
II	ZD	Sand	300	2	1.491
II	ZD	Sand	300	2	1.156
II	ZD	Sand	300	8	0.968
II	ZD	Sand	300	8	0.884
II	ZD	Sand	300	8	0.740
II	ZD	Sand	200	2	0.915
II	ZD	Sand	200	2	1.199
II	ZD	Sand	200	2	1.158

Structure Type	Soil Class	Soil Type	Shear Wave Velocity (m/s)	Embedment Depth (h)	Racking Coefficient
II	ZD	Sand	200	8	0.760
II	ZD	Sand	200	8	0.714
II	ZD	Sand	200	8	0.677
III	ZD	Sand	300	2	1.149
III	ZD	Sand	300	2	1.550
III	ZD	Sand	300	2	1.249
III	ZD	Sand	300	8	1.102
III	ZD	Sand	300	8	0.567
III	ZD	Sand	300	8	0.548
III	ZD	Sand	200	2	1.049
III	ZD	Sand	200	2	1.256
III	ZD	Sand	200	2	1.320
III	ZD	Sand	200	8	1.018
III	ZD	Sand	200	8	0.511
III	ZD	Sand	200	8	0.519
IV	ZD	Sand	300	2	1.116
IV	ZD	Sand	300	2	1.443
IV	ZD	Sand	300	2	1.245
IV	ZD	Sand	300	8	1.032
IV	ZD	Sand	300	8	0.476
IV	ZD	Sand	300	8	0.490
IV	ZD	Sand	200	2	0.941
IV	ZD	Sand	200	2	1.268
IV	ZD	Sand	200	2	1.243
IV	ZD	Sand	200	8	0.863
IV	ZD	Sand	200	8	0.458
IV	ZD	Sand	200	8	0.462
V (t=0.5 m)	ZD	Sand	300	2	1.814
V (t=0.5 m)	ZD	Sand	300	2	1.935
V (t=0.5 m)	ZD	Sand	300	2	1.368
V (t=0.5 m)	ZD	Sand	300	8	1.755
V (t=0.5 m)	ZD	Sand	300	8	1.949
V (t=0.5 m)	ZD	Sand	300	8	1.320
V (t=0.5 m)	ZD	Sand	200	2	1.430
V (t=0.5 m)	ZD	Sand	200	2	1.797
V (t=0.5 m)	ZD	Sand	200	2	1.541
V (t=0.5 m)	ZD	Sand	200	8	1.365
V (t=0.5 m)	ZD	Sand	200	8	1.292
V (t=0.5 m)	ZD	Sand	200	8	1.043
V (t=1.0 m)	ZD	Sand	300	2	1.434
V (t=1.0 m)	ZD	Sand	300	2	1.202
V (t=1.0 m)	ZD	Sand	300	8	0.900

Structure Type	Soil Class	Soil Type	Shear Wave Velocity (m/s)	Embedment Depth (h)	Racking Coefficient
V (t=1.0 m)	ZD	Sand	300	8	1.093
V (t=1.0 m)	ZD	Sand	300	8	0.839
V (t=1.0 m)	ZD	Sand	200	2	0.862
V (t=1.0 m)	ZD	Sand	200	2	1.122
V (t=1.0 m)	ZD	Sand	200	2	1.167
V (t=1.0 m)	ZD	Sand	200	8	0.652
V (t=1.0 m)	ZD	Sand	200	8	0.763
V (t=1.0 m)	ZD	Sand	200	8	0.696
I	ZE	Sand	150	2	0.970
I	ZE	Sand	150	2	1.008
I	ZE	Sand	150	2	1.091
I	ZE	Sand	150	8	0.897
I	ZE	Sand	150	8	0.897
I	ZE	Sand	150	8	0.605
I	ZE	Sand	120	2	0.918
I	ZE	Sand	120	2	0.955
I	ZE	Sand	120	2	1.010
I	ZE	Sand	120	8	0.820
I	ZE	Sand	120	8	0.831
I	ZE	Sand	120	8	0.567
II	ZE	Sand	150	2	0.836
II	ZE	Sand	150	2	0.979
II	ZE	Sand	150	2	1.036
II	ZE	Sand	150	8	0.648
II	ZE	Sand	150	8	0.701
II	ZE	Sand	150	8	0.547
II	ZE	Sand	120	2	0.774
II	ZE	Sand	120	2	0.874
II	ZE	Sand	120	2	1.045
II	ZE	Sand	120	8	0.570
II	ZE	Sand	120	8	0.608
II	ZE	Sand	120	8	0.487
III	ZE	Sand	150	2	0.984
III	ZE	Sand	150	2	1.029
III	ZE	Sand	150	2	1.158
III	ZE	Sand	150	8	0.948
III	ZE	Sand	150	8	0.946
III	ZE	Sand	150	8	0.408
III	ZE	Sand	120	2	0.941
III	ZE	Sand	120	2	0.965
III	ZE	Sand	120	2	1.069
III	ZE	Sand	120	8	0.897

Structure Type	Soil Class	Soil Type	Shear Wave Velocity (m/s)	Embedment Depth (h)	Racking Coefficient
III	ZE	Sand	120	8	0.911
III	ZE	Sand	120	8	0.500
IV	ZE	Sand	150	2	0.857
IV	ZE	Sand	150	2	0.935
IV	ZE	Sand	150	2	1.127
IV	ZE	Sand	150	8	0.759
IV	ZE	Sand	150	8	0.773
IV	ZE	Sand	150	8	0.342
IV	ZE	Sand	120	2	0.800
IV	ZE	Sand	120	2	0.865
IV	ZE	Sand	120	2	1.068
IV	ZE	Sand	120	8	0.693
IV	ZE	Sand	120	8	0.727
IV	ZE	Sand	120	8	0.419
V (t=0.5 m)	ZE	Sand	150	2	1.195
V (t=0.5 m)	ZE	Sand	150	2	1.462
V (t=0.5 m)	ZE	Sand	150	2	1.568
V (t=0.5 m)	ZE	Sand	150	8	1.117
V (t=0.5 m)	ZE	Sand	150	8	1.499
V (t=0.5 m)	ZE	Sand	150	8	0.838
V (t=0.5 m)	ZE	Sand	120	2	1.032
V (t=0.5 m)	ZE	Sand	120	2	1.172
V (t=0.5 m)	ZE	Sand	120	2	1.412
V (t=0.5 m)	ZE	Sand	120	8	0.930
V (t=0.5 m)	ZE	Sand	120	8	0.973
V (t=0.5 m)	ZE	Sand	120	8	0.726
V (t=1.0 m)	ZE	Sand	150	2	0.791
V (t=1.0 m)	ZE	Sand	150	2	1.007
V (t=1.0 m)	ZE	Sand	150	2	1.091
V (t=1.0 m)	ZE	Sand	150	8	0.543
V (t=1.0 m)	ZE	Sand	150	8	0.787
V (t=1.0 m)	ZE	Sand	150	8	0.595
V (t=1.0 m)	ZE	Sand	120	2	0.720
V (t=1.0 m)	ZE	Sand	120	2	0.888
V (t=1.0 m)	ZE	Sand	120	2	1.075
V (t=1.0 m)	ZE	Sand	120	8	0.466
V (t=1.0 m)	ZE	Sand	120	8	0.534
V (t=1.0 m)	ZE	Sand	120	8	0.488
I	ZD	Clay	300	2	1.109
I	ZD	Clay	300	2	1.068
I	ZD	Clay	300	8	1.162
I	ZD	Clay	300	8	1.239

Structure Type	Soil Class	Soil Type	Shear Wave Velocity (m/s)	Embedment Depth (h)	Racking Coefficient
I	ZD	Clay	300	8	1.116
I	ZD	Clay	200	2	1.021
I	ZD	Clay	200	2	1.020
I	ZD	Clay	200	2	1.220
I	ZD	Clay	200	8	1.023
I	ZD	Clay	200	8	1.025
I	ZD	Clay	200	8	1.034
II	ZD	Clay	300	2	1.022
II	ZD	Clay	300	2	1.019
II	ZD	Clay	300	8	1.037
II	ZD	Clay	300	8	1.017
II	ZD	Clay	200	2	0.820
II	ZD	Clay	200	2	0.937
II	ZD	Clay	200	2	0.928
II	ZD	Clay	200	8	0.758
II	ZD	Clay	200	8	0.866
II	ZD	Clay	200	8	0.872
III	ZD	Clay	300	2	1.123
III	ZD	Clay	300	2	1.118
III	ZD	Clay	300	2	1.077
III	ZD	Clay	300	8	1.125
III	ZD	Clay	300	8	1.107
III	ZD	Clay	300	8	1.134
III	ZD	Clay	200	2	0.437
III	ZD	Clay	200	2	0.465
III	ZD	Clay	200	2	1.032
III	ZD	Clay	200	8	1.037
III	ZD	Clay	200	8	1.043
III	ZD	Clay	200	8	0.824
IV	ZD	Clay	300	2	1.053
IV	ZD	Clay	300	2	1.052
IV	ZD	Clay	300	2	1.037
IV	ZD	Clay	300	8	1.056
IV	ZD	Clay	300	8	0.845
IV	ZD	Clay	300	8	0.945
IV	ZD	Clay	200	2	0.668
IV	ZD	Clay	200	2	0.963
IV	ZD	Clay	200	2	0.966
IV	ZD	Clay	200	8	0.881
IV	ZD	Clay	200	8	0.183
IV	ZD	Clay	200	8	0.638
V (t=0.5 m)	ZD	Clay	300	2	1.452

Structure Type	Soil Class	Soil Type	Shear Wave Velocity (m/s)	Embedment Depth (h)	Racking Coefficient
V (t=0.5 m)	ZD	Clay	300	2	1.271
V (t=0.5 m)	ZD	Clay	300	8	1.614
V (t=0.5 m)	ZD	Clay	300	8	2.309
V (t=0.5 m)	ZD	Clay	300	8	1.819
V (t=0.5 m)	ZD	Clay	200	2	1.390
V (t=0.5 m)	ZD	Clay	200	2	1.211
V (t=0.5 m)	ZD	Clay	200	2	1.226
V (t=0.5 m)	ZD	Clay	200	8	1.392
V (t=0.5 m)	ZD	Clay	200	8	1.333
V (t=0.5 m)	ZD	Clay	200	8	1.564
V (t=1.0 m)	ZD	Clay	300	2	0.981
V (t=1.0 m)	ZD	Clay	300	2	0.998
V (t=1.0 m)	ZD	Clay	300	8	0.952
V (t=1.0 m)	ZD	Clay	300	8	0.971
V (t=1.0 m)	ZD	Clay	200	2	0.723
V (t=1.0 m)	ZD	Clay	200	2	0.907
V (t=1.0 m)	ZD	Clay	200	2	0.895
V (t=1.0 m)	ZD	Clay	200	8	0.629
V (t=1.0 m)	ZD	Clay	200	8	0.798
V (t=1.0 m)	ZD	Clay	200	8	0.800
I	ZE	Clay	150	2	0.958
I	ZE	Clay	150	2	0.979
I	ZE	Clay	150	2	1.003
I	ZE	Clay	150	8	0.867
I	ZE	Clay	150	8	0.847
I	ZE	Clay	150	8	0.931
I	ZE	Clay	120	2	0.945
I	ZE	Clay	120	2	0.905
I	ZE	Clay	120	2	0.973
I	ZE	Clay	120	8	0.806
I	ZE	Clay	120	8	0.731
I	ZE	Clay	120	8	0.905
II	ZE	Clay	150	2	0.861
II	ZE	Clay	150	2	0.999
II	ZE	Clay	150	2	0.982
II	ZE	Clay	150	8	0.597
II	ZE	Clay	150	8	0.653
II	ZE	Clay	150	8	0.815
II	ZE	Clay	120	2	0.882
II	ZE	Clay	120	2	0.819
II	ZE	Clay	120	2	0.953
II	ZE	Clay	120	8	0.612

Structure Type	Soil Class	Soil Type	Shear Wave Velocity (m/s)	Embedment Depth (h)	Racking Coefficient
II	ZE	Clay	120	8	0.506
II	ZE	Clay	120	8	0.780
III	ZE	Clay	150	2	0.963
III	ZE	Clay	150	2	0.997
III	ZE	Clay	150	2	1.014
III	ZE	Clay	150	8	0.964
III	ZE	Clay	150	8	0.673
III	ZE	Clay	150	8	0.638
III	ZE	Clay	120	2	0.953
III	ZE	Clay	120	2	0.925
III	ZE	Clay	120	2	2.094
III	ZE	Clay	120	8	0.916
III	ZE	Clay	120	8	0.694
III	ZE	Clay	120	8	2.305
IV	ZE	Clay	150	2	0.844
IV	ZE	Clay	150	2	0.924
IV	ZE	Clay	150	2	0.985
IV	ZE	Clay	150	8	0.768
IV	ZE	Clay	150	8	0.470
IV	ZE	Clay	150	8	0.481
IV	ZE	Clay	120	2	0.864
IV	ZE	Clay	120	2	0.819
IV	ZE	Clay	120	2	0.956
IV	ZE	Clay	120	8	0.737
IV	ZE	Clay	120	8	0.471
IV	ZE	Clay	120	8	0.530
V (t=0.5 m)	ZE	Clay	150	2	1.188
V (t=0.5 m)	ZE	Clay	150	2	1.153
V (t=0.5 m)	ZE	Clay	150	2	1.122
V (t=0.5 m)	ZE	Clay	150	8	1.143
V (t=0.5 m)	ZE	Clay	150	8	1.334
V (t=0.5 m)	ZE	Clay	150	8	1.160
V (t=0.5 m)	ZE	Clay	120	2	1.075
V (t=0.5 m)	ZE	Clay	120	2	0.993
V (t=0.5 m)	ZE	Clay	120	2	1.064
V (t=0.5 m)	ZE	Clay	120	8	0.964
V (t=0.5 m)	ZE	Clay	120	8	0.839
V (t=0.5 m)	ZE	Clay	120	8	1.054
V (t=1.0 m)	ZE	Clay	150	2	0.807
V (t=1.0 m)	ZE	Clay	150	2	0.902
V (t=1.0 m)	ZE	Clay	150	2	0.986
V (t=1.0 m)	ZE	Clay	150	8	0.526

Structure Type	Soil Class	Soil Type	Shear Wave Velocity (m/s)	Embedment Depth (h)	Racking Coefficient
V (t=1.0 m)	ZE	Clay	150	8	0.617
V (t=1.0 m)	ZE	Clay	150	8	0.802
V (t=1.0 m)	ZE	Clay	120	2	0.851
V (t=1.0 m)	ZE	Clay	120	2	0.766
V (t=1.0 m)	ZE	Clay	120	2	0.954
V (t=1.0 m)	ZE	Clay	120	8	0.558
V (t=1.0 m)	ZE	Clay	120	8	0.449
V (t=1.0 m)	ZE	Clay	120	8	0.755

*t is represent lining thickness.

APPENDIX B - Flexibility ratio values based on different structure types and soil classes

Structure Type	Soil Class	Soil Type	Shear Wave Velocity (m/s)	Embedment Depth (h)	Flexibility Ratio
I	ZC	Sand	500	2	2.306
I	ZC	Sand	500	2	2.306
I	ZC	Sand	500	2	2.306
I	ZC	Sand	500	8	2.306
I	ZC	Sand	500	8	2.306
I	ZC	Sand	500	8	2.306
I	ZC	Sand	360	2	1.195
I	ZC	Sand	360	2	1.195
I	ZC	Sand	360	8	1.195
I	ZC	Sand	360	8	1.195
II	ZC	Sand	500	2	2.848
II	ZC	Sand	500	2	2.848
II	ZC	Sand	500	2	2.848
II	ZC	Sand	500	8	2.848
II	ZC	Sand	500	8	2.848
II	ZC	Sand	500	8	2.848
II	ZC	Sand	360	2	1.477
II	ZC	Sand	360	2	1.477
II	ZC	Sand	360	8	1.477
II	ZC	Sand	360	8	1.477
III	ZC	Sand	500	2	2.848
III	ZC	Sand	500	2	2.848
III	ZC	Sand	500	8	2.848
III	ZC	Sand	500	8	2.848
III	ZC	Sand	360	2	1.477
III	ZC	Sand	360	2	1.477
III	ZC	Sand	360	2	1.477
III	ZC	Sand	360	8	1.477
III	ZC	Sand	360	8	1.477
III	ZC	Sand	360	8	1.477
IV	ZC	Sand	500	2	3.874
IV	ZC	Sand	500	2	3.874
IV	ZC	Sand	500	8	3.874
IV	ZC	Sand	500	8	3.874
IV	ZC	Sand	360	2	2.008
IV	ZC	Sand	360	2	2.008
IV	ZC	Sand	360	2	2.008
IV	ZC	Sand	360	8	2.008

Structure Type	Soil Class	Soil Type	Shear Wave Velocity (m/s)	Embedment Depth (h)	Flexibility Ratio
IV	ZC	Sand	360	8	2.008
IV	ZC	Sand	360	8	2.008
V (t=0.5 m)	ZC	Sand	500	2	5.188
V (t=0.5 m)	ZC	Sand	500	2	5.188
V (t=0.5 m)	ZC	Sand	500	2	5.188
V (t=0.5 m)	ZC	Sand	500	8	5.188
V (t=0.5 m)	ZC	Sand	500	8	5.188
V (t=0.5 m)	ZC	Sand	360	2	2.689
V (t=0.5 m)	ZC	Sand	360	2	2.689
V (t=0.5 m)	ZC	Sand	360	8	2.689
V (t=0.5 m)	ZC	Sand	360	8	2.689
V (t=0.5 m)	ZC	Sand	360	8	2.689
V (t=1.0 m)	ZC	Sand	500	2	2.504
V (t=1.0 m)	ZC	Sand	500	2	2.504
V (t=1.0 m)	ZC	Sand	500	2	2.504
V (t=1.0 m)	ZC	Sand	500	8	2.504
V (t=1.0 m)	ZC	Sand	500	8	2.504
V (t=1.0 m)	ZC	Sand	500	8	2.504
V (t=1.0 m)	ZC	Sand	360	2	1.298
V (t=1.0 m)	ZC	Sand	360	2	1.298
V (t=1.0 m)	ZC	Sand	360	8	1.298
V (t=1.0 m)	ZC	Sand	360	8	1.298
I	ZD	Sand	300	2	0.786
I	ZD	Sand	300	2	0.786
I	ZD	Sand	300	8	0.786
I	ZD	Sand	300	8	0.786
I	ZD	Sand	300	8	0.786
I	ZD	Sand	200	2	0.349
I	ZD	Sand	200	2	0.349
I	ZD	Sand	200	2	0.349
I	ZD	Sand	200	8	0.349
I	ZD	Sand	200	8	0.349
I	ZD	Sand	200	8	0.349
II	ZD	Sand	300	2	0.971
II	ZD	Sand	300	2	0.971
II	ZD	Sand	300	8	0.971
II	ZD	Sand	300	8	0.971
II	ZD	Sand	300	8	0.971
II	ZD	Sand	200	2	0.432
II	ZD	Sand	200	2	0.432
II	ZD	Sand	200	2	0.432
II	ZD	Sand	200	8	0.432

Structure Type	Soil Class	Soil Type	Shear Wave Velocity (m/s)	Embedment Depth (h)	Flexibility Ratio
II	ZD	Sand	200	8	0.432
II	ZD	Sand	200	8	0.432
III	ZD	Sand	300	2	0.971
III	ZD	Sand	300	2	0.971
III	ZD	Sand	300	2	0.971
III	ZD	Sand	300	8	0.971
III	ZD	Sand	300	8	0.971
III	ZD	Sand	300	8	0.971
III	ZD	Sand	200	2	0.432
III	ZD	Sand	200	2	0.432
III	ZD	Sand	200	2	0.432
III	ZD	Sand	200	8	0.432
III	ZD	Sand	200	8	0.432
III	ZD	Sand	200	8	0.432
IV	ZD	Sand	300	2	1.321
IV	ZD	Sand	300	2	1.321
IV	ZD	Sand	300	2	1.321
IV	ZD	Sand	300	8	1.321
IV	ZD	Sand	300	8	1.321
IV	ZD	Sand	300	8	1.321
IV	ZD	Sand	200	2	0.587
IV	ZD	Sand	200	2	0.587
IV	ZD	Sand	200	2	0.587
IV	ZD	Sand	200	8	0.587
IV	ZD	Sand	200	8	0.587
IV	ZD	Sand	200	8	0.587
V (t=0.5 m)	ZD	Sand	300	2	1.769
V (t=0.5 m)	ZD	Sand	300	2	1.769
V (t=0.5 m)	ZD	Sand	300	2	1.769
V (t=0.5 m)	ZD	Sand	300	8	1.769
V (t=0.5 m)	ZD	Sand	300	8	1.769
V (t=0.5 m)	ZD	Sand	300	8	1.769
V (t=0.5 m)	ZD	Sand	200	2	0.786
V (t=0.5 m)	ZD	Sand	200	2	0.786
V (t=0.5 m)	ZD	Sand	200	2	0.786
V (t=0.5 m)	ZD	Sand	200	8	0.786
V (t=0.5 m)	ZD	Sand	200	8	0.786
V (t=0.5 m)	ZD	Sand	200	8	0.786
V (t=1.0 m)	ZD	Sand	300	2	0.854
V (t=1.0 m)	ZD	Sand	300	2	0.854
V (t=1.0 m)	ZD	Sand	300	8	0.854
V (t=1.0 m)	ZD	Sand	300	8	0.854

Structure Type	Soil Class	Soil Type	Shear Wave Velocity (m/s)	Embedment Depth (h)	Flexibility Ratio
V (t=1.0 m)	ZD	Sand	300	8	0.854
V (t=1.0 m)	ZD	Sand	200	2	0.380
V (t=1.0 m)	ZD	Sand	200	2	0.380
V (t=1.0 m)	ZD	Sand	200	2	0.380
V (t=1.0 m)	ZD	Sand	200	8	0.380
V (t=1.0 m)	ZD	Sand	200	8	0.380
V (t=1.0 m)	ZD	Sand	200	8	0.380
I	ZE	Sand	150	2	0.186
I	ZE	Sand	150	2	0.186
I	ZE	Sand	150	2	0.186
I	ZE	Sand	150	8	0.186
I	ZE	Sand	150	8	0.186
I	ZE	Sand	150	8	0.186
I	ZE	Sand	120	2	0.119
I	ZE	Sand	120	2	0.119
I	ZE	Sand	120	2	0.119
I	ZE	Sand	120	8	0.119
I	ZE	Sand	120	8	0.119
I	ZE	Sand	120	8	0.119
II	ZE	Sand	150	2	0.229
II	ZE	Sand	150	2	0.229
II	ZE	Sand	150	2	0.229
II	ZE	Sand	150	8	0.229
II	ZE	Sand	150	8	0.229
II	ZE	Sand	150	8	0.229
II	ZE	Sand	120	2	0.147
II	ZE	Sand	120	2	0.147
II	ZE	Sand	120	2	0.147
II	ZE	Sand	120	8	0.147
II	ZE	Sand	120	8	0.147
II	ZE	Sand	120	8	0.147
III	ZE	Sand	150	2	0.229
III	ZE	Sand	150	2	0.229
III	ZE	Sand	150	2	0.229
III	ZE	Sand	150	8	0.229
III	ZE	Sand	150	8	0.229
III	ZE	Sand	150	8	0.229
III	ZE	Sand	120	2	0.147
III	ZE	Sand	120	2	0.147
III	ZE	Sand	120	2	0.147
III	ZE	Sand	120	8	0.147
III	ZE	Sand	120	8	0.147

Structure Type	Soil Class	Soil Type	Shear Wave Velocity (m/s)	Embedment Depth (h)	Flexibility Ratio
III	ZE	Sand	120	8	0.147
IV	ZE	Sand	150	2	0.312
IV	ZE	Sand	150	2	0.312
IV	ZE	Sand	150	2	0.312
IV	ZE	Sand	150	8	0.312
IV	ZE	Sand	150	8	0.312
IV	ZE	Sand	150	8	0.312
IV	ZE	Sand	120	2	0.200
IV	ZE	Sand	120	2	0.200
IV	ZE	Sand	120	2	0.200
IV	ZE	Sand	120	8	0.200
IV	ZE	Sand	120	8	0.200
IV	ZE	Sand	120	8	0.200
V (t=0.5 m)	ZE	Sand	150	2	0.418
V (t=0.5 m)	ZE	Sand	150	2	0.418
V (t=0.5 m)	ZE	Sand	150	2	0.418
V (t=0.5 m)	ZE	Sand	150	8	0.418
V (t=0.5 m)	ZE	Sand	150	8	0.418
V (t=0.5 m)	ZE	Sand	150	8	0.418
V (t=0.5 m)	ZE	Sand	120	2	0.267
V (t=0.5 m)	ZE	Sand	120	2	0.267
V (t=0.5 m)	ZE	Sand	120	2	0.267
V (t=0.5 m)	ZE	Sand	120	8	0.267
V (t=0.5 m)	ZE	Sand	120	8	0.267
V (t=0.5 m)	ZE	Sand	120	8	0.267
V (t=1.0 m)	ZE	Sand	150	2	0.202
V (t=1.0 m)	ZE	Sand	150	2	0.202
V (t=1.0 m)	ZE	Sand	150	2	0.202
V (t=1.0 m)	ZE	Sand	150	8	0.202
V (t=1.0 m)	ZE	Sand	150	8	0.202
V (t=1.0 m)	ZE	Sand	150	8	0.202
V (t=1.0 m)	ZE	Sand	120	2	0.129
V (t=1.0 m)	ZE	Sand	120	2	0.129
V (t=1.0 m)	ZE	Sand	120	2	0.129
V (t=1.0 m)	ZE	Sand	120	8	0.129
V (t=1.0 m)	ZE	Sand	120	8	0.129
V (t=1.0 m)	ZE	Sand	120	8	0.129
I	ZD	Clay	300	2	0.786
I	ZD	Clay	300	2	0.786
I	ZD	Clay	300	8	0.786
I	ZD	Clay	300	8	0.786
I	ZD	Clay	300	8	0.786

Structure Type	Soil Class	Soil Type	Shear Wave Velocity (m/s)	Embedment Depth (h)	Flexibility Ratio
I	ZD	Clay	200	2	0.349
I	ZD	Clay	200	2	0.349
I	ZD	Clay	200	2	0.349
I	ZD	Clay	200	8	0.349
I	ZD	Clay	200	8	0.349
I	ZD	Clay	200	8	0.349
II	ZD	Clay	300	2	0.971
II	ZD	Clay	300	2	0.971
II	ZD	Clay	300	8	0.971
II	ZD	Clay	300	8	0.971
II	ZD	Clay	200	2	0.432
II	ZD	Clay	200	2	0.432
II	ZD	Clay	200	2	0.432
II	ZD	Clay	200	8	0.432
II	ZD	Clay	200	8	0.432
II	ZD	Clay	200	8	0.432
III	ZD	Clay	300	2	0.971
III	ZD	Clay	300	2	0.971
III	ZD	Clay	300	2	0.971
III	ZD	Clay	300	8	0.971
III	ZD	Clay	300	8	0.971
III	ZD	Clay	300	8	0.971
III	ZD	Clay	200	2	0.432
III	ZD	Clay	200	2	0.432
III	ZD	Clay	200	2	0.432
III	ZD	Clay	200	8	0.432
III	ZD	Clay	200	8	0.432
III	ZD	Clay	200	8	0.432
IV	ZD	Clay	300	2	1.321
IV	ZD	Clay	300	2	1.321
IV	ZD	Clay	300	2	1.321
IV	ZD	Clay	300	8	1.321
IV	ZD	Clay	300	8	1.321
IV	ZD	Clay	300	8	1.321
IV	ZD	Clay	200	2	0.587
IV	ZD	Clay	200	2	0.587
IV	ZD	Clay	200	2	0.587
IV	ZD	Clay	200	8	0.587
IV	ZD	Clay	200	8	0.587
IV	ZD	Clay	200	8	0.587
V (t=0.5 m)	ZD	Clay	300	2	1.769
V (t=0.5 m)	ZD	Clay	300	2	1.769

Structure Type	Soil Class	Soil Type	Shear Wave Velocity (m/s)	Embedment Depth (h)	Flexibility Ratio
V (t=0.5 m)	ZD	Clay	300	8	1.769
V (t=0.5 m)	ZD	Clay	300	8	1.769
V (t=0.5 m)	ZD	Clay	300	8	1.769
V (t=0.5 m)	ZD	Clay	200	2	0.786
V (t=0.5 m)	ZD	Clay	200	2	0.786
V (t=0.5 m)	ZD	Clay	200	2	0.786
V (t=0.5 m)	ZD	Clay	200	8	0.786
V (t=0.5 m)	ZD	Clay	200	8	0.786
V (t=0.5 m)	ZD	Clay	200	8	0.786
V (t=1.0 m)	ZD	Clay	300	2	0.854
V (t=1.0 m)	ZD	Clay	300	2	0.854
V (t=1.0 m)	ZD	Clay	300	8	0.854
V (t=1.0 m)	ZD	Clay	300	8	0.854
V (t=1.0 m)	ZD	Clay	200	2	0.380
V (t=1.0 m)	ZD	Clay	200	2	0.380
V (t=1.0 m)	ZD	Clay	200	2	0.380
V (t=1.0 m)	ZD	Clay	200	8	0.380
V (t=1.0 m)	ZD	Clay	200	8	0.380
V (t=1.0 m)	ZD	Clay	200	8	0.380
I	ZE	Clay	150	2	0.186
I	ZE	Clay	150	2	0.186
I	ZE	Clay	150	2	0.186
I	ZE	Clay	150	8	0.186
I	ZE	Clay	150	8	0.186
I	ZE	Clay	150	8	0.186
I	ZE	Clay	120	2	0.119
I	ZE	Clay	120	2	0.119
I	ZE	Clay	120	2	0.119
I	ZE	Clay	120	8	0.119
I	ZE	Clay	120	8	0.119
I	ZE	Clay	120	8	0.119
II	ZE	Clay	150	2	0.229
II	ZE	Clay	150	2	0.229
II	ZE	Clay	150	2	0.229
II	ZE	Clay	150	8	0.229
II	ZE	Clay	150	8	0.229
II	ZE	Clay	150	8	0.229
II	ZE	Clay	120	2	0.147
II	ZE	Clay	120	2	0.147
II	ZE	Clay	120	2	0.147
II	ZE	Clay	120	8	0.147
II	ZE	Clay	120	8	0.147

Structure Type	Soil Class	Soil Type	Shear Wave Velocity (m/s)	Embedment Depth (h)	Flexibility Ratio
II	ZE	Clay	120	8	0.147
III	ZE	Clay	150	2	0.229
III	ZE	Clay	150	2	0.229
III	ZE	Clay	150	2	0.229
III	ZE	Clay	150	8	0.229
III	ZE	Clay	150	8	0.229
III	ZE	Clay	150	8	0.229
III	ZE	Clay	120	2	0.147
III	ZE	Clay	120	2	0.147
III	ZE	Clay	120	2	0.147
III	ZE	Clay	120	8	0.147
III	ZE	Clay	120	8	0.147
III	ZE	Clay	120	8	0.147
IV	ZE	Clay	150	2	0.312
IV	ZE	Clay	150	2	0.312
IV	ZE	Clay	150	2	0.312
IV	ZE	Clay	150	8	0.312
IV	ZE	Clay	150	8	0.312
IV	ZE	Clay	150	8	0.312
IV	ZE	Clay	120	2	0.200
IV	ZE	Clay	120	2	0.200
IV	ZE	Clay	120	2	0.200
IV	ZE	Clay	120	8	0.200
IV	ZE	Clay	120	8	0.200
IV	ZE	Clay	120	8	0.200
V (t=0.5 m)	ZE	Clay	150	2	0.418
V (t=0.5 m)	ZE	Clay	150	2	0.418
V (t=0.5 m)	ZE	Clay	150	2	0.418
V (t=0.5 m)	ZE	Clay	150	8	0.418
V (t=0.5 m)	ZE	Clay	150	8	0.418
V (t=0.5 m)	ZE	Clay	150	8	0.418
V (t=0.5 m)	ZE	Clay	120	2	0.267
V (t=0.5 m)	ZE	Clay	120	2	0.267
V (t=0.5 m)	ZE	Clay	120	2	0.267
V (t=0.5 m)	ZE	Clay	120	8	0.267
V (t=0.5 m)	ZE	Clay	120	8	0.267
V (t=0.5 m)	ZE	Clay	120	8	0.267
V (t=1.0 m)	ZE	Clay	150	2	0.202
V (t=1.0 m)	ZE	Clay	150	2	0.202
V (t=1.0 m)	ZE	Clay	150	2	0.202
V (t=1.0 m)	ZE	Clay	150	8	0.202
V (t=1.0 m)	ZE	Clay	150	8	0.202

Structure Type	Soil Class	Soil Type	Shear Wave Velocity (m/s)	Embedment Depth (h)	Flexibility Ratio
V (t=1.0 m)	ZE	Clay	150	8	0.202
V (t=1.0 m)	ZE	Clay	120	2	0.129
V (t=1.0 m)	ZE	Clay	120	2	0.129
V (t=1.0 m)	ZE	Clay	120	2	0.129
V (t=1.0 m)	ZE	Clay	120	8	0.129
V (t=1.0 m)	ZE	Clay	120	8	0.129
V (t=1.0 m)	ZE	Clay	120	8	0.129

*t is represent lining thickness.